Global-Scale Rossby Waves on Stars

Thesis submitted in fulfillment of the requirements for the Ph.D. degree at the Ilia State University of Tbilisi, Faculty of Natural Sciences and Medicine and at the Georg-August Universität of Göttingen, Faculty of Physics

Mariam Albekioni

Lehman Haupt's International Doctoral Program

Scientific supervisors:
Prof. Dr. Vasil Kukhianidze (ISU),
Prof. Dr. Laurent Gizon (UGOE)

Ilia State University /Georg August Universität Göttingen
Tbilisi, Georgia
2024

აბსტრაქტი

როსბის ტალღები, იგივე r-მოდები, აღიძვრებიან მბრუნავ სფეროზე აბსოლუტური გრიგალობის შენახვის შედეგად. ეს ტალღები განაპირობებენ დედამიწის ატმოსფეროსა და ოკეანეების მსხვილ-მასშტაბიან დინამიკას. ამიტომ, მათი შესწავლა ათწლეულების განმავლობაში მიმდინარეობს. ბოლო წლებში მოხდა როსბის ტალღების დაკვირვება მზესა და ვარსკვალავებზე, რამაც გააღვიძა მათი თვისებების თეორიულად შესწავლის ინტერესი სხვადასხვა ასტროფიზიკურ სიტუაციაში. სადისერტაციო ნაშრომის მიზანია როსბის ტალღების თვისებების შესწავლა მზისა და ვარსკვლავების წიაღში.

ორგანზომილებიან ბეტა სიბრტყის მიახლოებაში, შესწავლილია განედური დიფერენციალური ბრუნვისა და სიბლანტის გავლენა მზის როსბის ტალღების დინამიკაზე. მიღებული შედეგები აჩვენებენ, რომ სიჩქარის საკუთარ ფუნქციებს აქვთ სინგულარობის წერტილი კრიტიკულ განედზე, სადაც როსბის ტალღის ფაზური სიჩქარე უტოლდება განედურ დიფერენციალურ ბრუნვას. არაბლანტი შემთხვევის განხილვისას, საკუთარი მნიშვნელობები ნამდვილი და უწვეტია, თუმცა სიბლანტის დამატების შემდეგ სპექტრი ხდება კომპლექსური და დისკრეტული. როდესაც რეინოლდის რიცხვის მნიშვნელობაა ~ 300, მაშინ ტალღის მილევა და ფუნქციის საკუთარი მნიშვნელობების რეალური ნაწილი თვისობრივ თანხვედრაშია მზეზე არსებულ დაკვირვებებთან. ასევე ნაჩვენებია, რომ თითოეული გრძედური ტალღური რიცხვი დაკავშირებულია განედურად სიმეტრიულ როსბის მოდასთან, რომელიც განედური დიფერენციალური ბრუნვის მიერ არის ჩაჭერილი ეკვატორის მახლობლად. ბლანტ მოდელში, როსბის ტალღებს გადააქვთ მნიშვნელოვანი იმპულსი შუა ფენებიდან ეკვატორის მიმართულებით.

კვლევის ფარგლებში, ასევე შესწავლილია როსბის ტალღები ერთგვაროვნად მბრუნავი ვარსკვლავების წიაღში ტემპერატურის რადიალური ცვლილების გათვალისწინებით. საწყისი სამგანზომილებიანი ჰიდროდინამიკული განტოლებები განვაცალეთ რადიალურ და ჰორიზონტალურ ნაწილებად ტრადიციული მიახლოების გამოყენებით და განცალების მუდმივით, რომელიც თავის მხრივ წარმოადგენს როსბის ტალღების ექვივალენტურ სიღრმეს თხელის წყლის მიახლოების მოდელში. აღმოჩნდა, რომ როსბის ტალღების რადიალური სტრუქტურა აღიწერება ბესელის ფუნქციებით და ფორმა განპირობებულია ვერტიკალური ტემპერატურული გრადიენტით. ზედაპირზე დაფიქსირებულმა სასაზღვრო პირობებმა მოგვცა შესაძლებლობა მიგვეღო ექვივალენტური სიღრმის დისკრეტული სპექტრი, რომელიც შეესაბამება დისკრეტულ ვერტიკალურ მოდებს. შედეგებმა უჩვენეს, რომ ვერტიკალური მოდები ძირითადად თავმოყრილნი არიან ზედაპირულ შრეში, რომლის სისქეც რამდენიმე ათეული სიმკვრივის მახასიათებელი სიღრმის ტოლია. შემდეგ, რადიალური განტოლებიდან მიღებული ექვივალენტური სიღრმის მნიშვნელობები გამოვიყენეთ ჰორიზონტალური განტოლების ამოსახსნელად და მივიღეთ შესაბამისი დისპერსიული თანაფარდობები როსბის, როსბი-გრავიტაციული და ინერციულ-გრავიტაციული ტალღებისთვის. ჰორიზონტალური ამონახსნები აღმოჩნდნენ კონცენტრირებულნი ეკვატორის მიდამოში და წარმოადგენენ ეკვატორულად ჩაჭერილ ტალღებს. ასევე ვაჩვენეთ, რომ ტალღების სიხშირეები დამოკიდებულია ვერტიკალურ ტემპერატურულ გრადიენტსა და ვარსკვლავის ბრუნვის სიხშირეზე. შესაბამისად, ვარსკვლავების სინათლის მრუდებში დაკვირვებული ტალღის სიხშირეები, ვარსკვლავის ცნობილ პარამეტრებთან ერთად (რადიუსი, ზედაპირის გრავიტაციული აჩქრება, ბრუნვის პერიოდი), შესაძლებლობას მოგცემს შევაფასოთ ტემპერატურული გრადიენტი ვარსკვლავების წიაღში. ამიტომ, როსბის ტალღები შეიძლება განვიხილოთ როგორც დამატებითი ინსტრუმენტი ასტეროსეისმოლოგიისთვის გრავიტაციულ და აკუსტიკურ ტალღებთან ერთად.

Abstract

Rossby waves (r-modes) arise due to the conservation of absolute vorticity on rotating spheres. The waves govern the large-scale dynamics of the Earth's atmosphere/oceans and have been intensively studied during decades. Recent discovery of the waves on the Sun and other stars revived the interest towards theoretical investigation of the wave properties in different astrophysical situations. This thesis aims to study the dynamics of the Rossby waves in solar/stellar interiors.

The influence of the latitudinal differential rotation and viscosity on the Rossby waves was studied using 2-dimensional beta-plane approximation on the Sun. Our results showed that the velocity eigenfunctions have a singularity at the critical latitude where the phase speed of the Rossby wave equals with the latitudinal differential rotation. Without viscosity, the eigenvalues are real and continuous, while they become discrete and complex in the presence of viscosity. For Reynolds number of ~ 300, the attenuation and the real part of eigenfunctions are in qualitative agreement with the solar observations. Each longitudinal wavenumber is associated with a latitudinally symmetric Rossby mode trapped at low latitudes by solar differential rotation. In the viscous model, Rossby modes transport significant angular momentum from the dissipation layers toward the equator.

We also studied the Rossby waves in the interiors of uniformly rotating stars with radiative envelopes in the presence of the vertical stratification of the temperature. The initial 3-dimensional linear hydrodynamic equations were separated into vertical and horizontal parts using traditional approximation with a separation constant, which actually is the equivalent depth of the Rossby waves. The vertical structure of the Rossby waves was found to be governed by the Bessel functions and strongly dependent on the vertical temperature gradient. Surface boundary conditions allowed us to obtain the discrete values of the equivalent depth, which correspond to the discrete vertical modes. It is found that the vertical modes are concentrated in the near-surface layer with a thickness of several tens of surface density scale height. Then the obtained equivalent depth was used to solve the horizontal structure equations and the corresponding dispersion relations for Rossby, Rossby-gravity, and inertia-gravity waves were obtained. The solutions were found to be confined around the equator leading to the equatorially trapped waves. It was shown that the wave frequency depends on the vertical temperature gradient as well as on the stellar rotation. Therefore, observations of wave frequency in light curves of stars with known parameters (radius, surface gravity, rotation period) could be used to estimate the temperature gradient in stellar outer layers. Consequently, the Rossby mode may be considered as an additional tool in asteroseismology apart from acoustic and gravity modes.

Aknowledgement

First of all, I want to thank my supervisors Vasil Kukhianidze and Laurent Gizon. Their scientific expertise and support, guide me through the entire process of research and dissertation writing. Vasil, I can never express my gratitude in words towards you as my scientific supervisor and as a friend too. You have consistently encouraged me to explore new methods for growth and development as a scientist, and I deeply appreciate it. Laurent, I am grateful to have had the chance to work with you, thank you for making me a part of that team while I was staying in Goettingen. I have learned a lot from you.

I would like to thank Teimuraz Zaqarashvili, as you were very busy but still made time for me to help. I appreciate your contribution as a mentor and a collaborator very much. Many thanks to Robert Cameron for his invaluable comments and suggestions regarding my research, as well as for the support he offered during my time in Goettingen. I am grateful to Johannes Wicht and Andreas Tilgner for their participation in the TAC meetings and the valuable feedback they provided.

I would like to express my gratitude to all the people who made the ”Lehman-Haupt International Doctoral Programme” possible and to thank our program coordinators Aleksandra Bovt and Vakhtang Pataridze.

Thanks to my friends and family. To my husband Murmani Gelava, your love and support always give me enormous strength. Thank you for everything you have done for me. To my sister, Elene, my dearest friend and my source of inspiration. To Eka Gurgenashvili, whom I met as a colleague and she is my closest friend now. To Mariam Chitishvili, my strength, and a friend since forever. Thanks to my dearest friend Tamar Zakareishvili, for all the support and inspiration. And to all of you guys: Grigol, Luka, Davit, Nika, Gogita. I could not have done it without you being always there for me.

Finally, I will thank my dad, and special thanks to my mom, Who is always proud of me and supports me unconditionally.

List of publications:

In the course of the doctoral research, four papers have been published with the involvement of Mariam Albekioni. Mariam is the first author in two papers and a co-author in the remaining two papers:

1. "Equatorially trapped Rossby waves in radiative stars" - M. Albekioni, T.V. Zaqarashvili, V. Kukhianidze, E. Gurgenashvili, P. Bourdin, Astronomical Notes, 344, 10

doi:https://doi.org/10.1002/asna.20230083

Contribution: M. Albekioni contributed to solving the problem analytically as well as modeling the results numerically. She provided the main scientific interpretation.

2. "Rossby waves on stellar equatorial β planes: Uniformly rotating radiative stars" - M. Albekioni, T.V. Zaqarashvili, V. Kukhianidze, A & A, 671, A91, 9
doi:https://doi.org/10.1051/0004-6361/202243985

Contribution: M. Albekioni contributed to solving the problem analytically as well as modeling the results numerically. She provided the main scientific interpretation.

3. "Rossby waves in astrophysics" - T.V. Zaqarashvili, M. Albekioni, J.L. Ballester, Y. Bekki, L. Biancofiore, A.C. Birch, M. Dikpati, L. Gizon, E. Gurgenashvili, E. Heifetz, A.F. Lanza, S.W. McIntosh, L. Ofman, R. Oliver, B. Proxauf, O.M. Umurhan, R. Yellin-Bergovoy, Space Science Reviews, 271, 15
doi:https://doi.org/10.1007/s11214-021-00790-2

Contribution: M. Albekioni contributed to writing chapter: 3.2.2. "Rossby Waves in shallow water approximation". She has reviewed the manuscript together with co-authors.

4. "Effect of latitudinal differential rotation on solar Rossby waves: Critical layers, eigenfunctions, and momentum fluxes in the equatorial β plane" - L. Gizon, D. Fournier, M Albekioni, A & A, 642, A178, 10
doi: https://doi.org/10.1051/0004-6361/202038525

Contribution: M. Albekioni contributed to solving the inviscid problem analytically with Prof. L. Gizon. She has reviewed the manuscript together with co-authors.

Contents

1 Introduction

1.1 Basics of Rossby waves

Rossby waves appear as large-scale waves in rotating fluids, whose frequency is several times less than the rotation frequency of the fluids. The waves essentially govern the global weather system of the Earth. Therefore, Rossby-type waves have been studied for decades, especially in the context of the Earth's atmosphere and oceans. For this reason, they are often called planetary waves (the waves are also called r-modes in astrophysical contexts). The waves were first identified by Carl-Gustaf Rossby; a Swedish oceanologist and meteorologist who was working on a long-range weather forecasting project at the Massachusetts Institute of Technology and the US Weather Bureau. During the study, he created 7-day and later 5-day mean charts for the pressure on the sea level and for the isentropic contours. This research together with Kelvin's circulation theorem became an inspiration for Rossby to describe the large-scale atmospheric dynamics in terms of the conservation of absolute vorticity (a sum of planetary and relative vorticities) on a rotating sphere, which forces the waves to propagate in the retrograde (opposite direction of the rotation) direction (Rossby, 1939).

The fluid vorticity is a curl of the flow velocity, $\vec{v}$, i.e. $\vec{\omega} = \nabla \times \vec{v}$. Consequently, the vorticity of a uniformly rotating sphere, i.e. planetary vorticity, is defined as $2\vec{\Omega}$, where $\vec{\Omega}$ is the angular velocity of the sphere. The absolute vorticity in the inertial frame thus can be written as $\vec{\omega}_a = 2\vec{\Omega} + \vec{\omega}$, where $\vec{\omega}$ is a vorticity in the rotating frame (relative vorticity). Due to the preferred direction of the rotation axis, the planetary vorticity is the function of the latitude being maximal at the poles and 0 at the equator. Therefore, the conservation of absolute vorticity yields the variation of relative vorticity with the latitude. The absolute value of planetary vorticity can be written as Coriolis parameter, $f = 2\Omega \sin\theta$, where θ is a latitude. Therefore, the Coriolis force is an essential component of the Rossby waves. The Coriolis force was named after Gaspard-Gustave de Coriolis, who first described the force in the context of the water wheels. Coriolis force arises in rotating frames, acts only on the moving bodies, does not do any work and deflects the motion at right (left) angles in the northern (southern) hemisphere. This is called the Coriolis effect. For example, when the fluid moves from the equator towards the poles it experiences eastward displacement, and the fluid moving towards the equator displaces westward. In order to conserve the absolute vorticity, the fluid gains a relative vorticity, which returns it to the starting point - Fig.1.

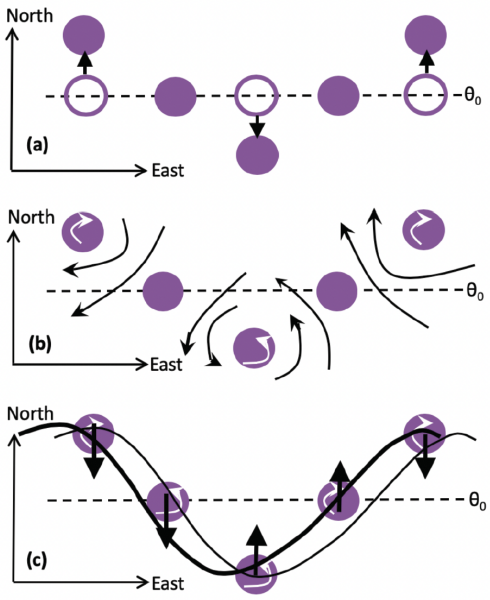

Figure 1: Graphical illustration of retrograde motion of Rossby wave due to the conservation of absolute vorticity. *The figure is reproduced from Dikpati et al. (2018b) by permission of the AAS*

The Coriolis effect is crucial for producing Rossby waves. The parameter, which shows the importance of rotation with regards to the inertial motions, is called Rossby number: $Ro = V/2\Omega L$, where V and L are the characteristic velocity and the length scale of fluid motions, respectively. A smaller Rossby number yields a stronger influence of rotation on the dynamics of the system.

The phase and group velocities of the Rossby waves have a retrograde and prograde direction, respectively. In the case of a uniform jet with velocity U, the phase and group velocities can be written as:

$$c_{phase} = U - \frac{\beta\lambda^2}{4\pi^2}, \tag{1}$$

$$c_{group} = U + \frac{\beta\lambda^2}{4\pi^2}, \tag{2}$$

where λ is a wavelength. Here $\beta = \partial f/\partial\theta = 2\Omega cos\theta/R$ with R being the radius of the sphere characterizes the latitudinal variation of the Coriolis parameter. For each value of U, there is the critical value of the wavelength $\lambda = 2\pi\sqrt{U/\beta}$, for which the waves become stationary, i.e. they do not have any displacement with regards to the Earth's surface.

The theoretical background of the Rossby waves has been developing for centuries since Hadley (1735). Laplace's (Laplace, 1893) tidal equations lead to

the basic mathematical descriptions of the waves, while Hough (Hough, 1897, 1898) found the solutions of Laplace's equations in terms of Legendre functions for Rossby-type waves (low-frequency waves in Hough's notation). A linearized system of the main equations (equations of motion, continuity, and energy) needs to be solved with appropriate assumptions. The analytical solutions for Rossby waves were found with different approximations, but the easiest one is related with only horizontal motion i.e. two-dimensional models with an incompressible fluid. This model provides solutions for two-dimensional Rossby waves and demonstrates key properties associated with these waves. The model incorporates the beta-plane approximation, which has been extensively utilized to investigate the large-scale dynamics of Earth's atmosphere and oceans. The crucial assumption of the approximation is that the scale of perturbations must be significantly smaller than the radius of the sphere. The beta-plane approximation in a 2D model yields the harmonic solutions with the dispersion relation:

$$\sigma = k_x U - \frac{k_x \beta}{k_x^2 + k_y^2}, \tag{3}$$

where σ is the wave frequency and k_x (k_y) is the toroidal (poloidal) wavenumber. However, for larger-scale perturbations, the curvature of the Earth's surface must be taken into account. In this case, the conservation of absolute vorticity in spherical coordinates leads to the Legendre equation (Haurwitz, 1940), which has bounded solutions in terms of Legendre polynomials. The corresponding dispersion relation for Rossby waves without a background flow is:

$$\sigma = -\frac{2m\Omega}{l(l+1)}. \tag{4}$$

m is an angular order (same as the toroidal wavenumber) and denotes the number of zeros around the equator in spherical harmonics. On the other hand, l is a degree and shows the number of nodes on a full spherical surface. When l is fixed and $m \neq 0$ ($|m| < l$), then the solutions are tesseral spherical harmonics. There are no nodal meridians for $m = 0$, therefore these are zonal harmonics. For $l = |m|$ there are no nodes between the poles, and the solutions are called sectoral harmonics.

The 2D model contains the basic physical properties of the Rossby waves, however, the real picture is much more complicated and the vertical stratification needs to be taken into account. Stratified fluids yield a non-uniform vertical density distribution due to gravity. In this scenario, the pressure may stay hydrostatic for a

small Rossby number. This assumption is common in studying geophysical and astrophysical flows.

In order to describe a stratified fluid, a shallow water model has been used since Laplace's (Laplace, 1893) tidal theory. There are certain conditions that need to be satisfied to consider a shallow water system. First of all, a fluid layer thickness must be much smaller than the scales of horizontal perturbations: $H/L \ll 1$, H is the width of the layer and it should correspond to the density scale height (to be less or equal to the scale height). Furthermore, inside the layer the density must be uniform and the pressure must be hydrostatic.

To investigate the properties of Rossby waves within a shallow water approximation, one can write Laplace's equations using a Cartesian coordinate system (Longuet-Higgins, 1965). These equations system has high and low-frequency solutions. The dispersion relation and the solutions depend on the Coriolis parameter. Away from the equator, $\beta y \ll f$ and the dispersion relation of the waves becomes

$$\sigma = -\frac{k_x \beta}{k_x^2 + k_y^2 + f_0^2/c2}. \tag{5}$$

Here, k_x (k_y) is a toroidal (poloidal) wavenumber, $c = \sqrt{gH}$ is the surface gravity speed and f_0 is the Coriolis parameter at the fixed latitude (g is the gravitational acceleration). When the scale of horizontal perturbations is much smaller than the Rossby radius of deformation ($k_x, k_y \gg f_0/c$), then this dispersion equation transforms into the 2D version (Eq. 3).

In the equatorial area, the Coriolis parameter can be approximated as $f \approx \beta y$. Then the Laplace tidal equations lead to the parabolic cylinder (the equation of quantum harmonic oscillator) equation. It has bounded solutions in terms of Hermite polynomials (e.g. Matsuno (1966)), which decrease exponentially towards the poles. The solutions strongly depend on the Lamb parameter and order of the Hermite polynomial. The Lamb parameter

$$\varepsilon = \frac{4\Omega^2 R^2}{gH} \tag{6}$$

characterizes shallow water systems. When this parameter is large, then the waves are trapped near the equator and they are called equatorial or equatorially trapped waves. The Rossby wave dispersion equation near the equator is described by the formula

$$\sigma = -\frac{k_x \beta}{k_x^2 + (2n+1)\beta/c}, \tag{7}$$

where $n = 0, 1, 2, ..$ is the order of Hermite polynomial and is equivalent to the $l - |m|$ quantity in spherical harmonics, that is the number of nodes between the poles. Hence, $n = 0$ corresponds to the sectoral harmonics $l = |m|$.

If the wavelength of the equatorially trapped Rossby waves is large enough, then the dispersion relation can be rewritten as:

$$\sigma \approx -\frac{k_x c}{2n+1}, \tag{8}$$

which shows that in shallow water system, the dynamics of the waves strongly depend on the gravitational acceleration and the width of the shallow layer.

In order to compare how spherical geometry changes the dispersion equation of the Rossby waves near the equatorial region, the solutions in spherical coordinates must be found (Longuet-Higgins, 1965). Laplace's tidal equations in spherical geometry have been solved analytically by expanding Legendre functions by Hough (Hough, 1897, 1898). Obtained dispersion equation depends on value of the Lamb parameter and in case of large ϵ it can be written as

$$\sigma \approx -\frac{2m\Omega}{(2n+1)\sqrt{\epsilon}} = -\frac{mc}{(2n+1)R}. \tag{9}$$

The equation is exactly the same as Eq.(8) for rectangular geometry replacing k_x by m/R. It is clear, that the spherical and rectangular coordinates do not give any difference in dispersion relation of equatorially trapped Rossby waves. Therefore, using rectangular coordinates in the equatorial β plane approximation is completely justified if we confine the analysis to low latitudes.

1.2 Stars

Stars are astrophysical objects where the matter is held together by self-gravity. They are born in the interstellar gaseous nebulae or molecular clouds. The matter start to collapse, which is a mandatory process for stellar formation, the Jeans criteria must be satisfied. If the mass is high enough, then the nebula breaks into smaller and denser parts. The temperature and pressure increase and the fragment forms as a rotational matter. The process continues before the matter starts adiabatic contraction, it gets rid of the extra fragments and forms an object called a protostar. The further evolution of protostars fully depend on their masses Fig.2.

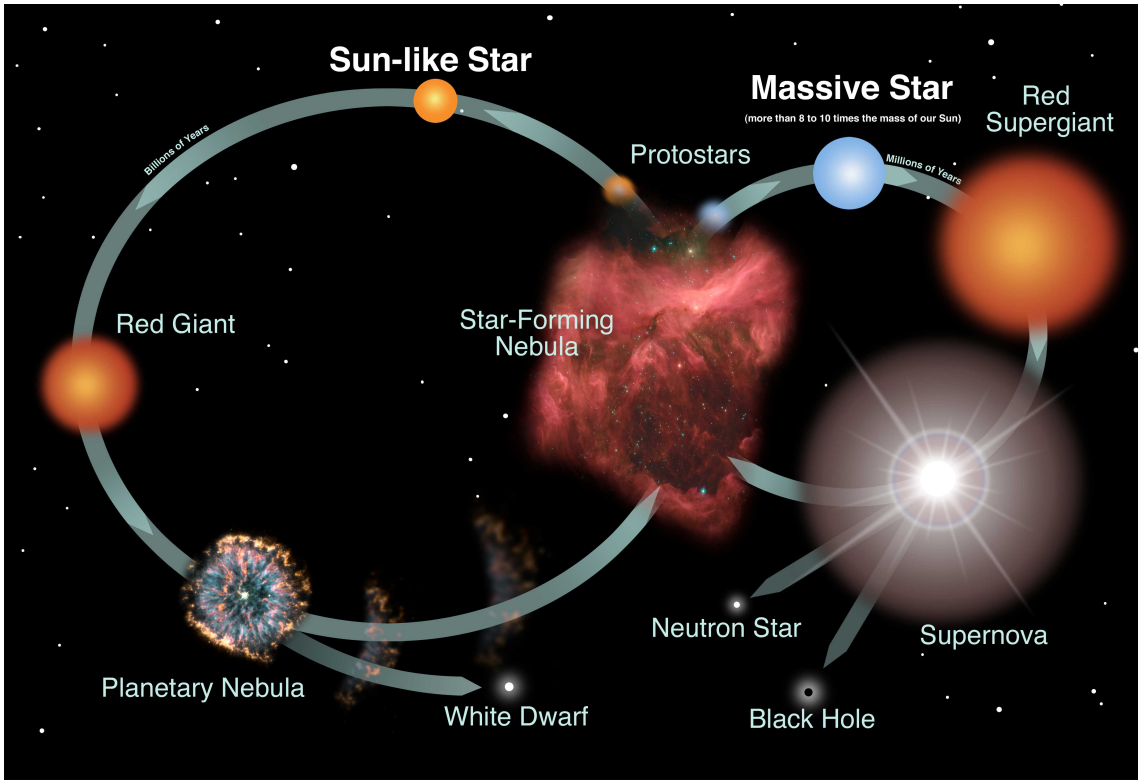

Figure 2: Stellar evolution chart, from birth to the remnant. *Credit: NASA and the Night Sky Network.*

The protostars with a mass of approximately $0.08M_{\odot}$ ($M_{\odot}$ denotes a solar mass 2×10^{30} kg) never reach the stage of nuclear fusion and they end up as brown dwarfs, the lowest right-hand side area in the Hertzsprung-Russel diagram (HRD). More massive protostars begin the nuclear reactions and move to the main sequence part of the HR diagram. The place of the stars in the diagram depends on their spectral type. The place on HRD defines the surface temperature vs luminosity relation of a star, which itself is determined by the mass. Mid-sized stars like

the Sun are called yellow dwarfs, they remain in the main sequence for approximately 10 billion years and are placed in the middle of the HRD. More massive stars fuse hydrogen faster and are placed on the upper part on the main sequence of HRD. They live much shorter comparing with solar-like stars.

Figure 3: The heat transfer inside stars with different masses. Massive stars ($> 1.5M_{\odot}$) have inner convective core and outer radiative envelope. The stars with average mass ($0.5 - 1.5M_{\odot}$), such as our Sun, have inner radiative and outer convective envelopes, and less massive stars ($< 0.5M_{\odot}$) stay convective. *Source: www.sun.org*

The Heat transfer (convective or radiative) inside a star is also defined by its mass (Fig.3). Less massive stars with $M < 0.5M_{\odot}$ stay almost fully convective. Solar-like stars - $0.5M_{\odot} < M < 1.5M_{\odot}$ develop inner radiative zone and outer convective envelope. Massive stars - $M > 1.5M_{\odot}$ have a convective core and a radiative outer shell.

1.3 The Sun

The Sun is our nearest star. It is a G2V-type main sequence star formed approximately 4.6 billion years ago. It is in the middle period of its lifetime. Sun generates its energy through nuclear fusion in the core (burning hydrogen into helium), where the temperature reaches $\approx$ 16 million K, while solar surface temperature is only 6 000 K. The internal structure of the Sun consists of different layers and the heat transfer mechanisms are distinct through each layer, accordingly (Fig.4). The core is the central part of the Sun, where the main thermonuclear fusion reactions take place. It is the densest part of the Sun with a radius of $0.2 - 0.25R_\odot$ ($R_\odot \approx 7 \times 10^5$ km is a radius of the Sun). The energy radiated in terms of photons during nuclear reactions transfers to the next layer called as the radiative zone with the thickness of $\approx 0.45R_\odot$, where the energy is transferred by radiation i.e. photons are absorbed and re-emitted by atoms. The temperature and density drop significantly at the top of a radiative zone so that the temperature gradient approaches the adiabatic value. A slightly super-adiabatic temperature gradient triggers convection near $\approx 0.7R_\odot$ and creates convection envelope, which extends to the surface. The heat transfer occurs through convection in this region and the temperature continuously reduces towards the surface (Fig.4). The solar atmosphere starts above the surface consisting in the photosphere, the chromosphere, and the corona. The photosphere is a visible surface that we can see on the Sun. There is a temperature minimum layer at approximately $500km$ distance above the solar surface, where the temperature reaches its minimum value of $\approx 4000K$. The temperature increases again with height reaching to 1-2 million K in the Corona. All visible events take place in the solar atmosphere and observations provide us with information over centuries.

The radiative and convective envelopes have qualitatively different rotation profiles. The radiative zone rotates as a solid body, while the convective envelope has both vertical and latitudinal differential rotation. The solar synodic rotational period at the equator is approximately 26 days, while it becomes $\sim$ 35 days at the poles, i.e. the rotation rate differs with latitudes. Solar differential rotation is described as:

$$\Omega_\odot = \Omega_0 - \Omega_1 sin^2\theta - \Omega_2 sin^4\theta \tag{10}$$

Where θ is a latitude, Ω_0 is the solar angular velocity at the equator, while Ω_1, Ω_2 are the coefficients obtained from the observations, which may change with the

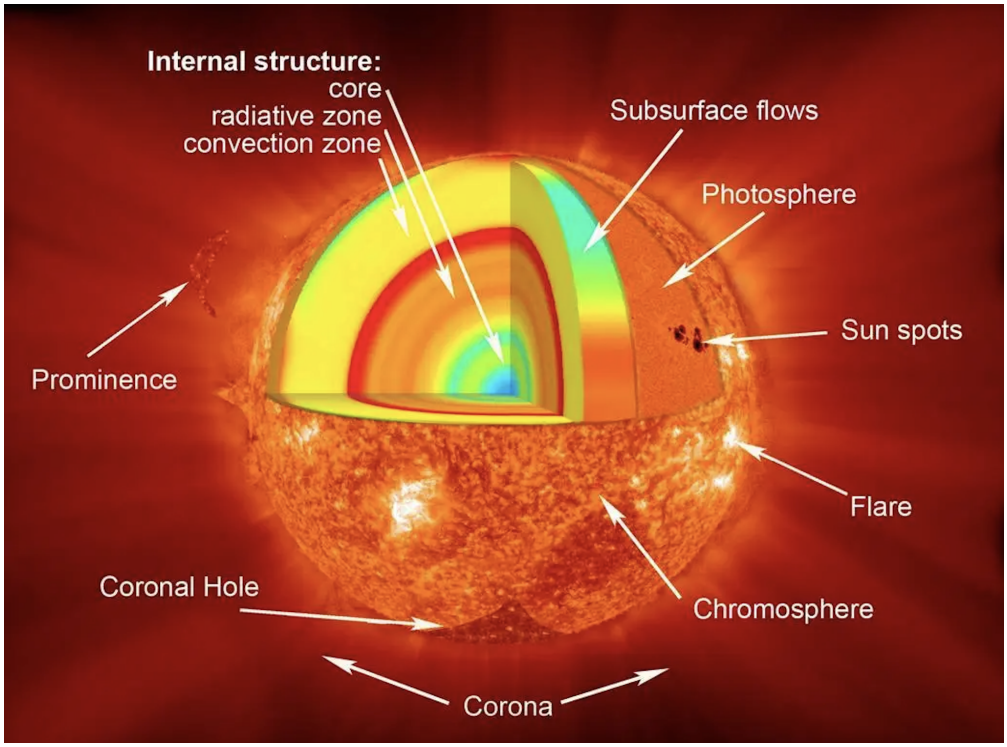

Figure 4: The solar structure: Internal layers and atmospheric configuration. Credit: NASA/Goddard Space Flight Center

depth and with phase of solar cycles (Newton & Nunn, 1951; Timothy et al., 1975; Snodgrass, 1984; Snodgrass & Ulrich, 1990; Brajša et al., 2001). The uniform rotation exists from the center up to $0.7R_{\odot}$ and then the rotation starts to depend both on the latitude and depth. The latitudinal differential rotation (or shear flows) may have a strong influence on the processes in the solar surface and interior.

1.4 Rossby waves on the Sun and stars

Rossby waves have been well described and observed in Earth's atmosphere and oceans for decades. As they are characteristic for rotating fluid systems, it was expected that they would also appear in other astrophysical objects. Beyond the Earth, the initial observations of Rossby waves in the solar system were predominantly performed on Jupiter and Saturn. Detection of the waves in stellar atmospheres is much more complicated. But the theoretical study of non-radial stellar oscillations in terms of r modes was started since Papaloizou & Pringle (1978). Then Provost et al. (1981) (see also Damiani et al. (2020)) studied r-modes in a uniformly rotating star using perturbation analysis with the approximation of slow rotation. Saio (1982) conducted research on r-mode oscillations in uniformly rotating stars, incorporating perturbations of the gravitational potential. In recent years, there has been considerable advancement in the theoretical understanding of Rossby waves within the solar interior (Gizon et al., 2020; Bekki et al., 2022; Dikpati et al., 2022).

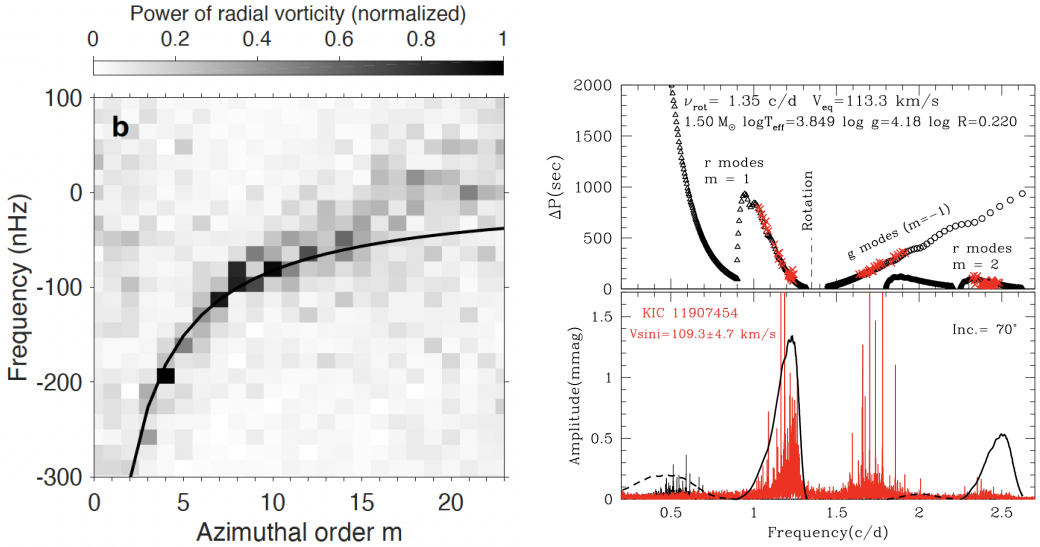

Figure 5: Left panel: Rossby wave frequency vs toroidal wavenumebr, m, obtained with granulation tracking method byLöptien et al. (2018). The black solid line represents the theoretical dispersion curve. Right panel: the period spacing (top) and amplitude spectra (bottom) for the γ Dor star KIC 11907454 from Saio et al. (2018).

While the theoretical background of solar and stellar Rossby waves was developing for decades, there were only some attempts to observe the Rossby waves on the Sun (Suess, 1971; Kuhn et al., 2000; Williams et al., 2007), but they were largely not successful. Recently, Löptien et al. (2018) found Rossby wave patterns

in the solar near-surface flows, whose dispersion relations was almost identical to classical Rossby wave dispersion relation on uniformly rotation sphere (see the left panel on Fig.5). In this work, the authors used 6 years of observational data obtained by the SDO/HMI instrument. Classical Rossby waves can be identified in horizontal velocity maps of the solar surface, where they appear as radial vorticity patterns. Only sectoral modes with toroidal wavenumber $3 \leq m \leq 15$ have been found with the granulation tracking method. Different methodologies of observational data analysis such as helioseismology and granular tracking techniques confirmed the existence of solar Rossby waves (Liang et al., 2019; Hanasoge & Mandal, 2019; Proxauf et al., 2020; Gizon et al., 2021; Hanson et al., 2022).

On the other hand, recent space missions such as TESS (Transiting Exoplanet Survey Satellite), CoRoT (Convection, Rotation and planetary Transit), and Kepler have gathered an extensive amount of observational data. The data has enabled the identification of Rossby waves in the light curves of various stars. first, Van Reeth et al. (2016) reported the signature of r-modes in Gamma Doradus stars through analysis of Kepler data. Subsequently, the waves have been detected in numerous stars mainly early type A, B, and F stars on a Hertzsprung-Russel diagram. Rossby waves are related to the variation of the flow vorticity, but they also cause pressure/density variations which makes it possible to detect r-modes in the light curves of the stars. It has been suggested that r-mode frequencies appear as a secondary peak in light curves, followed by the main peak which is believed to be the rotational frequency of the star (Saio et al., 2018) (see the right panel on Fig.5). It has been also suggested that the Rossby waves may lead to the observed short-term stellar cycles (Lanza et al., 2009; Bonomo & Lanza, 2012; Gurgenashvili et al., 2022).

It becomes increasingly clear that the Rossby waves have significant potential to be used for probing stellar interiors (Aerts, 2021). Therefore, the theoretical study of Rossby waves in solar/stellar interiors and consequent hint with observations is very important task in stellar astrophysics.

2 Results

2.1 Paper I: Rossby waves on stellar equatorial β planes: Uniformly rotating radiative stars

M. Albekioni, T.V. Zaqarashvili, V. Kukhianidze, A & A, 671, A91, 2023

doi: https://doi.org/10.1051/0004-6361/202243985

Contribution: M. Albekioni contributed to solving the problem analytically as well as modeling the results numerically. She provided the main scientific interpretation.

Abstract

Rossby waves arise due to the conservation of total vorticity in rotating fluids and may govern the large-scale dynamics of stellar interiors. Recent space missions have collected a lot of information about the light curves and activity of many stars, which triggered observations of Rossby waves in the stellar surface and interiors.

We aim to study the theoretical properties of Rossby waves in stratified interiors of uniformly rotating radiative stars with a sub-adiabatic vertical temperature gradient.

We used the equatorial beta-plane approximation and linear vertical gradient of temperature to study the linear dynamics of equatorially trapped Rossby and inertia-gravity waves in interiors of radiative stars. The governing equation was solved by the method of separation of variables in the vertical and latitudinal directions.

Vertical and latitudinal solutions of the waves are found to be governed by Bessel functions and Hermite polynomials, respectively. Appropriate boundary conditions at the stellar surface and poles define analytical dispersion relations for Rossby, Rossby-gravity, and inertia-gravity waves. The waves are confined in surface layers of 30-50 H_0, where H_0 is the surface density scale height, and they are trapped between the latitudes of $\pm 60^0$. Observable frequencies (normalised by the angular frequency of the stellar rotation) of Rossby waves with $m = 1$ ($m = 2$), where m is the toroidal wavenumber, are in the interval of 0.65-1 (1.4-2), depending on the stellar rotation, radius, and surface temperature.

Rossby-type waves can be systematically observed using light curves of Kepler and TESS (Transiting Exoplanet Survey Satellite) stars. Observations and theory then can be used for the sounding of stellar interiors.

1. Introduction

Rossby (planetary) waves are essential features of large-scale dynamics of rotating fluids. The theoretical background for the waves was first explored by Hadley (1735), while Laplace tidal equations created the basics for the mathematical description (Laplace, 1893). Hough (1897, 1898) found the solutions of the Laplace equations for the Rossby waves (low-frequency solution in Hough's terminology). However, the physical meaning of the waves was first described by Rossby (1939): the waves arise due to the conservation of total vorticity (planetary+relative) on a rotating sphere, which drives the propagating oscillations in the opposite direction of rotation.

Rossby waves are well studied in the Earth's context by observations and theory. Westward propagating waves with a predicted phase speed have been continuously observed in the terrestrial atmosphere (Hovmöller, 1949; Eliasen & Machenhauer, 1965; Yanai & Lu, 1983; Lindzen et al., 1984; Hirooka & Hirota, 1989; Madden, 2007) and oceans (Chelton & Schlax, 1996; Hill et al., 2000). The theory of terrestrial Rossby waves is also well studied (Haurwitz, 1940; Lindzen, 1967; Gill, 1982; Pedlosky, 1987). The detailed dynamics of the Rossby waves in the Earth's atmosphere and oceans is summarised in the reviews of Platzman (1968) and Salby (1984).

Recent direct observations of Rossby waves in the solar surface (Löptien et al., 2018) revived the interest for the study of Rossby waves on the Sun. The waves were observed by different methodologies such as granular tracking and helioseismology (Liang et al., 2019; Hanasoge & Mandal, 2019; Proxauf et al., 2020; Gizon et al., 2021; Hanson et al., 2022). The Rossby wave signature was also found in the dynamics of solar coronal bright points (McIntosh et al., 2017; Krista & Reinard, 2017). It was suggested that the magnetic Rossby waves may influence the short-term activity variations in the solar dynamo layer below the convection zone (Zaqarashvili et al., 2010; Zaqarashvili, 2018; Dikpati et al., 2018, 2020). The Rossby waves are important in the dynamics of many astrophysical objects such as Solar System planets, exoplanets, accretion disks, among others (Zaqarashvili et al., 2021).

The recent space missions CoRoT (Convection, Rotation and planetary Transits), Kepler, and TESS (Transiting Exoplanet Survey Satellite) have collected a lot of information about stellar light curves and activity. Van Reeth et al. (2016) reported the detection of Rossby waves in rapidly rotating γ Dor stars in period

spacing patterns. The pressure field of Rossby waves on the stellar surface may influence their light curves as suggested by Saio et al. (2018), hence the waves have been continuously observed in many Kepler stars with different spectral types (Saio et al., 2018; Li et al., 2019; Jeffery, 2020; Samadi-Ghadim et al., 2020; Takata et al., 2020; Henneco et al., 2021; Saio & Kurtz, 2022). Lanza et al. (2019) show that the Rossby waves may represent a source of confusion in the case of slowly rotating inactive stars that are preferential targets for a radial velocity planet search. Therefore, the theoretical description of stellar Rossby waves is important for stellar activity and exoplanetary research.

Rossby waves have been known as r modes in the stellar community since Papaloizou & Pringle (1978). Provost et al. (1981) made significant progress in the theoretical study of r modes in uniformly rotating stars by perturbation analysis (see also Damiani et al. (2020) for a similar topic of study). Saio (1982) examined the r-mode oscillations in the massive zero-age main sequence and ZZ Ceti stars. The studies generally concerned the slowly rotating stars, which allowed for perturbation analysis by a small expansion parameter for slow rotation (we note that Papaloizou & Pringle (1978) studied rapidly rotating stars, but for the high order harmonics of r modes). On the other hand, it is of vital importance to study the Rossby waves for stars with any rotation rate.

Here we aim to study the Rossby waves in stratified stellar interiors without approximation of slow rotation. We use the formalism of terrestrial Rossby waves, which has been well tested in Earth's atmosphere (e.g. Lindzen (1967)). The formalism allowed us to derive the exact solutions and dispersion relations for Rossby, Rossby-gravity, and inertia-gravity waves in rectangular equatorial beta-plane approximation. The periods of different harmonics can be used for observations of the waves in stellar light curves. In this paper, we are concerned with the radiative stars without an outer convection zone.

2. Governing equations

We started with linearised momentum, continuity, and energy equations in a frame of a uniformly rotating star:

$$\rho_0 \frac{\partial \vec{v}}{\partial t} + 2\rho_0 \vec{\Omega} \times \vec{v} = -\nabla p' + \rho' \vec{g}, \tag{11}$$

$$\frac{\partial \rho'}{\partial t} + (\vec{v} \cdot \nabla)\rho_0 + \rho_0 \nabla \cdot \vec{v} = 0, \tag{12}$$

$$\frac{\partial p'}{\partial t} + (\vec{v} \cdot \nabla) p_0 + \gamma p_0 \nabla \cdot \vec{v} = 0, \tag{13}$$

where $\vec{v}$ is the velocity, ρ_0 (p_0) is the unperturbed density (pressure), p' (ρ') is the perturbation of pressure (density), $\vec{g}$ is the gravitational acceleration, $\vec{\Omega}$ is the angular velocity of rotation, and $\gamma = c_p/c_v$ is the ratio of specific heats.

In the following, we adopt the Cartesian coordinates (x, y, z), where x is directed towards rotation, y is directed towards the north pole, and z is directed vertically upwards. An undisturbed medium was assumed to be in vertical hydrostatic balance

$$\frac{dp_0}{dz} = -g\rho_0 \tag{14}$$

and the ideal gas law is written as

$$p_0 = \frac{k_b}{m}\rho_0 T = g\rho_0 H, \tag{15}$$

where k_b is the Boltzman constant, $T(z)$ is the temperature, m is the mass of hydrogen atom, and $H(z) = k_b T(z)/mg$ is the density scale height. Then the substitution of Eq. (15) into Eq. (14) gives the vertical distribution of the density governed by the equation

$$\frac{d\rho_0}{dz} = -\frac{\rho_0}{H}\left(1 + \frac{dH}{dz}\right). \tag{16}$$

We closely followed to the formalism of Lindzen (1967), who considered the beta-plane approximation for the uniform temperature with depth. Our calculation, however, was performed for a non-uniform distribution of temperature with depth. Here we use the vertically hydrostatic assumption, which means that the vertical distribution of the pressure is only slightly disturbed from its static form as it is typical for geophysical and astrophysical flows with a small Rossby number. This means that the vertical velocity is small and it is neglected in the vertical momentum equation, while it is kept in the continuity equation. This approximation does not take internal gravity or acoustic waves into account and hence it is only valid for long-period waves.

We changed variables as

$$\tilde{v}_x = \sqrt{\rho_0} v_x, \tilde{v}_y = \sqrt{\rho_0} v_y, \tilde{v}_z = \sqrt{\rho_0} v_z, \tilde{p}' = \frac{p'}{\sqrt{\rho_0}}, \tilde{\rho}' = \frac{\rho'}{\sqrt{\rho_0}}, \tag{17}$$

so that Eqs. (11) - (13) could be written after the Fourier transform with $e^{i(-\sigma t + kx)}$ as

$$-i\sigma v_x - f v_y = -ikp', \tag{18}$$

$$-i\sigma v_y + f v_x = -\frac{\partial p'}{\partial y}, \tag{19}$$

$$\frac{\partial p'}{\partial z} - \frac{1}{2H}\left(1 + \frac{dH}{dz}\right) p' = -g\rho', \tag{20}$$

$$-i\sigma\rho' + ikv_x + \frac{\partial v_y}{\partial y} + \frac{\partial v_z}{\partial z} - \frac{1}{2H}\left(1 + \frac{dH}{dz}\right) v_z = 0, \tag{21}$$

$$i\sigma p' = i\gamma g H \sigma\rho' - g\left[1 - \gamma\left(1 + \frac{dH}{dz}\right)\right] v_z, \tag{22}$$

where $f = 2\Omega \sin\theta$ is the Coriolis parameter with θ being a latitude (we note that the tilde sign was not used for the variables). Due to the vertically hydrostatic assumption, the two terms $-i\sigma v_z$ and $-2\Omega_y v_x$ were omitted on the left-hand side of Eq. (20). The ratios of the omitted terms and the first term on the right-hand side of Eq. (20) are proportional to $\sigma^2 H/g$ and RH/λ^2, respectively, where R is the radius of the sphere and λ is the horizontal wavelength. The first ratio is very small for the Rossby wave timescales. The second ratio is proportional to $H/R \ll 1$ for the typical Rossby wavelengths. Hence, both terms are small and a vertically hydrostatic assumption is justified in the current consideration of Rossby-type waves.

Eqs. (18) and (19) lead to the equation

$$(f^2 - \sigma^2) v_y = i\sigma\left(\frac{k}{\sigma} f + \frac{\partial}{\partial y}\right) p'. \tag{23}$$

Eliminating ρ', v_z, and v_x from Eqs. (20)-(22), we obtain

$$\frac{\partial}{\partial z}\left[\frac{\gamma H}{1 - \gamma(1 + H')} \frac{\partial p'}{\partial z}\right] -$$

$$-\left[\frac{gk^2}{\sigma^2} + \frac{\gamma(1 + H')^2}{4H[1 - \gamma(1 + H')]} - \frac{\gamma H''}{2[1 - \gamma(1 + H')]^2}\right] p' +$$

$$+\frac{ig}{\sigma}\left[\frac{\partial}{\partial y} - \frac{k}{\sigma} f\right] v_y = 0, \tag{24}$$

where H' means the derivative of H by z.

We eliminated p' from Eqs. (23)-(24) and derived the single equation for v_y:

$$\frac{\partial}{\partial z}\left[\frac{\gamma H}{1 - \gamma(1 + H')} \frac{\partial v_y}{\partial z}\right] -$$

$$-\left[\frac{\gamma(1+H')^2}{4H[1-\gamma(1+H')]}-\frac{\gamma H''}{2[1-\gamma(1+H')]^2}\right]v_y-$$

$$-\frac{g}{f^2-\sigma^2}\left(\frac{\partial^2}{\partial y^2}-k^2-\frac{k}{\sigma}\frac{df}{dy}\right)v_y=0. \tag{25}$$

This equation can be solved by the separation of variables in appropriate boundary conditions. Here we note that the separation of variables is only possible in the case of a vertically hydrostatic assumption.

We represent v_y as

$$v_y = V(z)\Psi(y) \tag{26}$$

and after straightforward calculations with the separation constant $-h^{-1}$ we derived the two equations

$$\frac{\partial^2\Psi}{\partial y^2}+\left[\frac{\sigma^2-f^2}{gh}-k^2-\frac{k}{\sigma}\frac{df}{dy}\right]\Psi=0, \tag{27}$$

$$\frac{\partial}{\partial z}\left[\frac{\gamma H}{1-\gamma(1+H')}\frac{\partial}{\partial z}\right]V(z)-$$

$$-\left[\frac{\gamma(1+H')^2}{4H[1-\gamma(1+H')]}-\frac{\gamma H''}{2[1-\gamma(1+H')]^2}+\frac{1}{h}\right]V(z)=0. \tag{28}$$

Here Eq. (27) and Eq. (28) are the latitudinal and vertical equations governing the latitudinal and vertical structures of the waves, respectively. In fact, Eq. (27) is equivalent to the equation that governs shallow water equatorially trapped waves in a homogeneous layer with the width of h (e.g. Matsuno (1966)). This conclusion corresponds to the Taylor theorem (Taylor, 1936), which states that the dynamics of Rossby waves in stratified fluids is identical to the waves in a homogeneous layer that has a width of equivalent depth. The equivalent depth is different for different modes of Rossby waves. The theorem is valid for all compressible and stratified fluids (Pedlosky (1987); Zaqarashvili et al. (2021)). We first solved Eq. (28) in appropriate surface boundary conditions and found the equivalent depth, h. Then we used it to solve Eq. (27) and found the solutions in the y direction, satisfying bounded boundary conditions at poles. It should be noted that the value of equivalent depth, h, found from Eq. (28) defines the solutions of Eq. (27); therefore, the two equations are not independent, but interconnected by h.

Before starting to study the case of inhomogeneous distribution of temperature with depth, we present the solutions of the simplest case of uniform H, which

means an isothermal temperature profile. This is a very simplified approach, but it gives the basic physics of oscillations.

With $H = const$, Eq. (28) leads to

$$\frac{\partial^2 V(z)}{\partial z^2} - \left[\frac{1}{4H^2} - \frac{\kappa}{Hh}\right] V(z) = 0, \tag{29}$$

where $\kappa = (\gamma - 1)/\gamma$.

The solution of Eq. (29) involves either exponential or periodic functions depending on the value of the equivalent depth, h. We considered the exponential function for the close boundary condition v_z=0 at the surface, which corresponds to $z = 0$. The value for the scale height depends on the surface temperature. The surface temperature of 10 000 K gives $H = 300$ km and the corresponding equivalent depth found from the close boundary condition is $h \approx 500$ km.

The equivalent depth can be used to solve the latitudinal equation, Eq. (27). The solutions of Eq. (27) must satisfy boundary conditions in y directions, namely they must exponentially vanish at poles. Only the equivalent depth that satisfies the polar boundary conditions can be considered to be valid. The solution of the latitudinal equation for $h = 500$ km does not satisfy boundary conditions at poles; therefore, the exponential solution of Eq. (29) is not valid. The periodic solution of Eq. (29) leads to the value of equivalent depth, which satisfies the polar boundary conditions, but it corresponds to very high vertical wavenumber values.

When the temperature is a function of depth (generally increasing), then its gradient governs the state of the medium, which could be adiabatic, radiative, or convective. The Ledoux function, A, which defines the state, can be written using Eqs. (14)-(16) in terms of the density scale height as

$$A = \frac{R}{\rho_0}\frac{d\rho_0}{dz} - \frac{R}{\gamma p_0}\frac{dp_0}{dz} = -\frac{R}{H}\left(\frac{\gamma - 1}{\gamma} + \frac{dH}{dz}\right). \tag{30}$$

When $|dH/dz| = |H'| > (\gamma - 1)/\gamma$, that is $A > 0$, the temperature gradient is super-adiabatic and corresponds to convective stars. When $|H'| < (\gamma - 1)/\gamma$, in other words $A < 0$, the temperature gradient is sub-adiabatic, hence it corresponds to radiative stars. When $A = 0$, that is to say $|H'| = \kappa = (\gamma - 1)/\gamma = 2/5$, the star is neutrally stable so that the temperature gradient is adiabatic, which is a limiting case of super- and sub-adiabatic gradients. In this paper, we consider radiative stars; therefore, the condition of $|H'| < \kappa$ should be satisfied everywhere. This condition is most easily satisfied for the linear profile of temperature with a uniform vertical gradient. For other profiles, the vertical temperature gradient

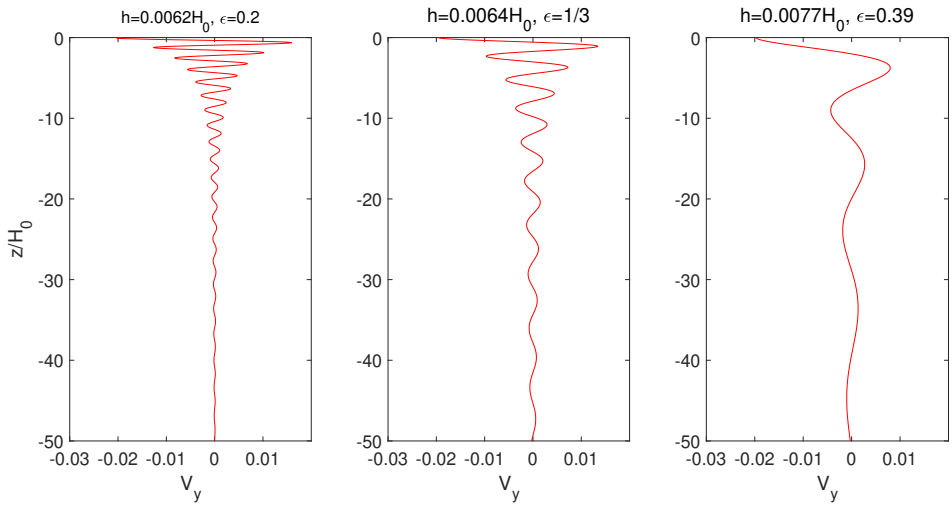

Figure 6: Vertical structure of Rossby waves for different vertical temperature gradients: $\epsilon = 0.2$ (left panel), $\epsilon = 1/3$ (middle panel), and $\epsilon = 0.39$ (right panel). Here v_y is plotted without $\sqrt{\rho_0}$ in Eq. (17) and normalised by ΩR.

generally increases with depth, which unavoidably leads to the violation of the radiative condition at some distance from the surface. Therefore, we assumed that the density scale height is a linear function of depth (readers should remember that $z > 0$ above the surface and $z < 0$ below the surface), that is

$$H = H_0 - \epsilon z. \tag{31}$$

This is equivalent to the temperature profile of the form

$$T = T_0 \left(1 - \epsilon \frac{z}{H_0}\right), \tag{32}$$

where T_0 is the temperature at the surface, $z = 0$. In this case, the radiative stars imply $\epsilon < \kappa$ and we use this criterion throughout the paper.

3. Free oscillations of radiative stars

We started to study free oscillations, meaning that we first solved the vertical structure equation (28) in corresponding boundary conditions. The solutions of the equation govern the spatial structure of Rossby waves along the vertical direction. The boundary conditions allowed us to find the discrete values of equivalent depth h. Then we used h to find latitudinal solutions of Eq. (27), which exponentially tend to zero at poles. These solutions correspond to the latitudinal structure of Rossby waves.

3.1 Vertical structure of Rossby waves

For the linear temperature profile, Eq. (28) is rewritten as

$$\frac{\partial}{\partial z}\left[\frac{\gamma H}{1-\gamma(1+H')}\frac{\partial}{\partial z}\right]V(z) - \left[\frac{\gamma(1+H')^2}{4H[1-\gamma(1+H')]} + \frac{1}{h}\right]V(z) = 0, \tag{33}$$

where $H' = dH/dz$. Using the new variable

$$x = 2\sqrt{H_0 - \epsilon z}\frac{\sqrt{\gamma(1-\epsilon)-1}}{\epsilon\sqrt{\gamma h}}, \tag{34}$$

Eq. (33) leads to

$$x^2\frac{\partial^2 V(x)}{\partial x^2} + x\frac{\partial V(x)}{\partial x} + (x^2 - n^2)V(x) = 0, \tag{35}$$

where $n = (1-\epsilon)/\epsilon$. This is the Bessel equation and its solutions are Bessel functions of order n, $J_n(x)$, and $Y_n(x)$. The solutions $J_n(x)$ and $Y_n(x)$ must satisfy certain boundary conditions at the surface. We used two different boundary conditions. The first condition yields the vertical velocity vanishing at the surface, that is $v_z = 0$ at $z = 0$, which is a close condition. The second condition yields the total Lagrangian pressure being zero at the surface, which is a free boundary condition. In both cases, vertical velocity and total pressure must be bounded towards the stellar centre.

We used different values of ϵ to find the vertical structure of Rossby waves for different vertical temperature gradients. We assumed $\epsilon = 0.2, 1/3, 0.39$, which give the order of Bessel functions as $n = 4, 2, 1.56$, respectively. We note that the adiabatic temperature gradient corresponds to $\epsilon = 0.4$, and therefore $\epsilon = 0.39$ is nearly the upper limit of the radiative temperature gradient.

3.1.1 Close boundary condition, v_z=0, at the surface

The close boundary condition, v_z=0, from Eqs. (20)-(23) yields the following equation:

$$\frac{\partial v_y}{\partial z} + \left[\frac{1}{\gamma H} - \frac{1}{2H} - \frac{H'}{2H}\right]v_y = 0. \tag{36}$$

Both solutions of Eq. (35), $J_n(x)$ and $Y_n(x)$, have similar vertical structures to the modes. Therefore, we considered $J_n(x)$ to be a solution and then Eq. (36) was

rewritten as

$$\frac{\partial}{\partial x} J_n(x) + \frac{1}{x}\left[\frac{1}{\epsilon} - 1 - \frac{2}{\gamma\epsilon}\right] J_n(x) = 0. \tag{37}$$

This is a transcendental equation, which has an infinite number of zeros. Each zero defines a certain value of equivalent depth, h, hence it corresponds to a certain wave mode. We first solved the equation for $\epsilon = 1/3$ and, for the first six zeros, we obtained the values of equivalent depth as $h \approx 1.05\,H_0$, $h \approx 0.058\,H_0$, $h \approx 0.025\,H_0$, $h \approx 0.014\,H_0$, $h \approx 0.009\,H_0$, and $h \approx 0.0064\,H_0$, respectively. As we mentioned above, only the values of equivalent depth (or wave modes), which result in the bounded conditions at poles, are valid. Solutions of the latitudinal equation (see the next subsection) show that the modes corresponding to the first five zeroes do not satisfy polar boundary conditions and hence they are not valid. On the other hand, the modes corresponding to the sixth (and larger) zero satisfy bounded conditions at poles. The solutions of Eq. (37) for the temperature gradient of $\epsilon = 0.39$ show that the mode, which corresponds to the second zero of the equation, already satisfies the polar boundary conditions. Therefore, all modes starting from the second mode in the vertical direction are valid for a nearly adiabatic temperature gradient. On the other hand, the temperature gradient of $\epsilon = 0.2$ yields the 17th and higher modes giving the bounded polar boundary conditions. Figure 6 shows the vertical structure of Rossby waves based on the solutions of Eq. (35) for different values of ϵ. We see that all solutions exponentially decrease with depth, hence the corresponding modes are trapped near the surface. All higher modes show a similar behaviour. The figure shows that the smaller values of ϵ, that is the smaller temperature gradient, yield the shorter vertical wavelength of Rossby waves and the stronger decay of the wave amplitude with depth. Therefore, the Rossby waves tend to be concentrated closer to the surface for a smaller temperature gradient.

3.1.2. Free boundary condition

In the free surface condition, the total Lagrangian pressure is zero at the surface. Using Eqs. (20) and (22), the condition is

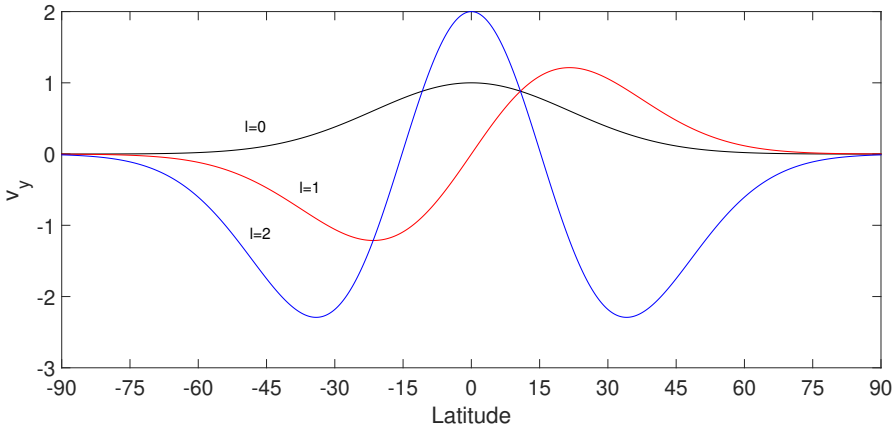

Figure 7: Latitudinal structure of equatorially trapped Rossby waves for the temperature gradient of $\epsilon = 1/3$ and the value of equivalent depth $\approx 0.0064 H_0$. The solutions exponentially decay towards poles above middle latitudes. Black, red, and blue curves show $l = 0$, $l = 1$, and $l = 2$ modes, respectively.

$$\frac{\partial v_y}{\partial z} + \frac{1}{H}\frac{3(1-\epsilon)}{2} v_y = 0, \tag{38}$$

which can be rewritten for the new variable x as

$$\frac{\partial J_n(x)}{\partial x} - \frac{1}{x}\frac{3(1-\epsilon)}{\epsilon} J_n(x) = 0. \tag{39}$$

This is also a transcendental equation and has an infinite number of zeros. We assumed $\epsilon = 1/3$ and for the first five zeroes we found $h \approx 0.069\, H_0$, $h \approx 0.027\, H_0$, $h \approx 0.015\, H_0$, $h \approx 0.0094\, H_0$, and $h \approx 0.0065\, H_0$, respectively. Only the modes corresponding to the fifth (and higher) zero satisfy the polar boundary conditions.

The value of h obtained from each zero with a free condition is similar to the value obtained from the next higher zero with a close condition. For example, the first zero with a free condition is near to the second zero with a close condition, etc. This happens because of the relation between the total Lagrangian pressure and vertical velocity. Therefore, close and free boundary conditions result in a similar spatial structure with a depth of the corresponding modes. Consequently, we only consider the closed boundary condition in the rest of the paper.

3.2. Latitudinal structure of Rossby waves

We now turn to the latitudinal equation (Eq. (27)) and find the solutions with

certain h satisfying bounded conditions at poles, which define dispersion relations of possible wave modes in the system. The solutions of Eq. (27) crucially depend on the parameter

$$\varepsilon = \frac{4\Omega^2 R^2}{gh}, \tag{40}$$

which actually corresponds to the parameter (sometimes referred to as the Lamb parameter) governing the dynamics of shallow water system of the layer thickness h. When this parameter is much larger than one (for fast rotation or small h), then Eq. (27) is most easily satisfied for small y. [1] Small y is equivalent to the equatorial region and hence the solutions are equatorially trapped. Third and higher zeroes with a close boundary condition with $h < 0.025\, H_0$ lead to the Lamb parameter of $\varepsilon > 10$ for solar radius, surface temperature, and rotation. Therefore, the modes corresponding to the higher zeroes with a close boundary condition are confined near the equatorial regions and decay sufficiently fast towards the poles. The modes, hence, can be considered by the equatorial beta-plane approximation, which would mean expanding the Coriolis parameter near the equator $\theta \approx 0$ and retaining only the first order term, $f = \beta y$, where $\beta = (2\Omega/R)$. In this case Eq. (27) tends to

$$\frac{\partial^2 \Psi}{\partial y^2} + \left[-\frac{k\beta}{\sigma} - k^2 + \frac{\sigma^2}{c^2} - \frac{\beta^2 y^2}{c^2} \right] \Psi = 0, \tag{41}$$

where $c = \sqrt{gh}$ is the surface gravity speed for corresponding equivalent depth h, which was obtained from the vertical structure equation as shown in the previous subsections.

It must be noted that the solutions under equatorial beta-plane approximation fairly correspond to the solutions of the spherical case. In fact, the governing equation of equatorially trapped Rossby waves in beta-plane approximation is identical to the spherical case Longuet-Higgins (1968); Zaqarashvili et al. (2021). Here we consider only the equatorially trapped waves for which the beta-plane approximation is justified.

Eq. (41) is a parabolic cylinder equation which has bounded solutions when

$$-\frac{k\beta}{\sigma} - k^2 + \frac{\sigma^2}{c^2} = \frac{\beta}{c}(2l + 1), \tag{42}$$

[1] see e.g. Longuet-Higgins (1968) for the similar topic of study in the spherical geometry.

where $l = 0, 1, 2, 3....$ Then the solution to this equation is

$$\Psi = \Psi_0 exp\left[-\frac{\beta}{2c}y^2\right] H_l\left(\sqrt{\frac{\beta}{c}}y\right), \tag{43}$$

where Ψ_0 is the value of v_y at the equator, $y = 0$, and H_l is the Hermite polynomial of the order l. The solution is oscillatory inside the interval $y < |\sqrt{(2l+1)c/\beta}| = |\sqrt{(2l+1)R^2/\sqrt{\varepsilon}}|$ and exponentially decreases towards poles outside. Smaller h or larger ε yields a stronger decrease in the solution. As it was discussed above, the values of h corresponding to the lower zeroes of Eqs. (37) and (39) lead to solutions which are not bounded at poles. The bounded solutions in the case of $\epsilon = 1/3$, which are shown in Figure 7, start to appear for the sixth (fifth) zero with a close (free) boundary condition, which yields $h \approx 0.0064\, H_0$. In this case, the Lamb parameter is around $\varepsilon \approx 43$ for the solar radius, surface temperature, and rotation. The temperature gradient of $\epsilon = 0.39$ allows for the second (and higher) zero with a close vertical boundary condition to lead to the bounded solution along latitudes. The critical latitude was estimated as $\theta_c = \arcsin\left(\sqrt{(2l+1)/\sqrt{\varepsilon}}\right)$, which for $l = 1$ modes gives around $\pm 40^0$, that is the solutions are oscillatory in the latitudes of $< 40^0$ and exponentially decay for $> 40^0$. Therefore, the solutions are mostly concentrated between the latitudes $\pm 60^0$ and are negligible at poles satisfying the boundary conditions there.

3.3. Dispersion equation

Eq. (42) defines the dispersion relation of waves

$$\sigma^3 - 4\Omega^2\left(\frac{k^2R^2}{\varepsilon} + \frac{2l+1}{\sqrt{\varepsilon}}\right)\sigma - 8\Omega^3\frac{kR}{\varepsilon} = 0. \tag{44}$$

This equation is identical to the dispersion relation of shallow water waves when the width of the shallow layer is replaced by the equivalent depth, h, as stated by the Taylor theorem. The dispersion relation governs the inertia-gravity, Rossby, and Rossby-gravity waves for each h.

For the high frequency limit ($\sigma \gg \Omega$) with $l \geq 1$, we have the dispersion relation

$$\sigma = \pm 2\Omega\sqrt{\frac{k^2R^2}{\varepsilon} + \frac{2l+1}{\sqrt{\varepsilon}}}, \tag{45}$$

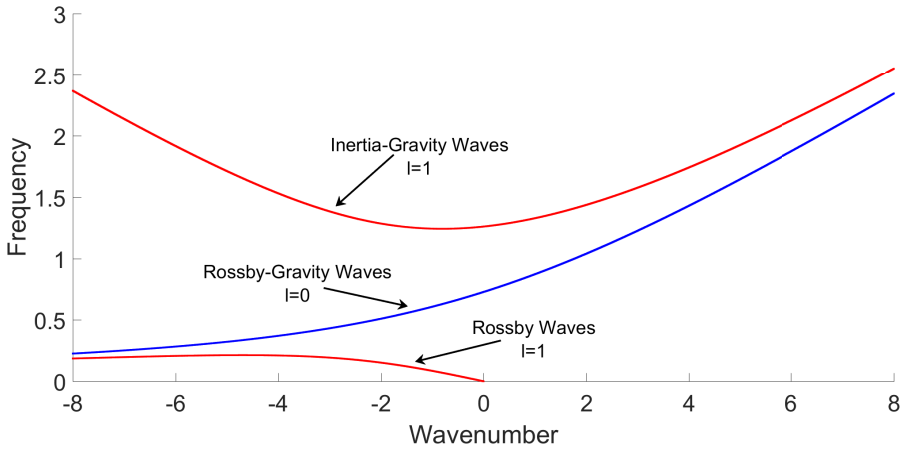

Figure 8: Solutions of the full dispersion equation (Eq. (44)) for $\varepsilon = 43$, which corresponds to the first valid vertical mode (with $h = 0.0064H_0$) in a star with the rotation, radius, and surface gravity of the Sun and the temperature gradient of $\epsilon = 1/3$. Red curves correspond to the inertia-gravity (upper) and Rossby (lower) waves with $l = 1$. The blue curve corresponds to the Rossby-gravity waves with $l = 0$. Wave frequency was normalised by the angular frequency of the star, Ω. The toroidal wavenumber, k, was normalised by the stellar radius, R.

which corresponds to the inertia-gravity waves.

For the low frequency limit ($\sigma \ll \Omega$) with $l \geq 1$, we have the dispersion relation

$$\sigma = -2\Omega \frac{kR}{k^2R^2 + (2l+1)\sqrt{\varepsilon}}, \tag{46}$$

which corresponds to the Rossby waves.

For $l = 0$, Eq. (44) leads to

$$\left(\sigma - 2\Omega\frac{kR}{\sqrt{\varepsilon}}\right)\left(\sigma^2 - 2\Omega\frac{kR}{\sqrt{\varepsilon}}\sigma - \frac{4\Omega^2}{\sqrt{\varepsilon}}\right) = 0. \tag{47}$$

The first solution of Eq. (46) is spurious; therefore, it must be neglected and the second solution defines the Rossby-gravity wave

$$\sigma = \Omega\frac{kR}{\sqrt{\varepsilon}}\left(1 \pm \sqrt{1 + \frac{4\sqrt{\varepsilon}}{k^2R^2}}\right). \tag{48}$$

The solutions of full dispersion equation (Eq. (44)) are displayed in Figure 8 for $\varepsilon = 43$, which corresponds to the equivalent depth, $h \approx 0.0064\, H_0$ (associated with the first valid vertical mode or the sixth zero with a close condition for the temperature gradient of $\epsilon = 1/3$) and a star with the rotation, radius, and surface

gravity of the Sun. We see that for large negative k, the dispersion curves of Rossby and Rossby-gravity waves merge, while for the large positive k the inertia-gravity and Rossby-gravity waves have the same behaviour. In the next subsection, we consider Rossby and Rossby-gravity waves in detail.

3.4. Rossby and Rossby-gravity waves

Eq. (46) is the dispersion relation for the Rossby waves on the equatorial beta plane. The positive frequency and the negative toroidal wavenumber indicate the retrograde (opposite to the rotation) propagation of waves. The dispersion relation crucially depends on the parameter ε. When this parameter is small (that is for slowly rotating stars or large equivalent depth, h), then the second term in denominator is smaller than the first one, which eventually leads to the dispersion relation of Rossby waves on the 2D surface with only longitudinal propagation ($k_y = 0$). This corresponds to sectoral harmonics in the spherical geometry. But a moderate value of the parameter significantly changes the dispersion relation of Rossby waves. In the considered case, this parameter has a moderate value due to the small h. For a star with solar parameters, that is $T_0 = 5770$ K, $\Omega = 3 \times 10^{-6}$ s^{-1}, $R = 7 \times 10^5$ km, and $h = 0.0064\, H_0$ km as estimated in the previous subsection, one can find that $\varepsilon \approx 43$. Therefore, one must keep the associated term in the dispersion relation. One should note that the parameter ε is equivalent to the parameter used by Provost et al. (1981) to study the r modes in slowly rotating stars, namely $\Omega^2 R^3/(GM)$, if one replaces h by R and divides by four. Provost et al. (1981) expanded all variables and the frequency with this parameter assuming it to be much smaller than unity. This could be correct if the equivalent depth, h, is of the order of the stellar radius. But our solution shows that $h \ll R$, that is the expansion parameter of Provost et al. (1981) is not small and cannot be appropriate in our consideration.

Rossby-gravity waves ($l = 0$) defined by Eq. (48) have mixed properties of Rossby and inertia-gravity waves. This mode is similar to Rossby waves when it propagates opposite to the rotation, but it is similar to the gravity wave when it propagates to the direction of the rotation. The wave has no oscillatory solution along latitudes and hence it corresponds to the sectoral modes in the spherical geometry.

4. Observational constraints

It is of importance to show how the theoretically obtained waves might be seen by observations. Recent progress in observations of Rossby waves using Kepler light curves suggest that the waves can also be detected in the data of the TESS mission. Here we provide hints for observers to detect the waves.

We used the rotating frame for the theoretical analysis of Rossby waves. On the other hand, observed light curves were obtained in the inertial frame; therefore, the observable frequency of the waves is expressed by

$$\sigma_{obs} = m\Omega + \sigma, \tag{49}$$

where σ is the theoretical wave frequency in the rotating frame and $m = kR$ is the normalised toroidal wavenumber.

Wave frequency depends on the parameter ε, which can be rewritten as

$$\varepsilon = 0.3 \left(\frac{h}{H_0}\right)^{-1} \left(\frac{T_0}{T_{sun}}\right)^{-1} \left(\frac{\Omega}{\Omega_{sun}}\right)^{2} \left(\frac{R}{R_{sun}}\right)^{2}, \tag{50}$$

where T_0 (T_{sun}), Ω (Ω_{sun}), and R (R_{sun}) are the surface temperature, the surface angular velocity, and the radius of a star (the Sun), respectively.

Figure 9 shows the dependence of the wave frequency in the inertial frame, σ_{obs} on ε. Only the frequency of lower order modes $m = 1$ and $m = 2$ are shown on this figure. The normalised frequencies of all modes (Rossby, Rossby-gravity, inertia-gravity) are increasing for higher ε, that is for the higher angular velocity of stars (with the same surface temperature and radius). The anti-symmetric harmonics with regards to the equator, $l = 1, 3...$, probably have negligible contributions to stellar light curves as the northern and southern parts of the modes cancel each other out.[2] Therefore, only symmetric harmonics, $l = 0, 2, 4$, are shown on this figure. Rossby waves with $m = 1$ have a frequency in the range of $0.65\,\Omega < \sigma_{obs} < \Omega$, that is less than the stellar angular velocity. The frequency of Rossby waves with $m = 2$ is in the range of $1.4\,\Omega < \sigma_{obs} < 2\Omega$. Inertia-gravity and Rossby-gravity waves have an order of magnitude higher frequencies than the angular velocity of stellar rotation. Observations can define the frequency of observed waves, which subsequently determine the corresponding value of ε using Figure 9. It is important to note that ε depends on the equivalent depth, h, and three

[2]This applies to stars whose rotation axes are perpendicular to the line of sight. For the stars with inclined rotation axes, the situation is more complicated.

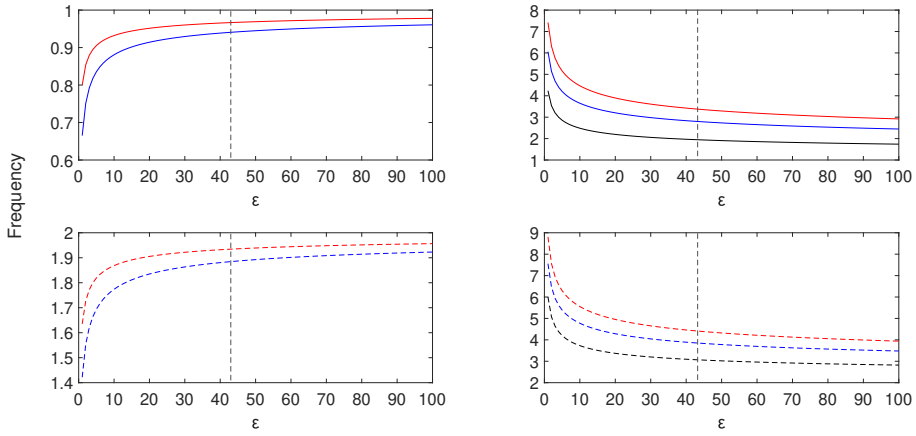

Figure 9: Wave frequency in the inertial frame as expected to be seen by observations vs ε. The frequency was normalised by the angular frequency of a star, Ω. Black, blue, and red curves correspond to the modes with $l = 0$, $l = 2$, and $l = 4$, respectively. The left panels display the Rossby modes with $m = 1$ (solid lines, upper panel) and $m = 2$ (dashed lines, lower panel). The upper (lower) right panel shows inertia-Gravity modes (Rossby-gravity modes). Grey dashed lines denote the value of ε calculated for the solar parameters and the equivalent depth of $h = 0.0064\, H_0$.

stellar parameters such as the surface temperature, the surface angular velocity, and the radius. The equivalent depth is calculated from the Rossby wave theory as discussed in the subsection 3.1. Consequently, if one knows two of the stellar parameters, one can estimate the value of the third one.

5. Discussion and conclusions

Rossby waves arise due to the conservation of absolute vorticity; therefore, vorticity is an essential ingredient of the waves. On the other hand, pressure variation is an equally important component in the waves. Therefore, the waves cause the periodic variations of surface pressure (temperature or density or both), which may lead to the periodical modulation of stellar radiance (Saio et al., 2018). Recent observations of Rossby waves in the light curves of Kepler and TESS stars (Saio et al., 2018; Li et al., 2019; Jeffery, 2020; Samadi-Ghadim et al., 2020; Takata et al., 2020; Henneco et al., 2021; Saio & Kurtz, 2022) have opened a new area for seismology of stellar interiors by the waves.

It is important to know the oscillation spectrum of the modes and how much deeper the modes penetrate in the stellar interior. Solving the full spherical 3D problem is generally also complicated with numerical simulations. In this paper,

we look into a more simplified rectangular problem taking into account the vertical stratification of density and temperature in stellar interiors. The rectangular geometry significantly simplifies the finding of wave dispersion relations, which are similar to those obtained under spherical geometry (Matsuno, 1966; Longuet-Higgins, 1968). Previous theoretical studies generally considered the spherical geometry in a slowly rotating limit (Provost et al., 1981; Saio, 1982; Damiani et al., 2020). Though the approximation of Papaloizou & Pringle (1978) includes rapidly rotating stars, it is valid for only higher order modes. On the other hand, our approximation is valid for stars with any rotation rate (except very rapidly rotating stars with significant distortion from the spherical symmetry); therefore, it is step forward in the study of stellar Rossby waves. Our mathematical formalism closely follows the consideration adapted in Earth's atmosphere Lindzen (1967). We considered the vertically hydrostatic assumption, so that the vertical distribution of the pressure is only slightly disturbed from its static form due to the waves. This approximation neglects the internal gravity and acoustic waves, hence it is valid for time and spatial scales of Rossby waves. For linear dynamics of the waves, we derived a single second-order partial differential equation for vertical and latitudinal variations, which was solved by the method of separation of variables. The two equations for the vertical and the latitudinal variations were obtained, which are connected by the separation constant defining the equivalent depth h.[3] The solutions of the two equations that satisfy certain boundary conditions give the exact analytical dispersion relations and the vertical structure of the waves in a certain distribution of background values.

The vertical structure of wave modes obviously depends on the vertical temperature profile. The super-adiabatic temperature gradient (positive Ledoux function, $A > 0$) corresponds to convective stars, while the sub-adiabatic gradient (negative Ledoux function, $A < 0$) describes the radiative stars. The limiting case from both gradients, that is $A = 0$, is the adiabatic temperature gradient, which fits the neutrally stable interior, where any plasma displacement in the vertical direction has no following dynamics. In this paper, we consider only radiative stars with the linear sub-adiabatic temperature gradient. [4] Other profiles of temperature lead the Ledoux function to change from a negative to positive value at some depth; therefore, they are inappropriate for the radiative stars. In the case of the linear

[3]We note that the relation between the separation constant and the wave frequency obtained from the solution of the latitudinal equations was studied by Townsend (2003).

[4]Convective stars with a near super-adiabatic temperature gradient will be studied in a forthcoming paper.

temperature profile, the vertical structure equation is transformed into the Bessel equation, which has exact analytical solutions in terms of Bessel functions.

To solve the latitudinal equation, we used the equatorial beta-plane approximation, which resulted in a parabolic cylinder equation with known solutions in terms of Hermite polynomials. Any solution on the equatorial beta plane, which decays sufficiently quickly towards the coordinate corresponding to the pole, is a correct approximation to the solutions on a sphere (Lindzen, 1967). Indeed, the governing equation and the dispersion relation of equatorially trapped waves are identical in the equatorial beta plane and spherical geometry (Longuet-Higgins, 1968; Zaqarashvili et al., 2021). Hence, the beta plane approximation is valid for the solutions decaying towards the poles. The solutions satisfy bounded boundary conditions at poles define the dispersion equation for Rossby, Rossby-gravity, and inertia-gravity waves, Eq. (44). Frequencies of modes with different wave numbers were then easily derived.

The solutions to the problem significantly depend on the boundary conditions for the vertical and latitudinal structure equations. We first solved the vertical structure equation in a close boundary condition at the surface (i.e. when the vertical velocity vanishes), which led to the equivalent depth, h. Then we used the depth to find the solutions of the latitudinal equation, which satisfied the bounded conditions at the poles.

Close boundary conditions at the surface led to the transcendental equation with Bessel functions (Eq. 37), which has an infinite number of zeroes corresponding to different wave modes. Each of the zeroes define the equivalent depth, which shapes the latitudinal structure of modes, and therefore only the modes that have bounded solutions at poles are valid. We found that the first valid zero yields the equivalent depth of $h = 0.0064\,H_0$ for the vertical temperature gradient of $\epsilon = 1/3$, where H_0 is the density scale height at the surface. In this case, the modes with $l = 0, 1, 2$, where l shows the number of zeroes between the poles, are concentrated around the equator between $\pm 60^0$ latitudes (see Fig. 2), so they are the equatorially trapped waves (Matsuno, 1966; Longuet-Higgins, 1968). The modes have oscillatory behavior along the vertical direction with the wavelength of several surface scale heights (see middle panel on Figure 1) and may penetrate to the depth of $\sim 50\,H_0$ (the scale height of a star with the surface temperature of 10 000 K and solar-type surface gravity is around 300 km). The vertical structure of modes significantly depends on the vertical temperature gradient rate. We found that the vertical wavelength of modes is longer for the stronger temperature

gradient (Figure 1) being of the order of density scale height for $\epsilon = 0.2$ and of the order of 10 density scale height for $\epsilon = 0.39$. Figure 1 also shows that the smaller temperature gradient leads to a stronger reduction in oscillation amplitude with depth, so that the waves are more concentrated near the surface. Generally, it is seen that the modes are confined near the surface layer of ~ 15 Mm. The dispersion equation is similar to that of equatorially trapped waves with $\varepsilon \gg 1$. The observable frequencies of the Rossby waves with $m = 1$ and $m = 2$ are in the range of $0.65\,\Omega < \sigma_{obs} < \Omega$ and $1.4\,\Omega < \sigma_{obs} < 2\Omega$, respectively, which depends on the stellar rotation, radius, and surface temperature (see Figure 4). Inertia-gravity and Rossby-gravity modes may have the observable frequency in the interval of $5\,\Omega < \sigma_{obs} < 20\,\Omega$.

Non-spherical distortion of a rotating star may influence the frequencies and the spatial structures of Rossby waves. We shall estimate the influence of non-sphericity from the analysis of Provost et al. (1981). They expanded all physical quantities in the small parameter $(\Omega/\Omega_g)^2$, where $\Omega_g = \sqrt{GM/R^3}$ is the characteristic frequency of the star. Consequently, they assumed the frequency of Rossby waves to be $\sigma = \sigma_0(1 + (\Omega/\Omega_g)^2\sigma_1)$, where σ_0 is the frequency of 2D classical Rossby waves and σ_1 is the first order frequency. Therefore, the correction due to the 3D consideration and non-spherical distortion is $(\Omega/\Omega_g)^2\sigma_1$. The value of $(\Omega/\Omega_g)^2$ is $\approx 1.7 \cdot 10^{-5}$ for a star with a solar radius, mass, and angular frequency, while it is $\approx 1.7 \cdot 10^{-3}$ for a star with the rotation that is ten times faster (i.e. with the period of 2.6 days). On the other hand, the largest frequency correction for radiative stars according to Provost et al. (1981) is $\sigma_1 = -1.121$, which corresponds to the mode with $n = 3$, $l = 3$, $m = 1$, and $k = 4$, where n is the polytropic index, l and m are the latitudinal and azimuthal numbers, respectively, and k is the number of radial nodes (see the fifth row of the first column in the table 1 of Provost et al. (1981)). Consequently, typical maximal correction of the 2D Rossby wave frequency due to the non-spherical distortion is $2 \cdot 10^{-5}$ for a slowly rotating star such as the Sun, and $2 \cdot 10^{-3}$ for a rapidly rotating star with a period of 2.6 days. Hence, the correction due to the non-spherical distortion is negligible in most cases. The situation can be changed for very rapidly rotating stars with a period of < 0.1 days. Therefore, our analysis may not be valid for these extreme cases.

It is known that the magnetic field has a significant influence on the dynamics of Rossby waves (Zaqarashvili et al., 2007; Márquez-Artavia et al., 2017; Zaqarashvili, 2018; Dikpati et al., 2018, 2020; Zaqarashvili et al., 2021). Therefore, the observed frequency of Rossby waves and their temporal variations might be

used for seismic estimations of the magnetic field strength near the surface and in the interiors of stars (Gurgenashvili et al., 2016; Zaqarashvili et al., 2021; Gurgenashvili et al., 2022). But a more thorough study (observational and theoretical) is surely required in that vein in the future.

To obtain the dispersion relations and vertical structure of Rossby waves, we considered the uniform rotation of stars. On the other hand, latitudinal differential rotation may lead to large-scale instabilities on stars (Watson, 1981; Gilman & Fox, 1997; Gilman et al., 2007), which may also lead to an instability and frequency modification of Rossby waves (Zaqarashvili et al., 2010; Gizon et al., 2020, 2021). Therefore, the inclusion of the latitudinal differential rotation in the consideration is desired in the future.

One can argue that anti-symmetric modes (with odd l) slightly contribute to stellar light curves as the southern and northern hemispheric parts of radiance may balance each other. This effect is unimportant for stars with a rotation axis being nearly parallel to the line of sight. Therefore, in most stars one can expect to observe only the symmetric modes with even l.

As it was discussed above, the rate of temperature gradient ϵ determines the equivalent depth, h, and hence defines the vertical structure and frequency of modes. On the other hand, systematic observations of wave frequency may lead to the estimation ε. Then one can determine the equivalent depth of the corresponding mode and hence roughly estimate the vertical temperature gradient in stellar interiors. This might be a useful tool for stellar seismology.

Considering the equatorial beta-plane approximation and linear vertical gradient of the temperature in the interior of radiative stars led to the exact analytical solutions for Rossby and inertia-gravity waves. Oscillation spectra and the radial structure of the waves with different wavenumbers were obtained. The waves may affect the light curves of stars; therefore, they could be further observed by recent space missions. The observed Rossby waves may be used for the seismology of stars with different spectral classes being at different evolutionary phases.

2.2 Paper II: Equatorially trapped Rossby waves in radiative stars

M. Albekioni, T.V. Zaqarashvili, V. Kukhianidze, E. Gurgenashvili, P. Bourdin, Astronomical Notes, 344, 10

doi: https://doi.org/10.1002/asna.20230083

Contribution: M. Albekioni contributed to solving the problem analytically as well as modeling the results numerically. She provided the main scientific interpretation.

Abstract

Observations by recent space missions reported the detection of Rossby waves (r-modes) in light curves of many stars (mostly A, B, and F spectral types) with outer radiative envelope. This paper aims to study the theoretical dynamics of Rossby-type waves in such stars. Hydrodynamic equations in a rotating frame were split into horizontal and vertical parts connected by a separation constant (or an equivalent depth). Vertical equations were solved analytically for a linear temperature profile and the equivalent depth was derived through free surface boundary condition. It is found that the vertical modes are concentrated in the near-surface layer with a thickness of several tens of surface density scale height. Then with the equivalent width, horizontal structure equations were solved, and the corresponding dispersion relation for Rossby, Rossby-gravity, and inertia-gravity waves was obtained. The solutions were found to be confined around the equator leading to the equatorially trapped waves. It was shown that the wave frequency depends on the vertical temperature gradient as well as on stellar rotation. Therefore, observations of wave frequency in light curves of stars with known parameters (radius, surface gravity, rotation period) could be used to estimate the temperature gradient in stellar outer layers. Consequently, the Rossby mode may be considered as an additional tool in asteroseismology apart from acoustic and gravity modes.

1. Introduction

Rossby (planetary) waves govern large-scale dynamics of rotating spheres[5]. The waves have been studied for centuries starting from Hadley (1735). They are characterized as low-frequency waves compared to the rotation frequency of the sphere and the solutions were found by Hough (Hough, 1897, 1898) based on Laplace tidal equations (Laplace, 1893). The existence of Rossby waves is associated with the Coriolis force and conservation of absolute vorticity on a rotating sphere. The first observational description and physical basics of the waves were discussed by Rossby (1939) in the Earth context during his work on a global weather forecast at the Massachusetts Institute of Technology. Consequently, the Rossby waves are well studied in Earth atmosphere and oceans by observations and theory (Hovmöller, 1949; Eliasen & Machenhauer, 1965; Yanai & Lu, 1983; Lindzen et al., 1984; Hirooka & Hirota, 1989; Madden, 2007; Chelton & Schlax, 1996; Hill et al., 2000; Haurwitz, 1940; Lindzen, 1967; Gill, 1982; Pedlosky, 1987; Platzman, 1968; Salby, 1984).

Rossby waves have an important role in the dynamic of different astrophysical objects like accretion disks, solar system planets, stars, etc. (Zaqarashvili et al., 2021). The waves have been recently detected on the Sun by granular tracking and helioseismology (Löptien et al., 2018; Liang et al., 2019; Hanasoge & Mandal, 2019; Proxauf et al., 2020; Gizon et al., 2021; Hanson et al., 2022) as well as by coronal bright points (McIntosh et al., 2017; Krista & Reinard, 2017). It is also suggested that the Rossby waves may lead to intermediate periodicity in solar activity (Zaqarashvili et al., 2010; Gurgenashvili et al., 2016, 2017; Dikpati et al., 2020). Theoretical description of Rossby waves in the solar interior and tachocline is also significantly developed in recent years (Zaqarashvili et al., 2007; Zaqarashvili, 2018; Gachechiladze et al., 2019; Dikpati et al., 2018, 2022; Gizon et al., 2020; Bekki et al., 2022; Horstmann et al., 2023).

Huge observational data collected by recent space missions TESS (Transiting Exoplanet Survey Satellite), CoRoT (Convection, Rotation, and planetary Transits), and Kepler led to the detection of Rossby waves in light curves of stars. First, Van Reeth et al. (2016) reported the evidence of r-modes in the Gamma Doradus stars using Kepler data. Then the waves have been observed in many stars with different spectral classes (Saio et al., 2018; Li et al., 2019; Jeffery, 2020; Samadi-Ghadim et al., 2020; Takata et al., 2020; Saio & Kurtz, 2022). It has been

[5]The waves are mostly known as r-modes in stellar physics (Papaloizou & Pringle, 1978)

also suggested that the Rossby waves may lead to the observed short-term stellar cycles (Lanza et al., 2009; Bonomo & Lanza, 2012; Gurgenashvili et al., 2022).

The theory of Rossby waves was developed in the context of the Earth's atmosphere and oceans mostly in the shallow water approximation, which considers the shallow layer of the sphere with a homogeneous density. This approximation is valid for the layers, which have smaller widths compared to the density scale height. On the other hand, stellar interiors generally cover many scale heights especially upper parts with lower temperatures. Therefore, the consideration of the radial direction is necessary to model the Rossby waves in stars. For this reason, the separation of horizontal and vertical equations allow us to find the solutions of Rossby waves in some approximations. Using expansions with small parameters, Papaloizou & Pringle (1978) studied the high order r-modes in 3D spherical geometry of rapidly rotating stars, while Provost et al. (1981) and Saio (1982) analyzed the low order modes in the slow rotation limit. However, it was shown by Taylor (1936) that the dynamics of Rossby waves in stratified fluids are identical to the waves in a homogeneous layer that has a width of the equivalent depth corresponding to the separation constant of horizontal and vertical equations. Then, the Rossby waves in stratified fluids (such as stellar interiors) can be described in shallow water approximation if the separation constant is known. Townsend (2003) used the spherical hydrodynamic equations in the traditional approximation and found the relation between wave frequency and separation constant (see also in Lee & Saio (1997)). It was found that the solutions of horizontal equations (in fact Laplace tidal equations) are approximated by parabolic cylinder equation (or Schrödinger equation) in the low-frequency limit, which has exact solutions in terms of Hermite polynomials. This phenomenon is well studied in the Earth context by Longuet-Higgins (1968) in spherical coordinates and by Matsuno (1966) in Cartesian coordinates. Namely, the low-frequency waves in shallow water approximation (obtained either in fast rotation or in a narrow width of the layer) are confined around the equator and hence are known as equatorially trapped waves. Equatorially trapped waves have the same solutions and dispersion relations in spherical and Cartesian coordinates (Zaqarashvili et al., 2021), which allows us to consider simpler rectangular symmetry. Recently Albekioni et al. (2023a) used the traditional approximation to solve the dynamics of Rossby waves in horizontal and vertical directions in rotating early-type stars with outer radiative envelopes. The horizontal behavior of the waves was found to be governed by a parabolic cylinder equation with the solutions of Hermite polynomials. While the vertical

behavior of the waves was governed by the Bessel equation for the linear vertical temperature gradient. Consequently, the vertical solutions were found in terms of Bessel functions and hence the free surface boundary conditions allowed us to find the vertical modes with corresponding separation constant. Then the separation constant was used in horizontal equations to find the frequencies of different wave modes with various horizontal wave numbers. However, Albekioni et al. (2023a) found the solutions only for the first vertical mode in a particular temperature gradient, while the formalism allows us to consider also overtone vertical modes and different values of temperature gradients. Vertical overtones lead to the construction of period spacing patterns, which are very important to compare the theory to observations (Aerts, 2021), therefore additional study related to vertical overtones is certainly required.

In this paper, we expand the results of Albekioni et al. (2023a) for various vertical modes of Rossby waves and different rates of vertical temperature gradients for stars with outer radiative envelopes.

2. Theoretical model

We use the linear adiabatic hydrodynamic equations in a rotating frame of stellar surface:

$$\rho_0 \frac{\partial \vec{v}}{\partial t} + 2\rho_0 \vec{\Omega} \times \vec{v} = -\nabla p' + \rho' \vec{g}, \tag{51}$$

$$\frac{\partial \rho'}{\partial t} + (\vec{v} \cdot \nabla)\rho_0 + \rho_0 \nabla \cdot \vec{v} = 0, \tag{52}$$

$$\frac{\partial p'}{\partial t} + (\vec{v} \cdot \nabla)p_0 + \gamma p_0 \nabla \cdot \vec{v} = 0, \tag{53}$$

where ρ_0 (p_0) is the equilibrium density (pressure), ρ' (p') is the perturbation of density (pressure), $\vec{v}$ is the perturbation of velocity, $\vec{g}$ is the gravitational acceleration, $\vec{\Omega}$ is the angular frequency of rotation and $\gamma = c_p/c_v$ is the ratio of specific heats. We note that solid body rotation is adopted throughout the paper. The effects of differential rotation will be studied in the future. Undisturbed medium is assumed to be in vertical hydrostatic balance, which with the ideal gas law gives the vertical distribution of undisturbed physical parameters (density, pressure, and temperature). Details of the initial setup and mathematical formalism can be found in Albekioni et al. (2023a) and we do not repeat it here.

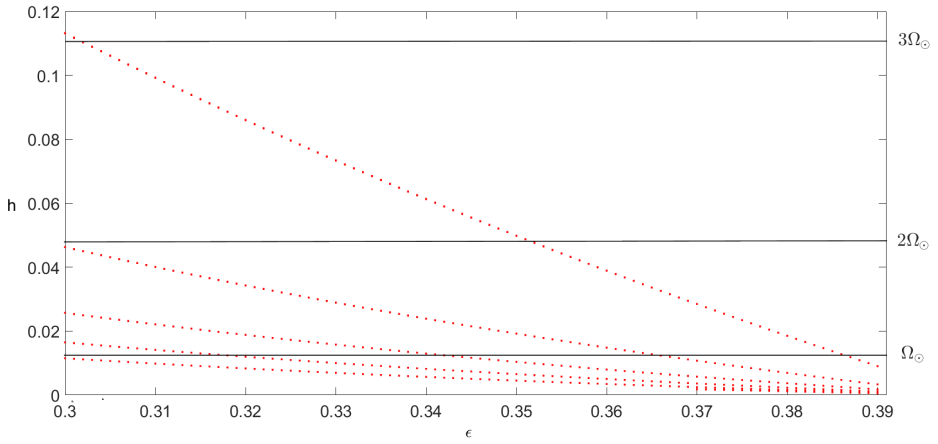

Figure 10: Equivalent depth (normalized by the surface scale height, H_0) vs the temperature gradient, ϵ, for the first five zeroes of Eq. (60) i.e. for the first five vertical modes (the first mode corresponds to the upper curve, and the fifth mode corresponds to the lower curve). Horizontal black lines show the upper limits of h_c, which satisfy the polar boundary conditions, for different stellar rotation rates ($\Omega_\odot$ is the angular frequency of the Sun). All values of $h < h_c$ for each rotation rate lead to the bounded solutions along the latitudinal direction.

Considering the Cartesian coordinate system, the Fourier transform of the form $e^{i(-\sigma t+kx)}$ and the vertically hydrostatic assumption of perturbed variables, Eqs. (51)-(53) lead to the two equations (see details in Albekioni et al. (2023a))

$$\frac{\partial^2\Psi}{\partial y^2}+\left[\frac{\sigma^2-f^2}{gh}-k^2-\frac{k}{\sigma}\frac{df}{dy}\right]\Psi(y)=0, \tag{54}$$

$$\frac{\partial}{\partial z}\left[\frac{\gamma H}{1-\gamma(1+H')}\frac{\partial}{\partial z}\right]V(z)-$$
$$-\left[\frac{\gamma(1+H')^2}{4H[1-\gamma(1+H')]}-\frac{\gamma H''}{2[1-\gamma(1+H')]^2}+\frac{1}{h}\right]V(z)=0, \tag{55}$$

where $\Psi(y)$ and $V(z)$ are the functions describing the latitudinal and the radial parts of the latitudinal velocity so that $v_y=\Psi(y)V(z)$, σ is the frequency of waves, k is the wavenumber along the x axis, $f=2\Omega\sin\theta$ is the Coriolis parameter (θ being as latitude) and $H(z)=k_bT(z)/mg$ is the density scale height (k_b is the Boltzmann constant and m is the mass of hydrogen atom). Here H' is the first derivative and H'' is the second derivative with z. Note that x, y, z axes are directed towards the rotation, the north pole, and vertically upwards, respectively. ρ_0 is absorbed in the expression of velocity so that v_y is multiplied by $\sqrt{\rho_0}$. We used the method of separation of variables to separate the equations into y- and z-dependent parts, so

that h is the separation constant. The physical meaning of h can be understood for a simple isothermal case, $H = const$. In this case, Eq. (55) has periodic solutions when $k_z^2 = (\gamma - 1)/(\gamma H h) - 1/4H^2 > 0$, which means that $h < 4H(\gamma - 1)/\gamma$. Then $k_z \sim h^{-1/2}$ i.e. smaller h yields the shorter vertical wavelength. A star with a surface temperature of 10 000 K yields $H = 300$ km, then h must be smaller than 480 km in order to have periodic solutions in vertical directions. The corresponding vertical wavelength is a few Mm and less, therefore the waves will have a small vertical extent near the surface, but may be increased with depth.

Eq. (54) is equivalent to the equation that governs shallow water equatorially trapped waves in a homogeneous layer with the width of h (e.g., Matsuno (1966)). In fact, this is the Taylor theorem (Taylor, 1936) stating that the dynamics of Rossby waves in stratified fluids are identical to the waves in a homogeneous layer that has a width of equivalent depth, h. Therefore, one can use the shallow water equations to describe the Rossby waves in a stratified fluid, if the equivalent depth of the corresponding wave mode is known. Note that the equivalent depth is different for different modes of Rossby waves.

Equations (54)-(55) govern the dynamics of Rossby and inertia-gravity waves in the vertical and horizontal directions. Note that the internal gravity and acoustic waves are neglected from the consideration using low-frequency approximation. This approximation is justified as the acoustic and internal gravity waves have time scales of minutes and hours respectively, while the Rossby and inertia-gravity waves have much longer time scale of the order of days. The equations (54)-(55) can be solved in two different ways. First, one can solve the latitudinal part of the equations and calculate the separation constant based on the boundary conditions at the poles. Then the obtained separation constant can be used to find the radial dependence of solutions through the solution of a system of vertical equations (this approach corresponds to the forced oscillation case in the Earth's atmospheric science). Lee & Saio (1997) and Townsend (2003) used the same approach in spherical geometry separating initial equations into two systems of equations with latitudinal and vertical dependence. They solved the latitudinal equations and derived the relations between the wave frequency and the separation constant. Second, one can first solve the radial part of the equations using the vertical boundary conditions and find the corresponding separation constant that is the equivalent depth (this approach corresponds to the so-called free oscillation case in the Earth's atmospheric science). Then one can use the equivalent depth to find the latitudinal dependence and frequency of the waves. Albekioni et al.

(2023a) used the second approach and found equatorially trapped Rossby waves satisfying the bounded conditions at poles. Here we use the approach as in Albekioni et al. (2023a), hence we will first solve Eq. (5) and find the equivalent depth according to the boundary conditions in the vertical direction.

3. Vertical structure of Rossby waves

Solutions of Eq. (55) are determined by the vertical variation of the density scale height, which actually depends on the vertical temperature gradient. In this paper, we use the linear profile of the scale height with a uniform vertical gradient

$$H = H_0 - \epsilon z, \tag{56}$$

which is equivalent to the temperature profile of the form

$$T = T_0 \left(1 - \epsilon \frac{z}{H_0}\right), \tag{57}$$

where H_0 and T_0 are the scale height and the temperature at the surface, $z = 0$, respectively.

In this paper, we consider early-type stars with outer radiative envelope, therefore $\epsilon < (\gamma - 1)/\gamma = 0.4$ should be satisfied. The linear temperature gradient assures the existence of a radiative environment through the considered extent of the stellar interior. For other profiles, the vertical temperature gradient generally increases with depth, which unavoidably leads to the violation of the radiative condition at some distance from the surface. It was shown by Albekioni et al. (2023a) that the Rossby waves are confined near-surface layers of stars with the thickness of 30-50 H_0, hence the linear profile is justified. Therefore, here we only consider an uniform linear profile of the temperature.

Eq. (55) leads to the Bessel equation for the linear temperature profile (Eq. (56))

$$x^2 \frac{\partial^2 V(x)}{\partial x^2} + x \frac{\partial V(x)}{\partial x} + (x^2 - n^2) V(x) = 0, \tag{58}$$

where

$$x = 2 \sqrt{H_0 - \epsilon z} \frac{\sqrt{\gamma(1-\epsilon) - 1}}{\epsilon \sqrt{\gamma h}} \tag{59}$$

and $n = (1 - \epsilon)/\epsilon$. Solutions of the equations are the Bessel functions of the order n, $J_n(x)$ and $Y_n(x)$. In Eq. (58), there are two unknown parameters, ϵ and

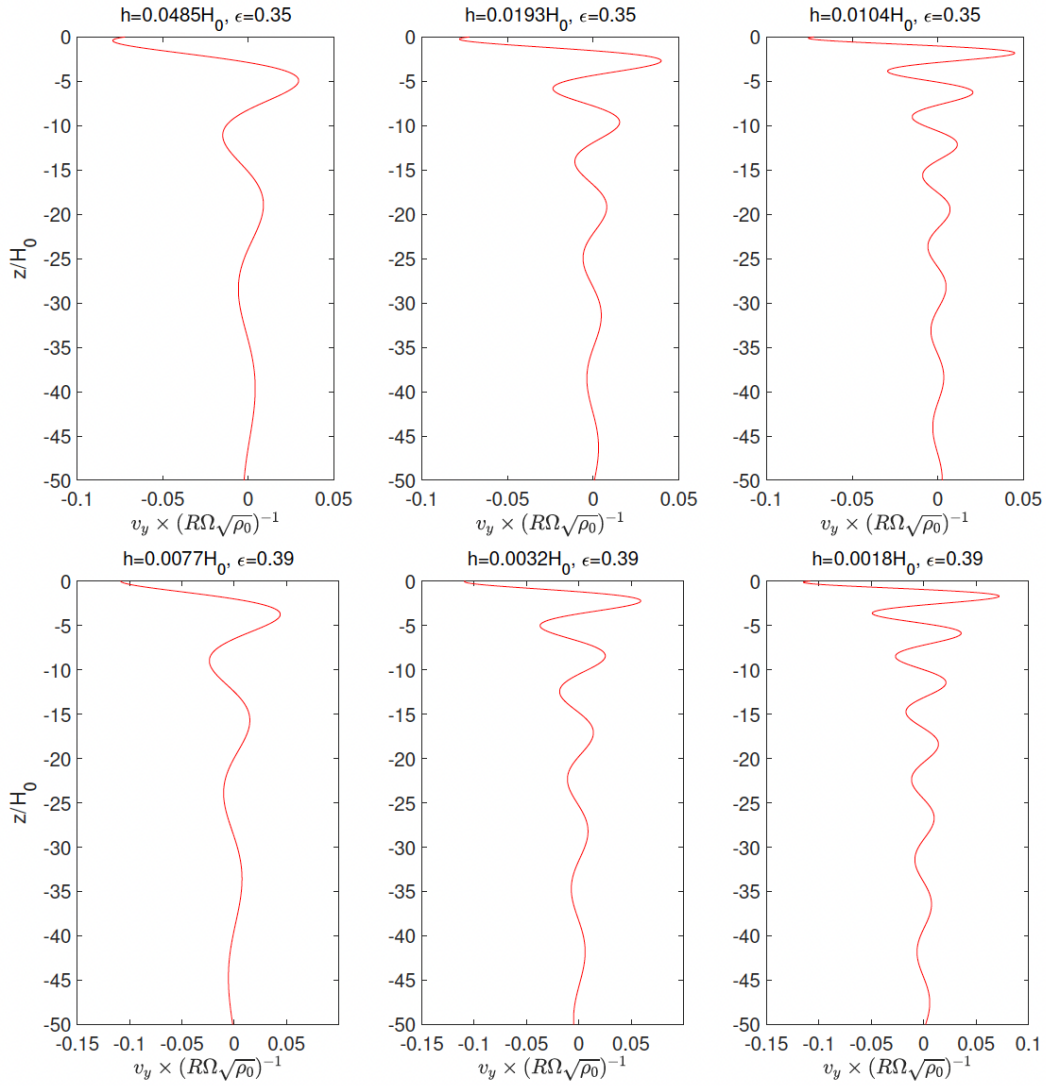

Figure 11: Vertical structure of first three vertical modes of Rossby waves for the temperature gradient of $\epsilon = 0.35$ (upper panels) and $\epsilon = 0.39$ (lower panels). Left, middle, and right panels correspond to the first, second, and third modes of Rossby waves, respectively. Note that ρ_0 is absorbed in the expression of velocity in the used formalism so that v_y is multiplied by $\sqrt{\rho_0}$. Therefore, the velocity plotted in this figure is non-dimensional.

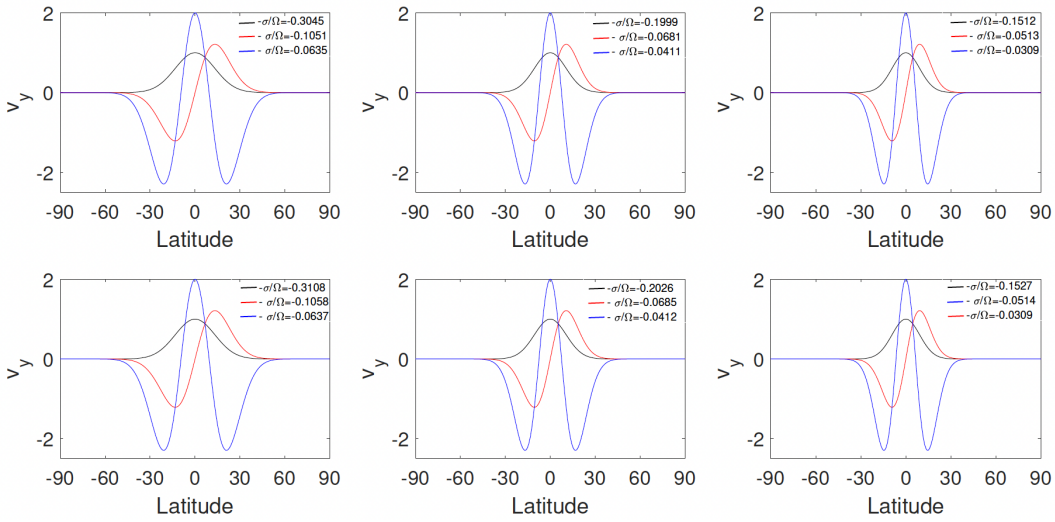

Figure 12: Latitudinal structure of Rossby waves for temperature gradient $\epsilon = 0.39$, stellar angular frequency of $3\Omega_\odot = 9\times10^{-6}s^{-1}$ (upper panel) and $5\Omega_\odot = 15\times10^{-6}s^{-1}$ (lower panel). Left, middle, and right columns display the first, second and third vertical modes. Black, red, and blue curves on each panel show $n = 0, n = 1, n = 2$ modes, respectively. All modes represent the equatorially trapped waves.

h, assuming that the surface temperature and hence H_0 is known. Then fixing the temperature gradient, ϵ, leads to the determination of h using boundary conditions. Both, $J_n(x)$ and $Y_n(x)$ are bounded for $z \to -\infty$ (i.e. towards stellar center). On the other hand, $Y_n(x) \to \infty$ for $x \to 0$ i.e. for $z \to H_0/\epsilon$. Therefore, $J_n(x)$ seems to be a more appropriate solution of Eq. (58). The free boundary condition (when the Lagrangian pressure is zero) at the surface $z = 0$, that is at $x = x(z = 0)$, leads to the equation (Albekioni et al., 2023a)

$$\frac{\partial J_n(x)}{\partial x} - \frac{1}{x}\frac{3(1-\epsilon)}{\epsilon}J_n(x) = 0. \tag{60}$$

For each value of ϵ, the free boundary condition, Eq. (60), gives an infinite number of zeros and hence an infinite number of h. Each of the zeroes and hence h corresponds to the particular vertical mode of waves.

Fig. (10) shows the equivalent depth vs different temperature gradients for different zeroes of Eq. (60).

Only the first five zeros, hence the first five vertical harmonics, are shown in this figure in the temperature gradient range of 0.3-0.39 (note that $\epsilon = 0.4$ is the upper limit of radiative medium). When the temperature gradient approaches the adiabatic limit ($\epsilon = 0.4$), then the corresponding equivalent depth is reduced for all five vertical harmonics. We need to keep in mind that each calculated equivalent

depth must lead to bounded solutions at poles when one inserts it in Eq. (54). This upper limit of the equivalent depth, h_c, is shown by black lines in Fig.(10) for different rotation rates of stars (Note, that here solar angular frequency has a value $\Omega_\odot = 3 \times 10^{-6} s^{-1}$). All the solutions with $h > h_c$ do not satisfy polar boundary conditions and, therefore are invalid for our consideration (see the next section). It is seen that the rapidly rotating stars allow all vertical harmonics in considered intervals of the temperature gradient to be bounded at poles. On the other hand, for the slowly rotating stars (similar to the Sun) only fifth and higher overtones are under the limit for the whole range of temperature gradient.

Next, we analyze the vertical structure of individual vertical modes and its dependence on the value of temperature gradient. We assume two different values of ϵ: 0.35 and 0.39. The first three values of equivalent depth corresponding to the first three vertical modes for $\epsilon = 0.35$ calculated from Eq. (60) are $h = 0.0485\, H_0, 0.0193\, H_0, 0.0104\, H_0$, respectively. For $\epsilon = 0.39$, the corresponding values are $h = 0.0077\, H_0, 0.0032\, H_0, 0.0018\, H_0$. The corresponding solutions of Eq.(55), which is the latitudinal velocity of the Rossby waves, are plotted Fig. (11). The figure shows that the wavelength is shorter for the higher modes as expected, but the higher modes penetrate slightly deeper in the interior. On the other hand, a larger temperature gradient yields a slightly longer wavelength of the waves as seen from the comparison of upper and lower rows.[6]

4. Latitudinal structure of Rossby waves

The obtained equivalent depths, h, which correspond to the different vertical modes of Rossby waves, must be inserted in Eq.(54) and the solutions satisfying the bounded conditions at poles must be found. Consequently, only the vertical modes that lead to the latitudinal solutions vanishing towards the poles are valid. The latitudinal structure of the waves described by Eq.(54) crucially depends on the equivalent depth. It is found by Albekioni et al. (2023a) that the sufficiently small equivalent depth results in the solutions, which are concentrated around the equator. The equivalent depth in Figure 1 has a small value for almost all modes

[6]Note, that the lower left panel of Figure 2 of this paper is the same as the right panel of Fig.1 in Albekioni et al. (2023a). However, the amplitudes at $z = 0$ are different in these two plots, as here we used the same amplitudes for all six plots for better comparison. This different normalisation obviously does not affect the vertical structure of the waves.

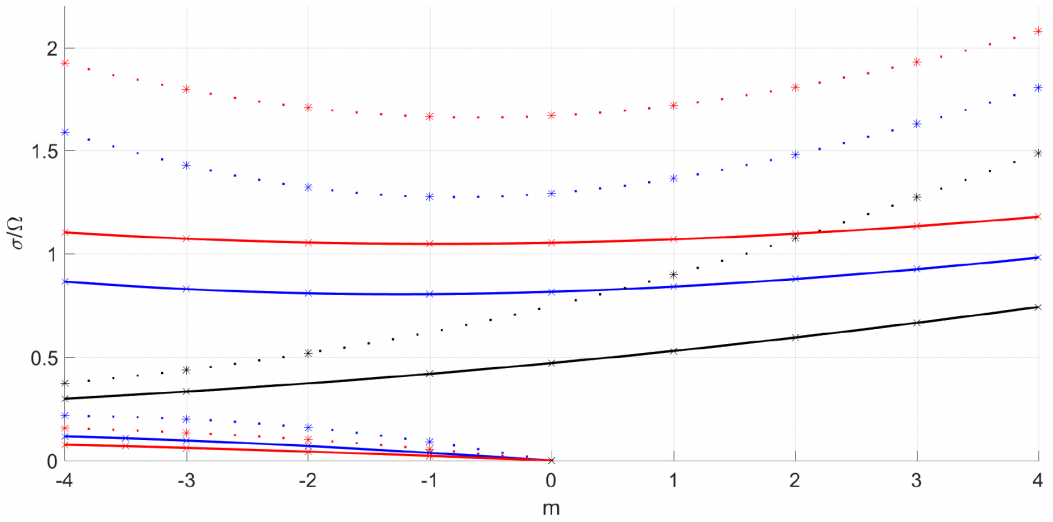

Figure 13: Frequencies of Rossby (lower curves), Rossby-gravity (middle curves with black color) and inertia-gravity waves (upper curves) vs toroidal wavenumber, m, obtained from Eq. 63. Black, blue and red colors show the modes with $n = 0$, $n = 1$, and $n = 2$, respectively. The frequencies match with the first vertical modes corresponding to the temperature gradients of $\epsilon = 0.39$ (solid lines) and $\epsilon = 0.35$ (dashed lines) for the stellar angular frequency of $3\Omega_\odot$.

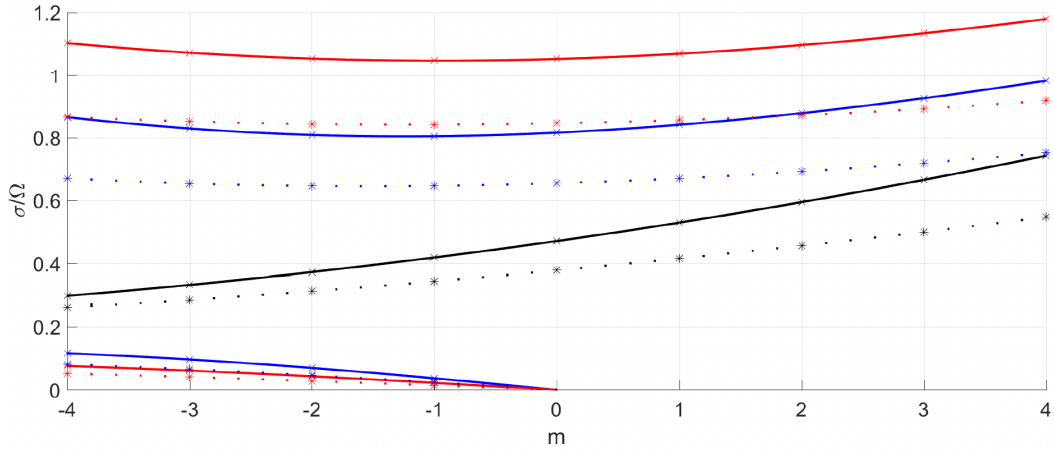

Figure 14: Frequencies of Rossby (lower curves), Rossby-gravity (middle curves with black color) and inertia-gravity waves (upper curves) vs toroidal wavenumber, m, obtained from Eq. 63. Black, blue and red colors show the modes with $n = 0$, $n = 1$, and $n = 2$, respectively. The frequencies match with the first (solid lines) and the second (dashed lines) vertical modes for the temperature gradient of $\epsilon = 0.39$ for the stellar angular frequency of $3\Omega_\odot$.

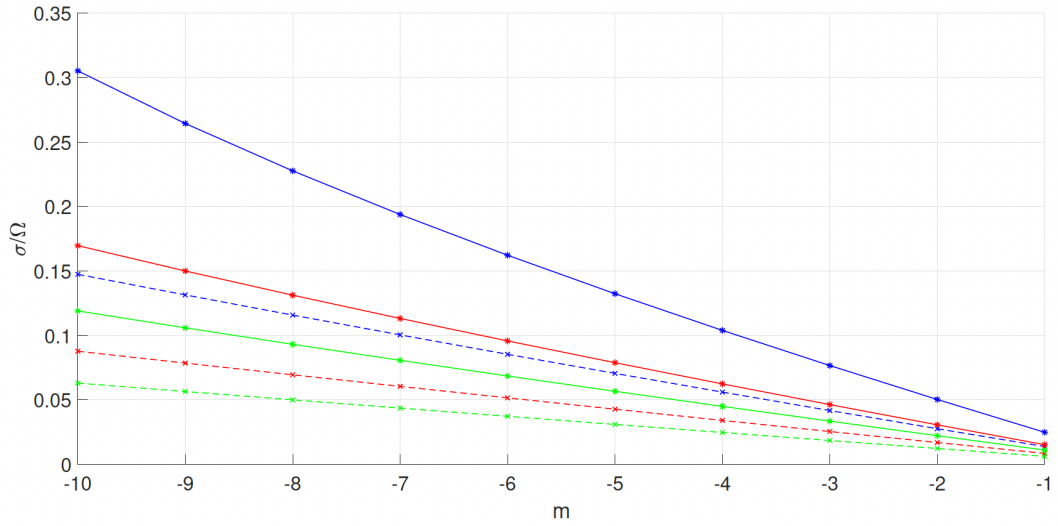

Figure 15: First (blue), second (red) and third (green) vertical harmonics of Rossby waves vs toroidal wavenumber, m, obtained from Eq. 63 for the temperature gradient of $\epsilon = 0.39$ and the stellar angular frequency of $3\Omega_\odot$. Solid and dashed lines correspond to the modes with $n = 2$ and $n = 4$, respectively.

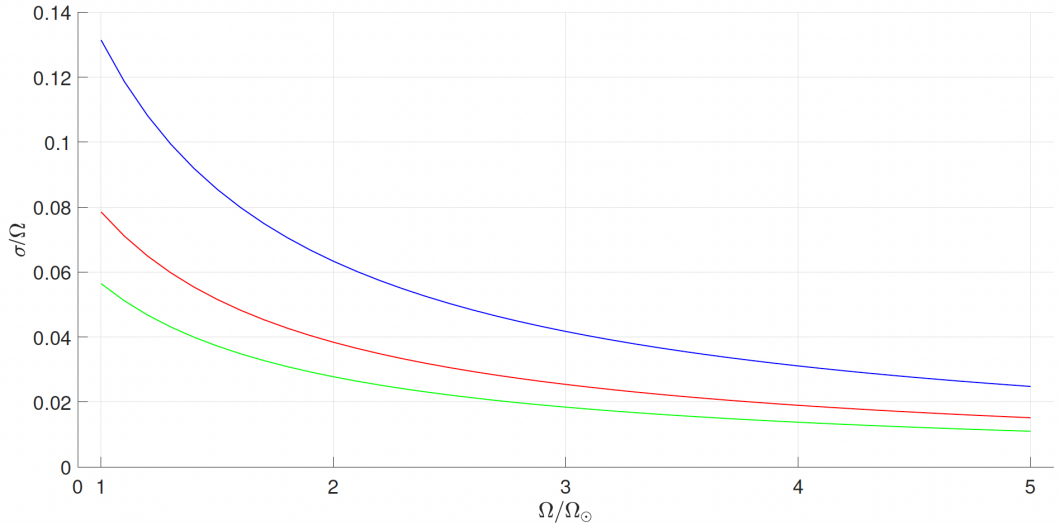

Figure 16: Frequency of different vertical modes of Rossby wave vs stellar rotation for a vertical temperature gradient of $\epsilon = 0.39$. Blue, red, and green lines correspond to the first, second, and third vertical modes, respectively. Here the toroidal and latitudinal wavenumbers are $m = -1$ and $n = 1$, respectively.

for rapid rotations ($\Omega > \Omega_\odot$), therefore, almost all vertical modes represent equatorially trapped waves. Near the equator, Coriolis parameter can be expanded as $f = \beta y$, where $\beta = 2\Omega/R$ and the Eq.(54) is transformed into parabolic cylinder equation

$$\frac{\partial^2 \Psi}{\partial y^2} + \left[-\frac{k\beta}{\sigma} + \frac{\sigma^2 - k^2 c^2}{c^2} - \frac{\beta^2 y^2}{c^2} \right] \Psi(y) = 0, \tag{61}$$

where $c = \sqrt{gh}$ is the surface gravity speed. When the Lamb parameter of particular wave mode with the equivalent depth h, $\varepsilon = 4\Omega^2 R^2/gh$, is much larger than unity, then the solutions of Eq.(61) are trapped in low latitudes and exponentially vanish towards poles. This happens for small equivalent depth, $h \ll H_0$, and fast rotation, $\Omega > \Omega_\odot$. In this case, the solutions of Eq.(61) are in terms of Hermite polynomials (see details in Albekioni et al. (2023a))

$$\Psi = \Psi_0 \exp\left(-\frac{\sqrt{\varepsilon}}{2} \frac{y^2}{R^2} \right) H_n\left(\varepsilon^{1/4} \frac{y}{R} \right), \tag{62}$$

and the waves are governed by the dispersion equation

$$\omega^3 - \frac{4}{\sqrt{\varepsilon}} \left(2n + 1 + \frac{m^2}{\sqrt{\varepsilon}} \right) \omega - \frac{8m}{\varepsilon} = 0, \tag{63}$$

where $\omega = \sigma/\Omega$ is the normalised wave frequency, $m = kR$ is the normalised toroidal wavenumber (can be assumed as discrete $m = 0, 1, 2...$), and $n = 0, 1, 2...$ denotes the number of zeroes along the latitudinal direction. $n = 0$ means that the mode has no zero along the latitudinal direction i.e. it corresponds to the sectoral harmonic, $n = 1$ has one zero at the equator, etc. For $n \geq 1$, the dispersion relation governs two higher frequency prograde and retrograde inertia-gravity waves and one lower frequency retrograde Rossby wave. For $n = 0$, Eq. (63) governs prograde and retrograde Rossby-gravity waves.

Eq. (62) shows that the latitudinal structure of the waves is governed by ε: larger ε leads to the stronger decrease in the wave amplitude. One can estimate the critical ε from Eq. (62) as $(\sqrt{\varepsilon} y^2/2R^2)_{y=\pi R/2} = 1$, which yields e-times decrease of polar values with regards to the equator. This gives the critical value of ε as ≈ 25. All modes with $\varepsilon > 25$ vanish towards poles, therefore they are valid solutions, while the modes with $\varepsilon < 25$ are not bounded at poles. Consequently, for each angular frequency, Ω, there is the critical value of the equivalent depth, h, which defines valid solutions of Rossby waves (here we assume fixed R and g). The critical equivalent depths for different angular velocities of stars are plotted by horizontal black lines in Fig.(10).

The upper panels of Fig. (12) show the latitudinal structure of the first three vertical modes in the case of the temperature gradient $\epsilon = 0.39$ and the angular frequency of $\Omega = 3\Omega_\odot$. It is seen that the waves are located between $\pm 50^0$, therefore they are equatorially trapped waves. Their amplitudes vanish towards the poles and hence satisfy the polar boundary conditions. The higher modes are more concentrated towards the equator. This happens because ε is inversely proportional to the equivalent depth, hence the smaller h yields the larger ε in the case of fixed stellar angular frequency. Lower panels of Fig. (12) display the structures of the same modes but for higher angular frequency $\Omega = 5\Omega_\odot$. It is seen that the wave profiles are squeezed towards the equator in comparison to the slower rotation and the waves are trapped between $\pm 30^0$ latitudes. Therefore, the stars with faster rotation display stronger trapping of Rossby waves around the equator.

5. Frequency of the waves

Eq. (63) shows that the wave frequency depends on the Lamb parameter, ε, and on the latitudinal wavenumber, n. On the other hand, ε is proportional to the frequency of stellar rotation (and radius) and inversely proportional to the equivalent depth, h (and the surface gravitational acceleration, g). As the equivalent depth is a function of the temperature gradient (see Figure 1) and has various values for different vertical modes, the wave frequency also depends on the two parameters.

Fig. (13) exhibits the solutions of Eq. (63) with regards to m for the different values of the temperature gradient. Solid lines show the first vertical modes of Rossby, Rossby-gravity, and inertia-gravity waves for the temperature gradient of $\epsilon = 0.39$. Lower (upper) blue and red curves display the first vertical modes of the Rossby (inertia-gravity) waves with a latitudinal wavenumber of $n = 1$ and $n = 2$, respectively. The middle black curve corresponds to the Rossby-gravity mode with $n = 0$. The dashed curves show the same modes for the temperature gradient of $\epsilon = 0.35$. The difference between the two temperature gradients is clear, so that the larger temperature gradient leads to the lower frequencies of all waves.

Fig. (14) presents the solutions of Eq. (63) with regards to m for the different vertical modes. Solid (dashed) lines show the first (the second) vertical modes of Rossby, Rossby-gravity, and inertia-gravity waves for the temperature gradient of $\epsilon = 0.39$. Lower (upper) blue and red curves display the Rossby (inertia-gravity) waves with a latitudinal wavenumber of $n = 1$ and $n = 2$, respectively. The middle

black curves correspond to the Rossby-gravity mode with $n = 0$. The difference between the various vertical modes is distinct so that the higher vertical modes lead to lower frequencies of all waves. Fig. (15) presents the solutions of Eq. (63) with regards to m for the different vertical modes of Rossby waves in the case of the temperature gradient $\epsilon = 0.39$ for $3\Omega_\odot$. Here the latitudinal wavenumbers are $n = 2$ and $n = 4$ and displayed by solid and dashed lines, respectively. The frequency difference of different vertical modes is clear.

As ε is also a function of angular frequency, then the wave frequency depends on the stellar rotation. Fig. (16) presents the frequency of various vertical modes of Rossby wave vs the stellar rotation. The Rossby wave frequency is inversely proportional to ε, which means that the wave frequency normalized by the stellar angular frequency is decreasing for faster-rotating stars, especially for the higher vertical modes. It is also seen that the difference between the frequencies of different vertical modes decreases for faster-rotating stars.

Fig. (17) presents the solutions of Eq. (63) vs $\varepsilon = 4\Omega^2 R^2/gh$ for Rossby waves with with different toroidal (m) and latitudinal (n) wavenumbers. Equivalent depth for particular vertical modes and temperature gradient in the stellar near surface interior can be determined from Fig. (10). Therefore, the observed frequency in light curves of a star with known rotation, surface gravity, and radius may determine the corresponding equivalent depth h from Fig. (17). Then Fig. (10) can be used to find suitable vertical temperature gradient and vertical mode of Rossby waves as well as the appropriate vertical structure of the waves. This could be an important tool for future seismology of stellar interior by Rossby-type waves.

6. Discussion and conclusion

Growing data of stellar light curves obtained by recent space missions requires improving indirect tools for the estimation of internal parameters. Acoustic and gravity waves are obvious choices for asteroseismology, but it becomes increasingly clear that the Rossby waves also have significant potential to be used for probing stellar interiors (Aerts, 2021). The theory of stellar Rossby waves (or r-modes) was developed using expansions with a small parameter for high-order modes of rapidly rotating stars (Papaloizou & Pringle, 1978) and for low-order modes in slowly rotating stars (Provost et al., 1981; Saio, 1982). On the other hand, Lee & Saio (1997) and Townsend (2003) used traditional approximation to separate the horizontal and vertical equations in order to obtain the Laplace tidal

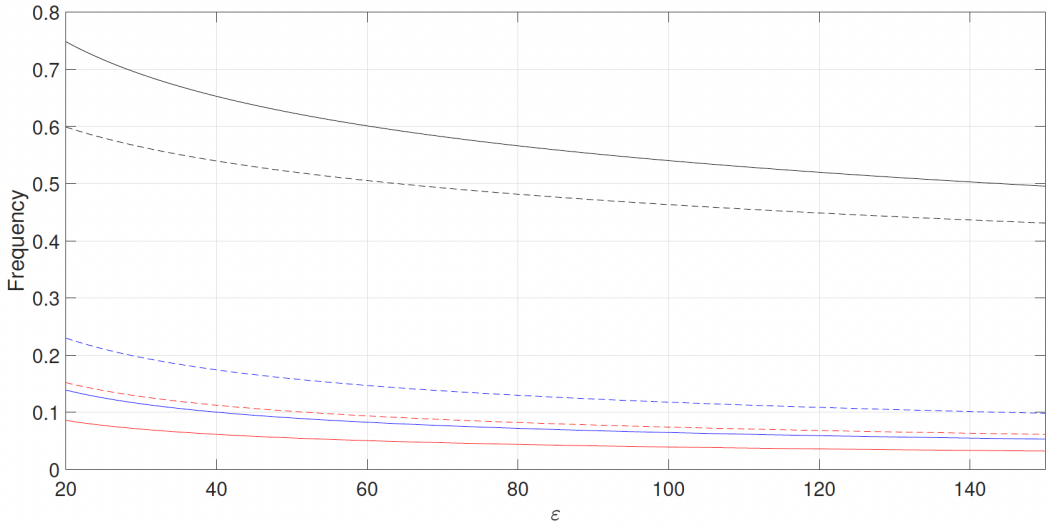

Figure 17: Frequency of Rossby waves vs $\varepsilon = 4\Omega^2 R^2/gh$. The black solid (dashed) curve corresponds to the Rossby-gravity mode with $(n, m) = (0, -1)$ ($(n, m) = (0, -2)$). The blue solid (dashed) curve corresponds to Rossby waves with $(n, m) = (1, -1)$ ($(n, m) = (1, -2)$). The red solid (dashed) curve corresponds to Rossby waves with $(n, m) = (2, -1)$ ($(n, m) = (2, -2)$). The vertical mode of the waves can be determined by corresponding equivalent depth, h, from Fig. (10) fixing the vertical temperature gradient.

equation for horizontal variations. Then they solved the Laplace tidal equations and obtained the dependence of wave frequency and separation constant. Then one can find the separation constant for each wave frequency and use it to solve the vertical equations to obtain the vertical structure of the modes. In the recent paper (Albekioni et al., 2023a), we used the same formalism of separation, but first solved the vertical equations for the linear temperature profile in free surface boundary conditions and found the corresponding value of separation constant, which is actually an equivalent depth of Rossby waves. Consequently, we derived the oscillation spectrum of Rossby waves from the horizontal equations for the first vertical mode and fixed vertical temperature gradient. It was found that the equivalent depth derived from surface boundary conditions has a small value, therefore corresponding horizontal solutions are concentrated around the equator leading to the equatorially trapped waves. This solution justifies the use of Cartesian coordinates as the solutions and frequencies of equatorially trapped Rossby waves are identical in rectangular and spherical considerations (Matsuno, 1966; Longuet-Higgins, 1968; Zaqarashvili et al., 2021). On the other hand, the difference in periods of various vertical modes, e.g. period spacing pattern, is often used to identify observed wave modes (Aerts, 2021) and hence is very useful in

asteroseismology. Consequently, it is of vital importance to study various vertical modes in the discussed formalism. Here we continue the similar study for various values of temperature gradient and vertical overtones of waves.

Figure 1 shows the dependence of equivalent depth, which was obtained from the solution of vertical equations using free boundary condition, on vertical temperature gradient ($|dT/dz| \sim \epsilon$) for the first five vertical modes. The value of the equivalent depth decreases for higher vertical overtones and for larger temperature gradients. We note that $\epsilon = 0.4$ corresponds to the adiabatic temperature gradient, therefore the radiative (or convectively stable) medium yields $\epsilon < 0.4$. The corresponding vertical structure of the modes is plotted in Figure 2 for different temperature gradients. We see that the vertical wavelength decreases significantly for higher overtones and imperceptibly for stronger temperature gradients. In all cases, the amplitude of latitudinal velocity decreases with depth so that the Rossby modes are concentrated near the surface layer with a thickness of 50 surface scale height. Higher overtones penetrate slightly deeper. It must be noted that the rotation kernels and vertical structure of $m = 1$ Rossby mode in the recent paper by Van Reeth et al. (2018) showed only a slight decrease of the wave amplitude with depth in upper layers and subsequent growth toward the center of stars for solid body rotation. The difference between the results depicted in Figure 2 of Van Reeth et al. (2018) and Figure 11 in the current paper arises due to the density factor, ρ_0. In Figure 2 of our paper, the displayed velocity does not include density as indicated by the figure labels. But in Figure 2 of Van Reeth et al. (2018), the rotation kernels incorporate density (Aerts et al., 2010), which leads to the mentioned discrepancy. If one plots the velocity with the factor of $\sqrt{\rho_0}$ in Figure 2 in our paper, then one can find only a gradual decrease in amplitude with depth in coincidence with Van Reeth et al. (2018). The absence of amplitude growth in deeper layers in Figure 2 is probably caused due to the used linear temperature gradient. The inclusion of differential rotation obviously will lead to new vertical profiles of the waves.

Small values of equivalent depth lead to the parabolic cylinder equation for horizontal direction with bounded solutions in terms of Hermite polynomials and with corresponding dispersion relation of Rossby, Rossby-gravity, and inertia-gravity waves. The latitudinal structure of the waves depends on the parameter $\varepsilon = 4\Omega^2 R^2/gh$ as shown by Eq. (63). Larger ε leads to the stronger equatorial confinement of the waves. Figure 3 shows the latitudinal structure of the first three vertical modes for different rotation rates. The waves are strongly trapped near the

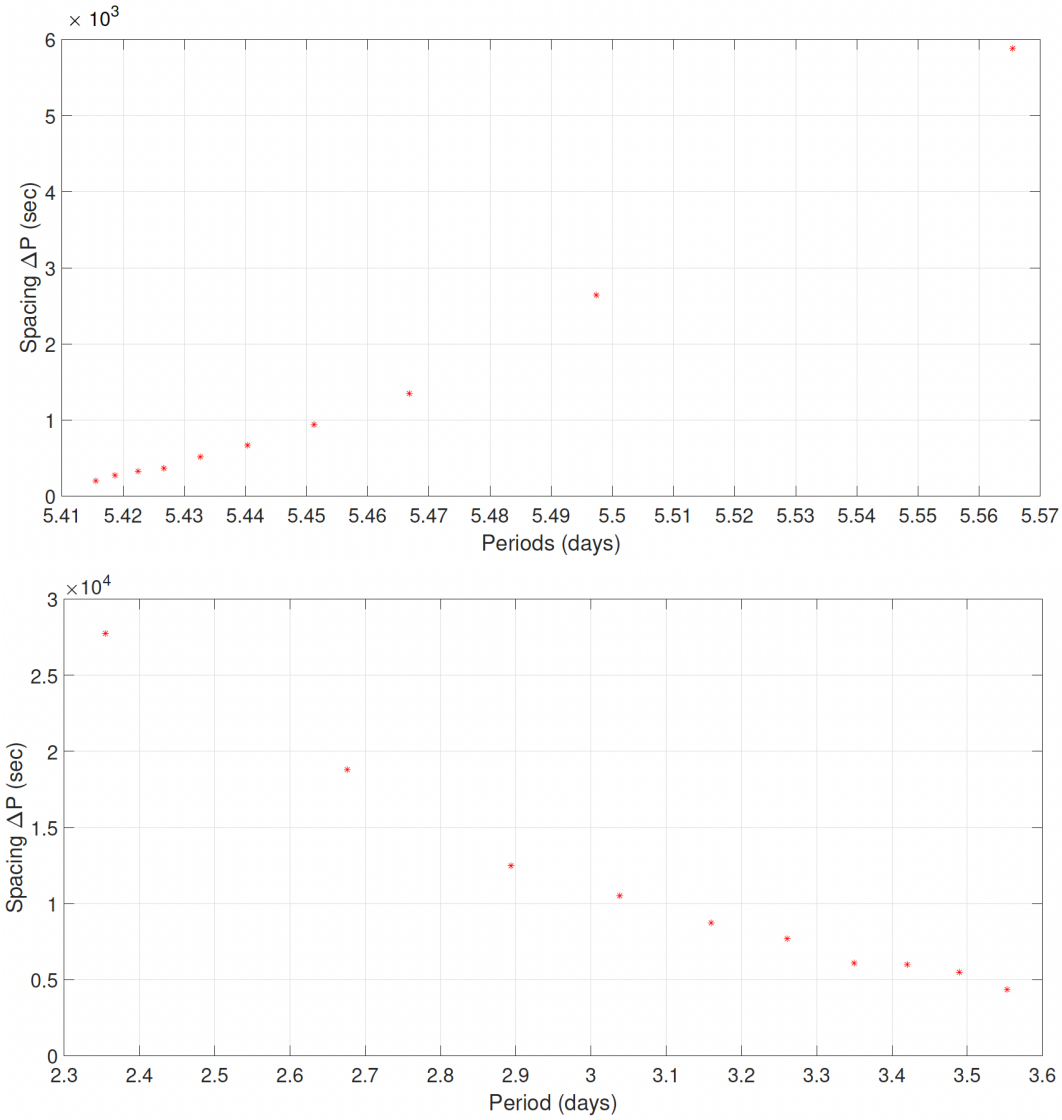

Figure 18: Spacing (ΔP) vs period patterns for Rossby (upper panel, $m = -1$ and $n = 2$ mode) and inertia-gravity (lower panel, $m = 1$ and $n = 2$ mode) waves for the vertical temperature gradient of $\epsilon = 0.39$ and the stellar angular frequency of $\Omega = 5\Omega_\odot$ (i. e. the rotation period of ~ 5.4 days). Wave periods are calculated in the inertial frame. The first ten vertical modes are used to construct the period-spacing patterns; the vertical order of the modes is increasing from left to right.

equator for rapidly rotating stars: the waves are confined between latitudes of $\pm 30^0$ for 5 $\Omega_\odot$. In this paper, we consider the stars with outer radiative zones, which occupy the upper part of the Hertzsprung-Russel diagram. These stars generally have rapid rotation compared to $\Omega_\odot$ due to the weak magnetic breaking (Kraft, 1967). Therefore, the stars considered in this paper are fast rotators, hence the waves are trapped around the equator for almost all modes and the value of the temperature gradient.

The wave frequency strongly depends on ε, hence on the surface rotation frequency and corresponding equivalent depth. As the equivalent depth is a function of the temperature gradient, the wave frequency also hinges on it. Figure 4 shows that the frequency of all wave modes significantly depend on the gradient, which implies that observations may provide the estimation of the parameter. Wave frequency also significantly depends on stellar rotation as seen from Figure 7 for the Rossby node with $m = -1$ and $n = 1$. The dependence seems more important at the slow rotation part of the interval but becomes imperceptible for rapid rotations.

Observations of light curve variations may provide asteroseismic sounding of some parameters. Here we consider solid body rotation without magnetic field, therefore we can estimate the vertical temperature gradient. Incorporation of differential rotation (Gizon et al., 2020) and the magnetic field (Zaqarashvili, 2018) in the model may widen the application further to magnetic field strength and the differential rotation rate. The frequency of Rossby waves is smaller than the angular frequency of rotation, while the frequency of inertia-gravity waves is comparable to the rotation frequency (see Figures 4-5). It should be noted that the wave frequency is calculated in the rotating frame in this paper, therefore one needs to transform it in the inertial frame in order to compare with observations. Transformation of frequency occurs with $\sigma_{obs} = m\Omega + \sigma$. Hence, the Rossby waves with $m = -1$ will have a slightly lower frequency compared to the rotational frequency $|\sigma| < \Omega$, while the waves with $m = -2$ will have the frequency in the interval of $\Omega < |\sigma| < 2\Omega$.

We mentioned above that the vertical modes are important to construct the period-spacing patterns, which are used to compare the theory with observations. As an example, we plot the period-spacing patterns for Rossby and inertia-gravity waves on Fig. 18 for a specific value of the temperature gradient, $\epsilon = 0.39$. We calculated the first ten vertical modes for the stellar angular frequency of $\Omega = 5\Omega_\odot$ and the horizontal wavenumbers of $n = 2$ and $|m| = 1$. We see that the Rossby and inertia-gravity waves show expected behavior as shown in the literature (Aerts,

2021). This analysis may serve as another valuable tool to facilitate comparisons between observations and theoretical predictions.

Observations of frequency in the light curves of stars can be compared with the theoretical spectra of the waves. Figure 8 displays the dependence of wave frequency on ε for several modes of Rossby waves with different m and n. The observed frequency will then determine the corresponding equivalent depth h if the radius, surface gravity, and rotational frequency of the star are known. Once the equivalent depth is estimated, one can use Fig.10 to identify the corresponding ϵ and vertical mode number of the waves. Consequently, one can estimate the vertical temperature gradient and the vertical structure of different harmonics. This methodology could potentially serve as an important tool for future asteroseismic studies of stellar interiors.

2.3 Paper III: Effect of latitudinal differential rotation on solar Rossby waves: Critical layers, eigenfunctions, and momentum fluxes in the equatorial β plane

L. Gizon, D. Fournier, M. Albekioni, A & A, 642, A178

doi: https://doi.org/10.1051/0004-6361/202038525

Contribution: M. Albekioni contributed to solving the inviscid problem analytically with Prof. L. Gizon. She has reviewed the manuscript together with co-authors.

Abstract

Retrograde-propagating waves of vertical vorticity with longitudinal wavenumbers between 3 and 15 have been observed on the Sun with a dispersion relation close to that of classical sectoral Rossby waves. The observed vorticity eigenfunctions are symmetric in latitude, peak at the equator, switch sign near $20° - 30°$, and decrease at higher latitudes.

We search for an explanation that takes solar latitudinal differential rotation into account.

In the equatorial β plane, we studied the propagation of linear Rossby waves (phase speed $c < 0$) in a parabolic zonal shear flow, $U = -\overline{U}\,\xi^2 < 0$, where $\overline{U} = 244\ ms^{-1}$ and ξ is the sine of latitude.

In the inviscid case, the eigenvalue spectrum is real and continuous, and the velocity stream functions are singular at the critical latitudes where $U = c$. We add eddy viscosity to the problem to account for wave attenuation. In the viscous case, the stream functions solve a fourth-order modified Orr-Sommerfeld equation. Eigenvalues are complex and discrete. For reasonable values of the eddy viscosity corresponding to supergranular scales and above (Reynolds number $100 \leq Re \leq 700$), all modes are stable. At fixed longitudinal wavenumber, the least damped mode is a symmetric mode whose real frequency is close to that of the classical Rossby mode, which we call the R mode. For $Re \approx 300$, the attenuation and the real part of the eigenfunction is in qualitative agreement with the observations (unlike the imaginary part of the eigenfunction, which has a larger amplitude in the model).

Each longitudinal wavenumber is associated with a latitudinally symmetric R mode trapped at low latitudes by solar differential rotation. In the viscous model, R modes transport significant angular momentum from the dissipation layers toward the equator.

1. Introduction

In the atmosphere of Earth, Rossby (1939) waves are global-scale waves of radial vorticity that propagate in the direction opposite to rotation (retrograde). They originate in the conservation of vertical absolute vorticity, that is, the sum of planetary and wave vorticity (see, e.g., Platzman, 1968; Gill, 1982).

Equatorial Rossby waves have recently been observed on the Sun with longitudinal wavenumbers in the range $3 \leq m \leq 15$ (Löptien et al., 2018; Liang et al., 2019). In the corotating frame, their dispersion relation is close to that of classical sectoral ($l = m$) Rossby waves, $\omega = -2\Omega/(m+1)$, where $\Omega/2\pi = 453.1$ nHz is the equatorial rotation rate.

The observed variation of the eigenfunctions with latitude, however, differs noticeably from $P_m^m(\sin\lambda) \propto (\cos\lambda)^m$, where λ is the latitude, which is the expected answer for sectoral modes in a uniformly rotating sphere (e.g., Saio, 1982; Damiani et al., 2020). Instead, the observed eigenfunctions have real parts that peak at the equator, switch sign near $20^\circ - 30^\circ$, and decay at higher latitudes (Löptien et al., 2018). Their imaginary parts are small (Proxauf et al., 2020).

An ingredient that is obviously missing in models of solar Rossby waves is latitudinal differential rotation. The solar rotation rate decreases fast with latitude: the difference between the rotation rate at mid-latitudes and at the equator is not small compared to the frequencies of the Rossby waves of interest. For m larger than 5, we show that a critical latitude exists at which the (negative) wave frequency equals the (negative) differential rotation rate counted from the equator.

To capture the essential physics while keeping the problem simple, we chose to work in two dimensions and in the equatorial β plane. This simplification is acceptable for wavenumbers that are large enough (about ≥ 6).

The stability and dynamics of parabolic (Poiseuille) shear flows in the presence of critical layers was summarized by Drazin & Reid (2004), for example. Kuo (1949) included the β effect in the problem. In the inviscid case, critical layers lead to a singular eigenvalue problem (see, e.g., (Balmforth & Morrison, 1995)). The stream functions are continuous but not differentiable (Sect.4), thus they cannot be compared directly to actual observations of the vorticity. Because we also wish to explain the lifetime of the modes (Löptien et al., 2018), we introduce a viscous term in the Navier-Stokes equations to model damping by turbulent convection. As shown in Sect. 2, this leads to a new equation for the stream function: an Orr-Sommerfeld equation whose coefficients are modified by the β effect.

The viscosity removes singularities and the eigenfunctions are regular across the viscous critical layer (see Sect. 3). To solve the eigenvalue problem accurately, we use a numerical method based on the Chebyshev decomposition proposed by Orszag (1971). As shown in Sect. 5, the eigenvalue spectrum includes a symmetric Rossby mode in addition to the other modes that are known to exist in the $\beta = 0$ case (Mack, 1976). We focus on the eigenvalue problem here. We do not discuss the nonlinear dynamics in the critical layers, which would require solving the nonlinear evolution equation (e.g., Stewartson, 1977).

In addition to the practical advantages of studying 2D Rossby waves in the β plane, the physics of this problem has been extensively discussed in Earth and planetary sciences. In the terrestrial atmosphere and oceans, Rossby waves encounter critical layers (see Frederiksen & Webster, 1988; Vallis, 2006; **?**). They play a role in the global dynamics by transporting angular momentum through Reynolds stresses, and they modify the mean flow (e.g., Bennett & Young, 1971; Webster, 1973; Geisler & Dickinson, 1974).

Our model can be further extended to include the effect of the solar meridional flow using the method of Orszag (1971), see Sect. 6. In Sect. 7 we compare the predictions of the model to solar observations of the mode frequencies and damping rates and to observations of the vorticity eigenfunctions. Finally, in Sect. 8 we discuss the implications of the model for angular momentum transport and the dynamics of solar differential rotation.

2. Waves in a sheared zonal flow: Equations of motion in the equatorial β plane

In the equatorial β plane, we study the propagation of 2D Rossby waves through a steady zonal flow representative of solar differential rotation. Several β-plane approximations have been proposed (see, e.g., Dellar, 2011). Here we choose the sine transformation:

$$x = R\phi, \tag{64}$$

$$y = R \sin \lambda, \qquad -R \leq y \leq R, \tag{65}$$

where ϕ is longitude, λ is latitude, and $R = 696$ Mm is the solar radius. The x coordinate increases in the prograde direction, and the y coordinate increases northward. To first order in y/R, the x and y components of the velocity vector

in the β plane are equal to their ϕ and λ components on the sphere (Ripa, 1997), respectively.

The total velocity is the sum of the background zonal flow $U(y)\hat{\mathbf{x}}$ and the horizontal wave velocity $\mathbf{u}(x, y, t)$ with

$$\mathbf{u}(x, y, t) = u_x(x, y, t)\hat{\mathbf{x}} + u_y(x, y, t)\hat{\mathbf{y}}. \tag{66}$$

By choice, $U(0) = 0$ at the equator. The latitudinal shear is specified by the parabolic (Poiseuille) profile

$$U(y) = -\overline{U}\,(y/R)^2, \tag{67}$$

where the amplitude $\overline{U}$ is chosen such that $U(y)$ approximates the solar surface differential rotation at low and mid-latitudes. From the standard solar angular velocity profile given by Beck (2000), $\Delta\Omega = -0.35[(y/R)^2 + (y/R)^4]$ μrad s^{-1}, we find that the value $\overline{U} = 244$ m s^{-1} is a good choice, see Fig. 19.

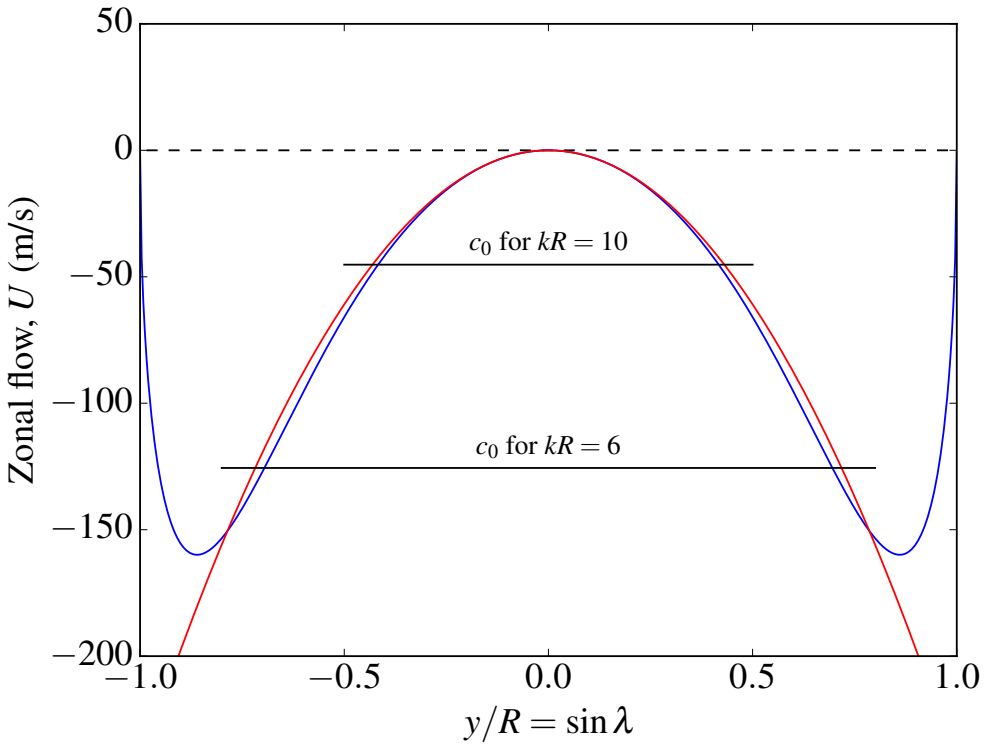

Figure 19: Parabolic zonal flow U (red curve, Eq. 67) in the frame rotating at the equatorial rotation rate, which approximates the solar rotational velocity at the photosphere (blue curve). The horizontal black lines indicate the phase speed of Rossby waves, $c_0 = -(\beta - U'')/k^2$, for longitudinal wavenumbers $kR = 6$ and $kR = 10$. At critical latitudes, $U = c_0$.

The 2D Navier-Stokes equations in the equatorial β plane are

$$\left(\frac{\partial}{\partial t} + U\frac{\partial}{\partial x}\right)u_x + u_y U' + \mathbf{u}\cdot\nabla u_x = -\frac{1}{\rho}\frac{\partial p}{\partial x} + \nu\Delta u_x + f u_y, \tag{68}$$

$$\left(\frac{\partial}{\partial t} + U\frac{\partial}{\partial x}\right)u_y + \mathbf{u}\cdot\nabla u_y = -\frac{1}{\rho}\frac{\partial p}{\partial y} + \nu\Delta u_y - f u_x, \tag{69}$$

where ν is the viscosity, and the equatorial Coriolis parameter is $f = \beta y$ with $\beta = 2\Omega/R$. The prime denotes a derivative, for example, $U' = \mathrm{d}U/\mathrm{d}y$.

To enforce mass conservation, we introduce the stream function Ψ such that

$$u_x = \frac{\partial\Psi}{\partial y}, \qquad u_y = -\frac{\partial\Psi}{\partial x}. \tag{70}$$

Assuming a barotropic fluid, we can eliminate the pressure term by combining the two components of the momentum equation to obtain

$$\left(\frac{\partial}{\partial t} + U\frac{\partial}{\partial x}\right)\Delta\Psi + (\beta - U'')\frac{\partial\Psi}{\partial x} + (\mathbf{u}\cdot\nabla)\Delta\Psi = \nu\,\Delta^2\Psi. \tag{71}$$

3. Critical latitudes

3.1. Linear inviscid case: critical points

In the linear inviscid case, we search for wave solutions of the form

$$\Psi(x, y, t) = Re\left\{\psi(y)\exp[i(kx - \omega t)]\right\}. \tag{72}$$

When the nonlinear and viscous terms are dropped, Eq. (71) becomes the Rayleigh-Kuo equation (Kuo, 1949),

$$(U - c)\left(-k^2\psi + \psi''\right) + (\beta - U'')\,\psi = 0, \tag{73}$$

where $c = \omega/k$ is the phase speed. This equation differs from the RayleighLord Rayleigh (1879) equation only through the β term. It can be rewritten as a Helmholtz equation,

$$\psi'' + K(y)\psi = 0, \tag{74}$$

with

$$K(y) = -k^2 + \frac{\beta - U''}{U - c}. \tag{75}$$

The squared latitudinal wavenumber, $K(y)$, is singular at the critical points $y = \pm y_c$ such that $U(y_c) = c$. The critical points divide the low-latitude region where the solution is locally oscillatory ($K > 0$ for $|y| < y_c$) from the high-latitude regions, where it is locally evanescent ($K < 0$ for $|y| > y_c$).

Equation (73), supplemented by boundary conditions $\psi(\pm R) = 0$, is an eigenvalue problem that can be solved in the complex plane. It admits a continuum of neutral modes with real eigenfrequencies. According to Rayleigh's theorem (adapted for the Rayleigh-Kuo equation, see Kuo, 1949), there is no discrete mode because $\beta - U'' \neq 0$ everywhere. We can thus solve the initial value problem given by Eq. (73) for any particular real value of c to obtain the associated eigenfunction (e.g., Drazin & Howard, 1966; Drazin et al., 1982; Balmforth & Morrison, 1995). These eigenfunctions are singular at the critical points.

Because U'' is constant in our problem and $U(0) = 0$, Eq. (75) implies that each mode can be associated with a value of $K(0)$ such that

$$c = -\frac{\beta - U''}{k^2 + K(0)}. \tag{76}$$

For equatorial propagation, $K(0) = 0$ is a natural choice, and we may consider the eigenvalue

$$c_0 = -(\beta - U'')/k^2 \tag{77}$$

as an example. In our case, $\beta - U'' = 1.12\beta$, therefore waves propagate faster than in the no-flow case. The critical points $y = \pm y_c$ where $U(\pm y) = c_0$ are given by

$$k y_c = \sqrt{\beta R^2/\overline{U} + 2} = 4.31. \tag{78}$$

Thus, for $kR > 4.31$, there are critical latitudes at $\lambda = \pm\lambda_c$, such that

$$\lambda_c = \arcsin(4.31/kR). \tag{79}$$

To obtain the eigenfunctions, Eq. (73) should be solved separately for $|y| < y_c$ and $|y| > y_c$. The analytical and numerical solutions are discussed in Sect. 4. The stream function is continuous ($u_y = -ik\psi$ is continuous), but its first and second derivatives diverge at the critical layer (see, e.g., Haynes, 2003).

3.2. Viscous critical layer

Bulk viscosity removes singularities. The linear viscous equation for ψ is

$$(c - U)\,(-k^2\psi + \psi'') - (\beta - U'')\,\psi = \frac{i\nu}{k}(k^4\psi - 2k^2\psi'' + \psi''''). \tag{80}$$

For $\beta = 0$, this is Orr-Sommerfeld equation (Orr, 1907; Sommerfeld, 1909). Equation (80) is a fourth-order differential equation, which requires four boundary conditions, such as $\psi(\pm R) = 0$ and $\psi'(\pm R) = 0$ for a no-slip boundary condition. The critical layer of the inviscid case is replaced by a viscous critical layer around $y = \pm y_c$. The width of this viscous layer, δ, is obtained by balancing the dominant viscous term with the dominant term on the left-hand side, $(U - c)\psi'' \sim \nu\psi''''/k$. Close to the viscous layer, we write $d/dy \sim 1/\delta$ and $U - c \approx U'(y_c)(y - y_c) \sim (\overline{U}y_c/R^2)\delta$, so that the width of the viscous layer is approximately

$$\delta/R \sim (ky_c\, Re)^{-1/3}, \tag{81}$$

where

$$Re = R\overline{U}/\nu \tag{82}$$

is the Reynolds number.

The width of the layer is controlled by Re. As discussed by Rüdiger (1989), ν should be understood as an eddy viscosity due to turbulent convection. As an example, we may estimate the Reynolds number associated with solar supergranulation. For supergranulation, the turbulent viscosity $\nu \approx 250$ km^{2}s^{-1} (Simon & Weiss, 1997; Duvall, Jr. & Gizon, 2000) implies $Re \approx 700$ and $\delta \approx 0.07R$ for $kR = 10$. Not surprisingly, the width of the viscous layer is comparable in this case to the spatial scale of supergranulation.

3.3 Nonlinear critical layer

In order to assess whether it is legitimate to drop the nonlinear term $(\mathbf{u}\cdot\nabla)\Delta\Psi$ in Eq. (71), we estimate the width of the nonlinear critical layer δ_{NL}. It is obtained by balancing the advection term $k(U-c)\psi''$ and the nonlinear term $u_y\psi'''$. We find

$$\delta_{NL}/R \sim \left(u_{\max}/\overline{U}\right)^{1/2} (ky_c)^{-1/2}, \tag{83}$$

where $u_{\max}$ is a characteristic velocity amplitude for the Rossby waves. On the Sun, Liang et al. (2019) measured $u_{\max} \approx 2$ ms^{-1} for the maximum latitudinal velocity of a mode at the equator. For $kR = 10$, the width of the nonlinear critical layer is $\delta_{NL} \approx 0.04R$.

Introducing the threshold $Re_* = (u_{\max}/\overline{U})^{-3/2}(ky_c)^{1/2}$, the ratio between the widths of the viscous and nonlinear critical layers is

$$\delta/\delta_{NL} \approx (Re/Re_*)^{-1/3}. \tag{84}$$

For $Re < Re_*$ the critical layer is linear and dominated by dissipation over the width δ. For $kR = 10$, we find $Re_* \approx 3000$, which is much larger than the Reynolds number $Re \approx 700$ estimated in the previous section for solar supergranulation. It is therefore reasonable to study the linear problem, as we do in the remainder of this paper. However, we caution that there is some uncertainty about the appropriate value for the viscosity.

4. Inviscid modes of oscillations

In the inviscid case, the spectrum for the Rayleigh-Kuo equation, Eq. (73), is real and continuous. We fix the value of c to c_0 (Eq. 77) and compute the corresponding eigenfunctions. There are two singular solutions, both real: a solution that is symmetric in latitude and an antisymmetric solution. These solutions can be obtained by solving the equation analytically or numerically in two distinct intervals, $0 \le y < y_c$ and $y_c \le y \le R$.

In the inner region, we solve the ODE with the conditions $\psi(0) = 1$ and $\psi'(0) = 0$ to obtain the symmetric solution. For the region $y > y_c$, we impose continuity with the inner solution and use the boundary condition $\psi(R) = 0$. The symmetric solution can be expressed as a series in each regions. We write $\psi(y) = \sum_{p\ge 0} a_p \xi^{2p}$ with $\xi = y/R$ for $|y| < y_c$ and $\psi(y) = \sum_{p\ge 1} b_p (\xi^2 - 1)^p$ for $|y| > y_c$. The coefficients a_p and b_p are computed by recurrence. when we set Set $\kappa = kR$ and $\xi_c = y_c/R$, the inner solution is given by

$$a_0 = 1, \tag{85}$$

$$a_1 = 0, \tag{86}$$

$$a_p = \frac{2(p-1)(2p-3)a_{p-1} - \kappa^2 a_{p-2}}{2\xi_c^2 p(2p-1)} \quad \text{for } p \ge 2. \tag{87}$$

For the outer solution,

$$b_2 = -\, b_1/4, \tag{88}$$

$$b_3 = -\,\frac{[\kappa^2 + 3(1-\xi_c^2)]b_2}{6(1-\xi_c^2)}, \tag{89}$$

$$b_p = -\,\frac{[(1-\xi_c^2)(2p-3) + 2(p-2)]b_{p-1}}{2(1-\xi_c^2)p} + \frac{[\kappa^2 - 2(p-2)(2p-5)]b_{p-2} + \kappa^2 b_{p-3}}{4(1-\xi_c^2)(p-1)p} \quad \text{for } p \geq 4. \tag{90}$$

The coefficient b_1 is chosen such that the solution is continuous at the critical point.

To validate the series solution, we also solved the problem numerically. In the inner region, we have an initial value problem that can be solved using classical libraries, for example `odeint` from `SciPy`. In the outer region, the problem is a boundary value problem that can be converted into an initial value problem using the shooting method (Keller, 1968).

We find an excellent agreement between the analytical and the numerical solutions, therefore we only plot the analytical solution in Fig. 20 for $kR = 10$. The symmetric eigenfunction ψ_s switches sign before the critical latitude and evanesces above it. The location of the critical layer is close to the zero-crossing of the observed vorticity eigenfunctions from Löptien et al. (2018) and Proxauf et al. (2020). Unfortunately, in the inviscid case, the vorticity $\zeta = k^2\psi - \psi''$ diverges at the critical latitude and thus the comparison with the observations is difficult.

We note that for each eigenvalue $c = c_0$ an antisymmetric eigenfunction, ψ_a, also exists. This solution can be obtained like above, but with different boundary conditions at the equator. We set $\psi_a(0) = 0$ and $\psi_a'(0) = \psi_0'$, where ψ_0' can be chosen to control the maximum value of ψ_a, for example unity. The other conditions are the same as before, that is, $\psi_a(\pm R) = 0$ and ψ_a continuous at the critical point. The antisymmetric solution can be expanded as $\psi_a(y) = \sum_{p\geq 0} A_p \xi^{2p+1}$ for $|y| < y_c$ and $\psi_a(y) = \sum_{p\geq 1} B_p \xi(\xi^2-1)^p$ for $|y| > y_c$. The coefficients A_p an B_p are again obtained by recurrence. Figure 21 shows example antisymmetric eigenfunctions.

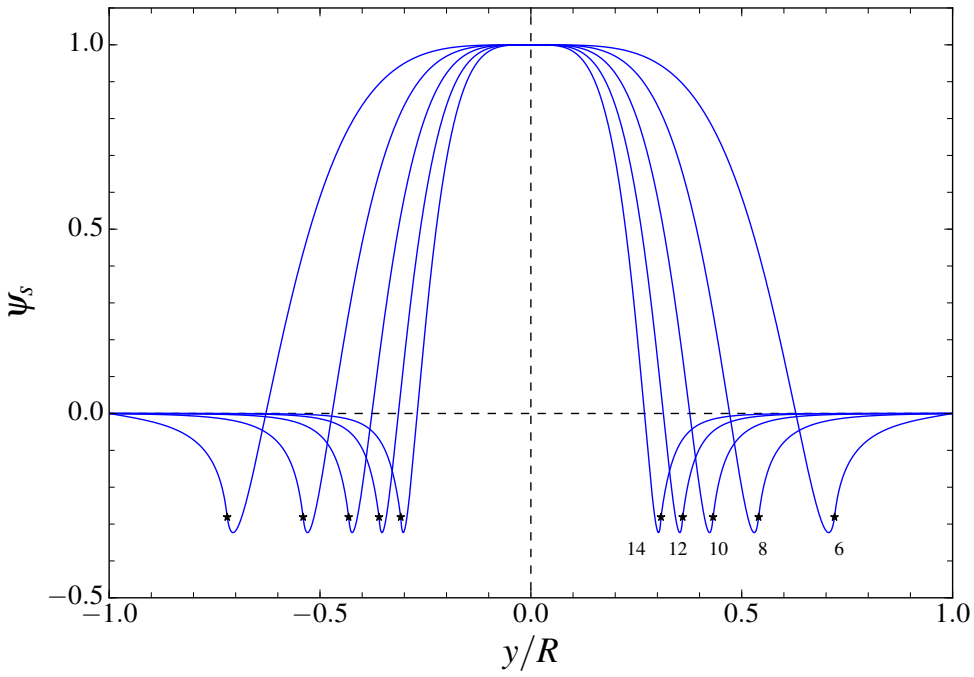

Figure 20: Symmetric inviscid eigenfunctions for the eigenvalue $c_0 = -(\beta - U'')/k^2$ and $kR = 6, 8, 10, 12$ and 14. The stars mark the critical points.

5. Viscous modes of oscillation

5.1. Numerical method

In order to remove the singularities at the critical latitudes, we now include viscosity. The viscosity is specified through the Reynolds number, Re, which is a free parameter in our problem. For example, $Re = 700$ for supergranular turbulent viscosity.

To facilitate the numerical resolution of the modified Orr-Sommerfeld equation, Eq. (80), it is convenient to introduce dimensionless quantities. We define $\xi = y/R$, $\kappa = kR$, and $\hat{\beta} = \beta R^2/\overline{U}$. The dimensionless eigenvalues $\hat{c} = c/\overline{U}$ and eigenfunctions $\hat{\psi}(\xi) = \psi(y)/(R\overline{U})$ solve the equation

$$(\hat{c} + \xi^2)\hat{D}\hat{\psi} - (\hat{\beta} + 2)\hat{\psi} = i(\kappa\, Re)^{-1}\, \hat{D}^2\hat{\psi}, \tag{91}$$

where $\hat{D} = -\kappa^2 + d^2/d\xi^2$ is the Laplacian, and the prime now denotes derivation with respect to ξ. For $\overline{U} = 244$ ms^{-1}, we have $\hat{\beta} = 16.4$. We consider values of the dimensionless longitudinal wavenumber in the range $8 \leq \kappa \leq 15$.

We follow the numerical approach of Orszag (1971), originally developed for the Orr-Sommerfeld eigenvalue problem. We use the Matlab package `Chebfun` to

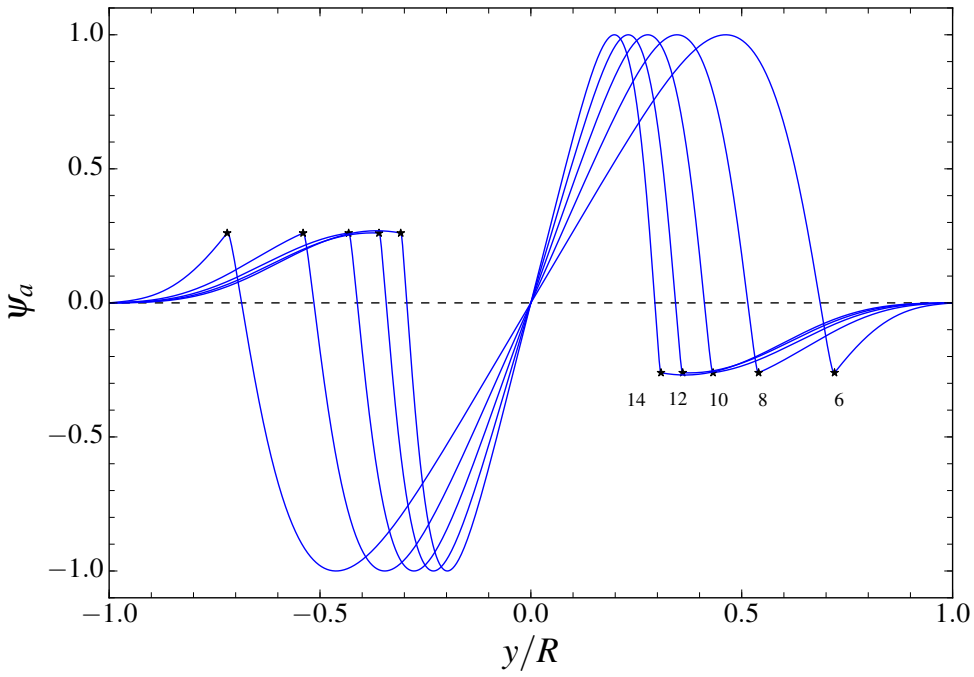

Figure 21: Antisymmetric inviscid eigenfunctions for $c = c_0$ and $kR = 6, 8, 10, 12$ and 14. The stars mark the critical points.

project functions onto Chebyshev polynomials and to compute spatial derivatives analytically (Driscoll et al., 2014). This package also provides practical tools to solve differential equations and eigenvalue problems (only a few lines of codes are needed).

To obtain the symmetric solutions, we solve the above eigenvalue problem on $[0, 1]$ with the boundary conditions

$$\hat{\psi}_s'(0) = \hat{\psi}_s'''(0) = 0 \quad \text{and} \quad \hat{\psi}_s(1) = \hat{\psi}_s'(1) = 0. \tag{92}$$

The antisymmetric solutions are obtained by setting

$$\hat{\psi}_a(0) = \hat{\psi}_a''(0) = 0 \quad \text{and} \quad \hat{\psi}_a(1) = \hat{\psi}_a'(1) = 0. \tag{93}$$

In both cases, the numerical solutions (eigenvalues and eigenfunctions) are complex.

5.2. Spectrum

In Fig. 22 the eigenvalues $c = c_r + ic_i$ are shown in the complex plane for $\kappa = 10$ and $Re = 300$. In the figure, these eigenvalues are normalized by $|c_0| > 0$.

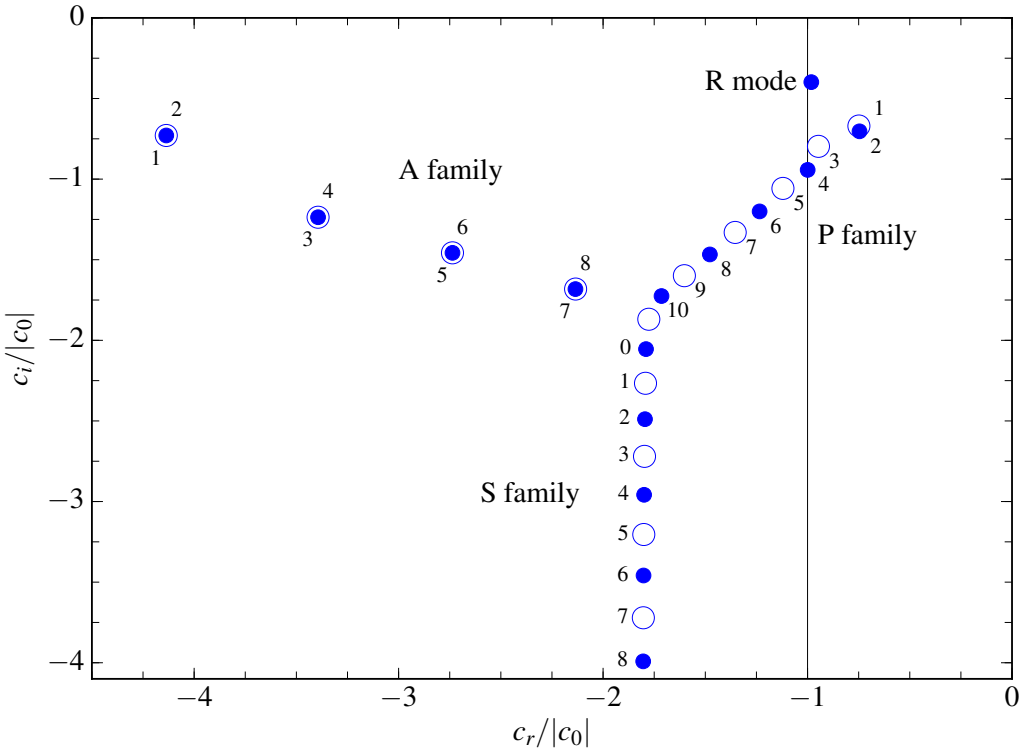

Figure 22: Eigenvalues $c = c_r + ic_i$ in the complex plane for $kR = 10$ and $Re = 300$, normalized by the reference eigenvalue $|c_0| = (\beta - U'')/k^2$. The R mode is clearly identifiable (the least damped mode), as are the three families of modes: the wall modes (A family), the center modes (P family), and the damped modes (S family). The modes with symmetric eigenfunctions are shown with full circles and those with antisymmetric eigenfunctions with open circles. All modes have $c_r < 0$ and $c_i < 0$, i.e. they are stable and propagate in the retrograde direction. The vertical line corresponds to the phase speed of the standard Rossby wave, $c_r = c_0$. The modes in each family are labeled with integers that increase with attenuation.

All modes are stable because none of the imaginary parts of the eigenfrequencies are positive. In the complex plane, the eigenvalues are distributed along three main branches that correspond to different types of eigenfunctions. The same branches appear in the standard plane Poiseuille problem; they were called A, P and S by Mack (1976). Example eigenfunctions are displayed in Fig. 23 and Fig. 24. The A branch, for which the eigenfunctions have large amplitudes at high latitudes, refers to the "wall modes". The P branch refers to the "center modes", which oscillate near the viscous layers. The S branch corresponds to the "damped modes" (Schensted, 1961). Schensted (1961) showed that the A and P branches have a finite number of eigenvalues and the S branch has an infinite number of eigenvalues. She obtained approximate equations for the three branches. We labelled the modes

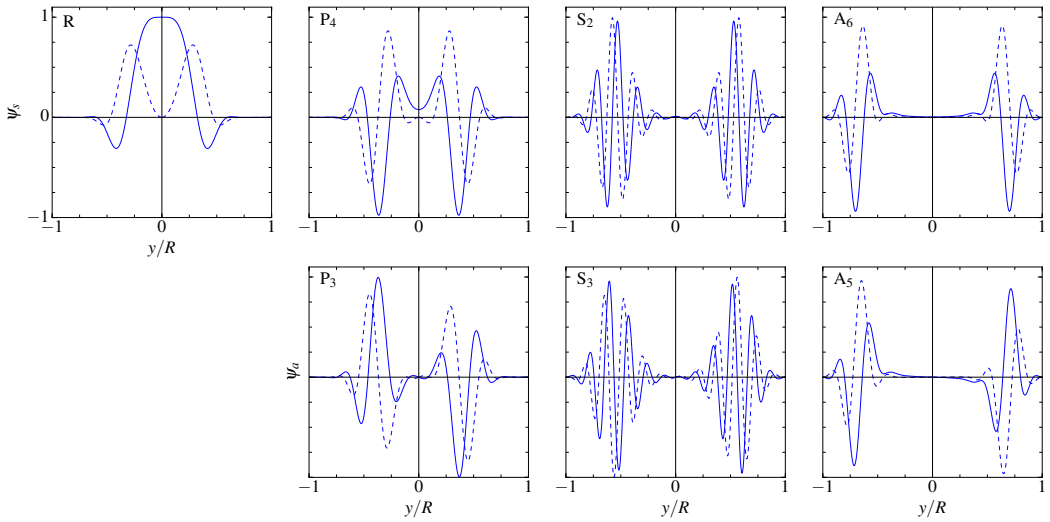

Figure 23: Eigenfunctions for the symmetric modes R, P_4, S_2, and A_6 (*top row,* ψ_s) and for the antisymmetric modes P_3, S_3, and A_5 (*bottom row,* ψ_a). See Fig. 22 for the position of the corresponding eigenvalues in the complex plane. The real and imaginary parts are plotted with solid and dashed lines respectively. The modulus of the eigenfunctions is normalized to one. By choice, all imaginary parts are zero at the equator.

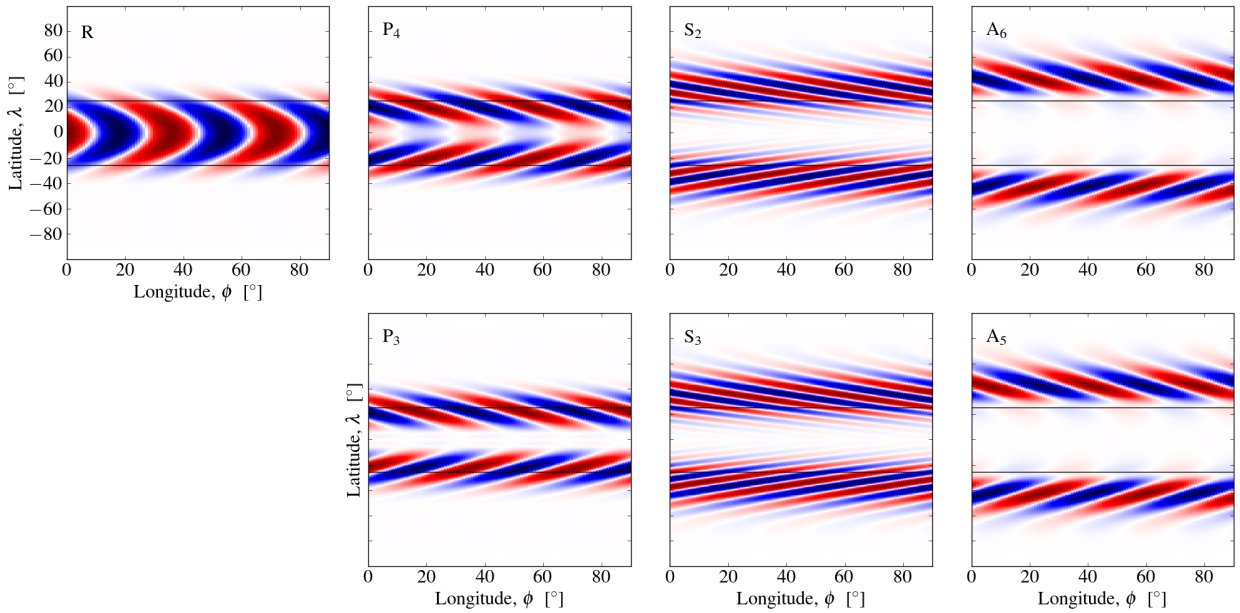

Figure 24: Stream functions in real space for all the modes shown in Fig. 23. The horizontal black lines show the central latitudes of the viscous layers, $\lambda = \pm 25°$ for $kR = 10$. The R mode (*top left panel*) is confined to the equatorial region between the viscous layers.

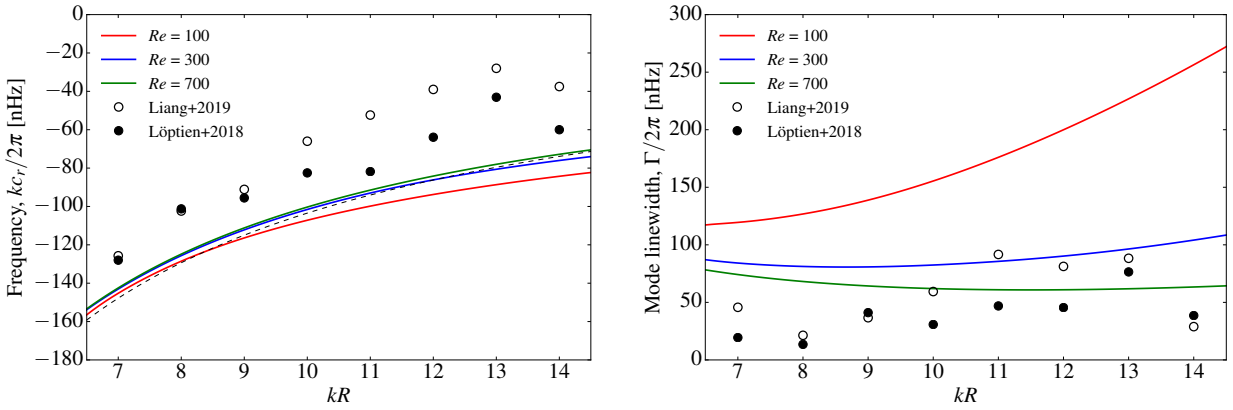

Figure 25: *Left panel*: R-mode dispersion relations $\omega = kc_r$ for $Re = 100$, 300 and 700 (red, blue and green). The dashed black curve is the reference dispersion relation $\omega = kc_0$. For comparison, the frequencies of each mode m observed by Löptien et al. (2018) and Liang et al. (2019) are multiplied by the factor $(m + 1)/kR$ and plotted at abscissa kR (this simple conversion factor is derived from the dispersion relations for classical Rossby waves in spherical and local Cartesian geometries). *Right panel*: Plot of $\Gamma = -2kc_i$ for $Re = 100$, 300 and 700. The observed full widths at half maximum for each mode m are plotted at abscissa kR for comparison.

with integers in Fig. 22, such that even integers refer to the symmetric eigenfunctions and odd integers to the antisymmetric eigenfunctions. As noted by Drazin & Reid (2004), the even and odd modes in the A branch have nearly the same eigenfrequencies. As seen in Fig. 24, the A modes have significant amplitudes only at latitudes above the viscous layers.

Our problem differs from the standard plane Poiseuille problem through the β term. As a result, one additional mode appears in the eigenvalue spectrum (Fig. 22). This mode, which we call the R mode for an obvious reason, is symmetric and has an eigenfrequency whose real part is close to that of the classical equatorial Rossby mode, $c_r \approx c_0$. The R mode has the longest lifetime in the spectrum. It is also the mode for which $\int_{-1}^{1} |\hat{\psi}''|^2 d\xi$ is the smallest. As shown in Fig. 23, the real part of the R-mode eigenfunction resembles the eigenfunction of the symmetric mode found in the inviscid case (Fig. 20), except that it is smooth everywhere (no infinite derivative at the critical points). In the viscous case, the complex R-mode eigenfunctions look like chevrons in real space (Fig. 24).

For some modes in the P branch, c_r is close to c_0 (P_3 and P_4), but these modes have a far shorter lifetime than the R mode (by a factor of two to three at $Re = 300$) and eigenfunctions that differ significantly from the observations.

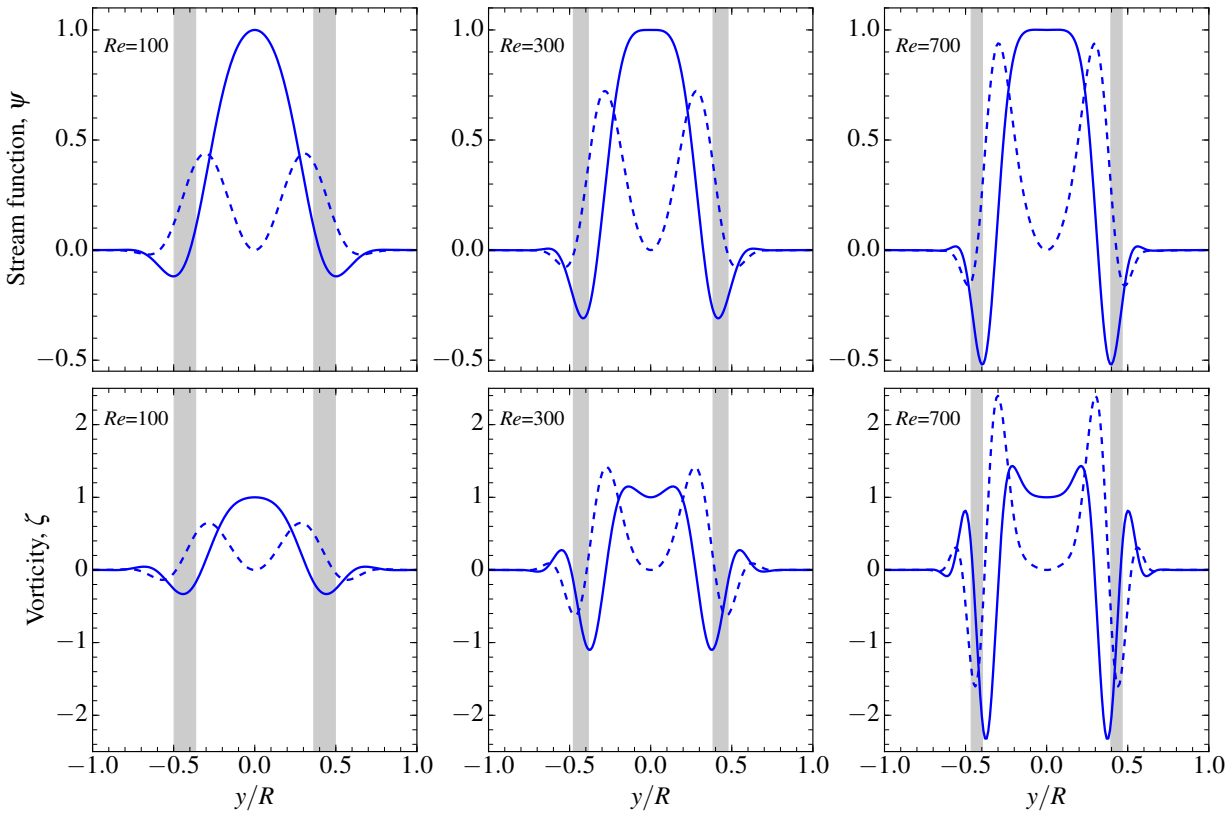

Figure 26: Stream function (*top row*) and vertical vorticity (*bottom row*) for R modes with $kR = 10$. The Reynolds number is $Re = 100$, 300 and 700 from left to right. The solid and dashed curves correspond to the real and imaginary parts. The shaded areas indicate the locations of the viscous critical layers for each value of Re.

5.3. R modes

Figure 25 shows the R-mode eigenfrequencies as a function of wavenumber kR for different values of the viscosity. The value of the viscosity has a rather weak effect on the dispersion relation. At fixed wavenumber, the real part of the eigenfrequency changes with Re by less than 10 % over the range $100 \geq Re \geq 700$. On the other hand, the imaginary part c_i changes significantly with the value of Re. For $Re < 700$, the attenuation $\Gamma = -2kc_i$ increases with k. For $Re = 300$, we find that the theoretical mode linewidths ($\Gamma/2\pi = -kc_i/\pi$ in nHz) are in the range 70 – 100 nHz, that is, they agree reasonably well with the observed mode line widths ($\Gamma/2\pi$ from Liang et al., 2019). The e-folding lifetime of a mode is given by $\tau = 2/\Gamma$.

The top row of Fig. 26 shows the R-mode stream functions for different values of the Reynolds number. The normalization is such that at $\xi = 0$, the real part is one and the imaginary part is zero. As Re decreases, the stream function varies more slowly around the viscous layer, and its imaginary part decreases in amplitude. The bottom row of Fig. 26 shows the vertical vorticity eigenfunctions. For $Re = 700$, the vorticity varies fast near the viscous layer; here ψ'' is largest.

6. Effect of the meridional flow

In addition to the rotational shear U, we consider the effect of the meridional flow V on the R mode. The total velocity is

$$U(y)\hat{\mathbf{x}} + V(y)\hat{\mathbf{y}} + \mathbf{u}(x, y, t), \tag{94}$$

where the meridional flow is approximated by

$$V(y) = \overline{V}\,\frac{y}{R}\left[1 - \left(\frac{y}{R}\right)^2\right], \tag{95}$$

with

$$\overline{V} = \frac{3\sqrt{3}}{2} \times 15 ms^{-1} \tag{96}$$

The value of $\overline{V}$ is chosen such that the maximum value of V is 15 ms^{-1} (near latitude $\lambda = 35°$).

When the meridional flow is included, the 2D linearized Navier-Stokes equa-

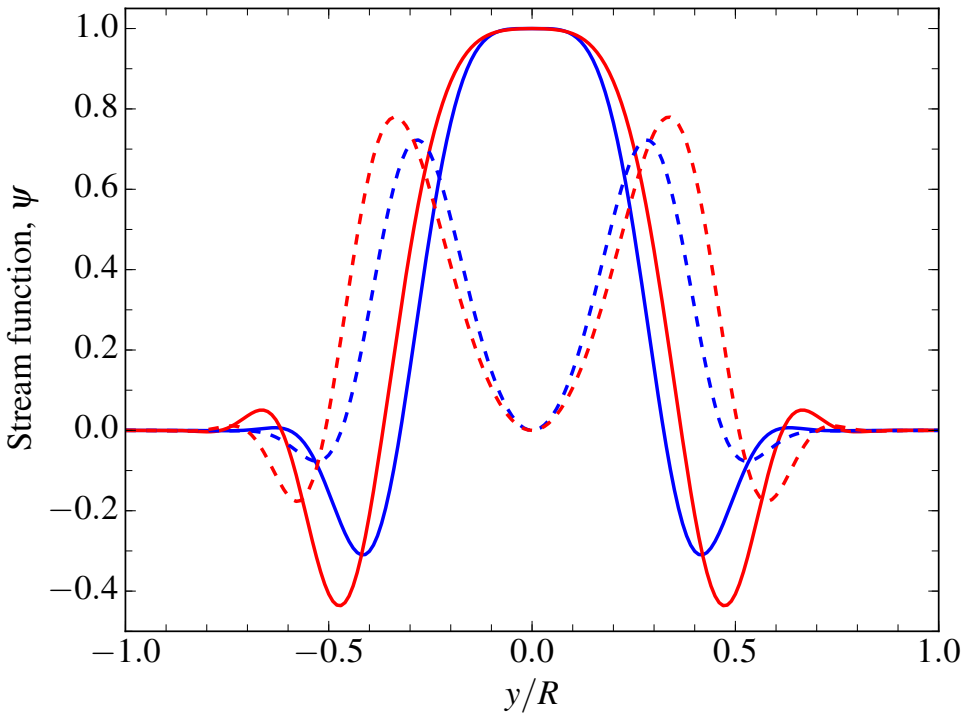

Figure 27: Effect of the meridional flow V on the R-mode stream function for $Re = 300$ and $kR = 10$ (red curves). For comparison, the blue curves show the stream function when only the zonal flow U is included. The real and imaginary parts correspond to the solid and dashed curves.

tions in the equatorial β plane become

$$\left(\frac{\partial}{\partial t} + U\frac{\partial}{\partial x} + V\frac{\partial}{\partial y}\right)u_x + u_y U' = -\frac{1}{\rho}\frac{\partial p}{\partial x} + \nu\Delta u_x + f u_y, \tag{97}$$

$$\left(\frac{\partial}{\partial t} + U\frac{\partial}{\partial x} + V\frac{\partial}{\partial y}\right)u_y + u_y V' = -\frac{1}{\rho}\frac{\partial p}{\partial y} + \nu\Delta u_y - f u_x. \tag{98}$$

When these equations are combined, the fourth-order differential equation for the stream function (linear problem) is

$$\left(c - U + \frac{iV'}{k}\right)D\psi + \frac{iV}{k}D\psi' - (\beta - U'')\,\psi = \frac{i\nu}{k}D^2\psi, \tag{99}$$

with $D = -k^2 + d^2/dy^2$. Compared to the previous problem with U only, the term in front of $D\psi$ is now complex, and an additional term involving the first and third derivatives of the stream function appears.

We consider only the symmetric solutions and focus on the R mode. The boundary conditions are $\psi'(0) = \psi'''(0) = 0$ and $\psi(R) = \psi'(R) = 0$. Like before, we follow the procedure by Orszag (1971) to solve the eigenvalue problem.

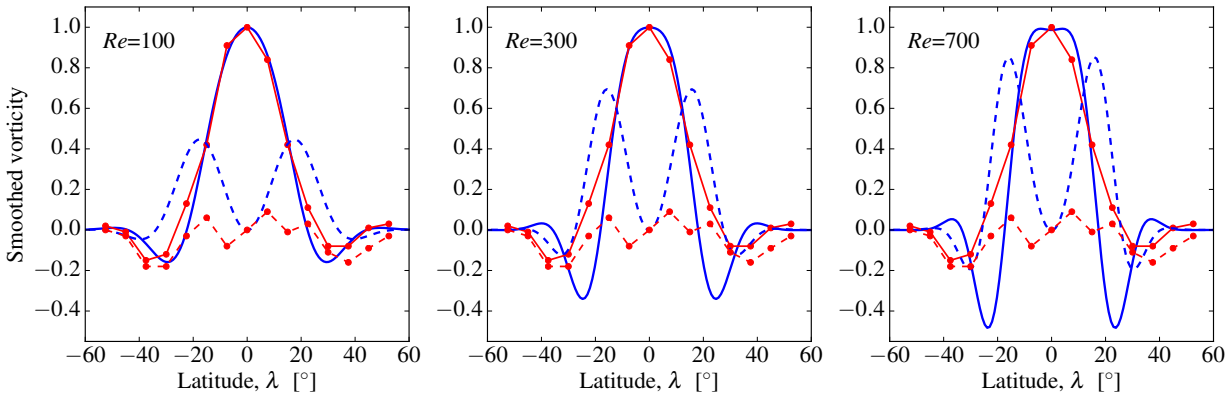

Figure 28: Real (blue solid lines) and imaginary (blue dashed lines) parts of the R-mode vertical vorticity at $kR = 10$ after smoothing the maps of horizontal velocities with a 2D Gaussian kernel with $\sigma = 6°$. Three different values of Re are shown. For comparison, the red curves with points show the ring-diagram helioseismic observations for $m = 10$ near the surface (Proxauf et al., 2020).

The eigenfrequencies are not affected significantly by the meridional flow. For $Re = 300$ and $kR = 10$, we find $c/|c_0| = -0.986 - 0.446i$ when U and V are included, compared to $c/|c_0| = -0.982 - 0.398i$ when only U is included. Figure 27 shows the real and imaginary parts of the R-mode eigenfunction at fixed $kR = 10$ for $Re = 300$. The meridional flow V has a small but measurable effect on the ψ eigenfunction: it is stretched towards higher latitudes, and its real part has a larger amplitude near the viscous layers.

7. Comparison with observations

Proxauf et al. (2020) measured and characterized the vorticity eigenfunctions of the solar Rossby modes using a ring-diagram helioseismic analysis. To enable a direct comparison between observations and theory, some smoothing must be applied to the model because the observed flows have a resolution of only $\sigma = 6°$ in ϕ and λ. After remapping the theoretical flows on a longitude-latitude grid, we convolve u_ϕ and u_λ with a 2D Gaussian kernel with standard deviation σ in both coordinates. From the smoothed velocities, we compute the vertical vorticity. As seen in Fig. 28, the smoothing has a significant effect on the theoretical vorticity near the viscous layer.

The functional form of the real part of the observed eigenfunction was described by several parameters by Proxauf et al. (2020): a full width at half maxi-

mum W, the latitude λ_0 at which the sign changes, the latitude $\lambda_{\rm min}$ at which the vorticity is most negative, and the value $\zeta_{\rm min}$ of the vorticity at $\lambda_{\rm min}$. These parameters are provided in Table 1 for three different values of kR in three different cases: (a) smoothed theoretical vorticity when the zonal shear flow U is included, (b) smoothed theoretical vorticity when U and V are both included and (c) observations from Proxauf et al. (2020). For $Re = 300$, we find that the widths for cases (a) and (b) are within $\approx 3^\circ$ of the observed values. For (a), the zero-crossing latitude varies from $\lambda_0 = 17^\circ$ for $kR = 12$ to $\lambda_0 = 21^\circ$ for $kR = 8$. For (b) the values of λ_0 are slightly higher by $\approx 2^\circ$, while the observed $\lambda_0 \approx 28^\circ$ does not vary much with k. The theoretical values of $\lambda_{\rm min}$ vary slightly faster with kR than λ_0, and theory agrees better with observations for $kR = 8$. The observed values of $\zeta_{\rm min}$ range from -0.3 to -0.1, about half of the theoretical values. However, the values of $\zeta_{\rm min}$ depend on Re, with more negative values for larger values of Re. On the other hand, the values of W, λ_0, and $\lambda_{\rm min}$ in the table are not very sensitive to the Reynolds number for $100 \leq Re \leq 700$.

The imaginary part of the vorticity eigenfunctions is far more difficult to measure (Proxauf et al., 2020). It is significantly different from zero for some values of m, but it is noisy, and its functional form cannot be described by a simple parametric function. According to Proxauf et al. (2020), the sign of the observed imaginary part appears to be positive for the lowest values of m and negative for $m > 5$. The comparison provided in Fig. 28 shows that, at latitudes below the viscous layer, the amplitude of the imaginary part is far higher in the model than in the observations.

8. R-mode momentum fluxes

The complex eigenfunctions in our model imply that R modes transport a net momentum flux in latitude. It is interesting to obtain an estimate of this momentum flux (even though the model eigenfunctions have imaginary parts that differ from the observations). The purpose of this exercise is to establish whether R modes play a significant role in the balance of forces that shape differential rotation.

We consider a time-dependent zonal flow $U(y, t)$ that evolves slowly according to the x-component of the momentum equation averaged over x (see, e.g., Geisler & Dickinson, 1974):

$$\frac{\partial U}{\partial t} = -\frac{\partial}{\partial_y}\langle u_x u_y \rangle + \nu U'' + V(\beta y - U'), \tag{100}$$

Table 1: Parameters W, λ_0, $\lambda_{\rm min}$ and $\zeta_{\rm min}$ that characterize the functional form of the real part of the R-mode vorticity eigenfunctions. **Notes**. The smoothed eigenfunctions from theory ($Re = 300$) are given for the cases when (a) only the zonal flow U is included and (b) both U and the meridional flow V are included. The theoretical values are compared with the observations from Proxauf et al. (2020).

	Case	$kR = 8$	$kR = 10$	$kR = 12$
W (°)	U	17.6	13.1	11.2
	U & V	20.2	15.8	13.1
	Obs.	17.1 ± 0.8	14.7 ± 1.1	13.8 ± 1.4
λ_0 (°)	U	21.1	18.4	17.5
	U & V	24.8	20.2	19.4
	Obs.	25.8	27.8 ± 1.6	28.9 ± 1.0
$\lambda_{\rm min}$ (°)	U	29.3	24.8	22.9
	U & V	32.9	27.4	24.8
	Obs.	36.5 ± 1.8	34.5 ± 2.1	39.8 ± 1.8
$\zeta_{\rm min}$	U	−0.69	−0.35	−0.17
	U & V	−0.86	−0.49	−0.28
	Obs.	−0.28	−0.11	−0.14

where the prime denotes a y-derivative and angle brackets $\langle\cdot\rangle$ denote the average over x. We used $\partial_x u_x + \partial_y u_y = 0$ to obtain the term involving $\langle u_x u_y\rangle$ on the right-hand side of the equation. The various terms in Eq. (100) have been discussed in detail by Rüdiger (1989) in spherical geometry. These terms must balance exactly to explain the steady-state differential rotation.

The horizontal Reynolds stress has two components, the first due to rotating turbulent convection (the Λ effect), and the second due to the Rossby waves,

$$\langle u_x u_y\rangle = \langle u_x u_y\rangle_\Lambda + \langle u_x u_y\rangle_{\rm R}. \tag{101}$$

We estimate $\langle u_x u_y\rangle_{\rm R}$ in the model for a single R mode. It is related to the stream function through

$$\begin{aligned}\langle u_x u_y\rangle_{\rm R} &= -\left\langle \frac{\partial\Psi}{\partial y}\,\frac{\partial\Psi}{\partial x}\right\rangle \\ &= -\left\langle {\rm Re}\left(\psi' e^{ik(x-c_r t)-t/\tau}\right)\,{\rm Re}\left(ik\psi e^{ik(x-c_r t)-t/\tau}\right)\right\rangle \\ &= -\frac{k}{2}\,{\rm Im}\left(\psi'\psi^*\right)e^{-2t/\tau} =: Q_{xy}\,e^{-2t/\tau},\end{aligned} \tag{102}$$

where τ is the mode lifetime mentioned in Sect. 5.3. We normalize the R-mode stream function such that the velocity amplitude at the equator is equal to its observed value,

$$k\psi(0) = u_{\rm max} \approx 2ms^{-1}. \tag{103}$$

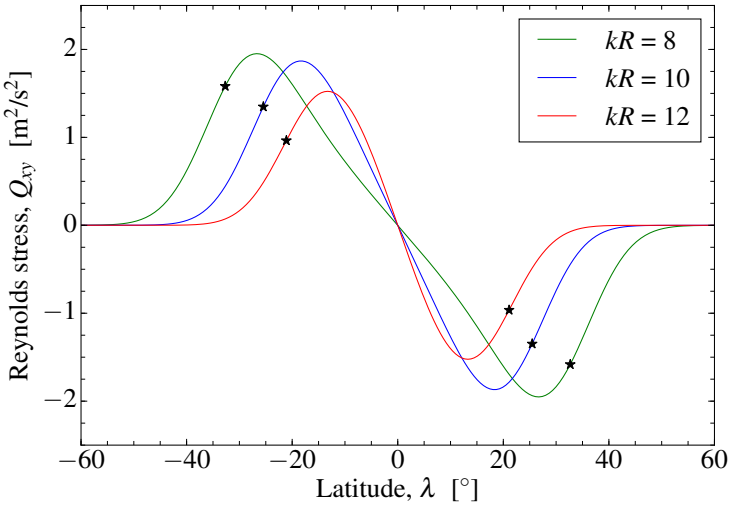

Figure 29: Horizontal Reynolds stress Q_{xy} vs. latitude for R modes with $kR = 8$, 10 and 12. The Reynolds number is $Re = 300$, and mode amplitudes were normalized according to Eq. (103). Both the zonal flow U and the meridional flow V were included to compute the mode eigenfunctions. The stars show the locations of the viscous critical layer for the different values of kR.

The Reynolds stress Q_{xy} is plotted in Fig. 29 for R modes with $Re = 300$ and $kR = 8$, 10 and 12. We find that $Q_{xy} < 0$ in the north, below the viscous critical layer. For example, for $kR = 10$, Q_{xy} reaches the minimum value of -2 m^{2}s^{-2} at latitude 20°. This means that R modes transport angular momentum from the dissipation layer to the equator, or in the other words, they reinforce latitudinal differential rotation. This is the expected result for idealized Rossby waves incident on a critical layer (see, e.g., Vallis, 2006).

Summing Q_{xy} over several R modes would lead to a horizontal Reynolds stress that is comparable in amplitude and sign to the value reported at large spatial scales by Hathaway et al. (2013). On the other hand, Q_{xy} has the opposite sign and is much smaller in amplitude than the (viscous) Reynolds stress associated with convective flows at supergranulation scales (Hanasoge et al., 2016, their figure 10). The acceleration $-\partial_y Q_{xy}$ is plotted in Fig. 30 and compared to the measurements described above. The Rossby waves in our model contribute to the equatorial acceleration at a significant level.

9. Conclusion

Using a simple 2D setup in the β plane, we have shown that latitudinal differential rotation and viscosity must play an important role in shaping the horizontal

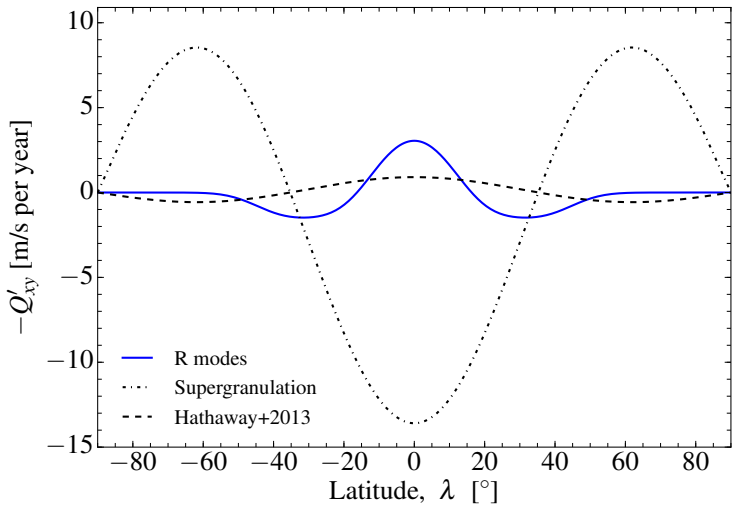

Figure 30: Equatorial acceleration $-\partial_y Q_{xy}$ obtained by superposition of nine viscous R modes for $kR = 7, 8, \ldots 15$ (solid blue curve). The dot-dashed and dashed curves show $-\partial_y \langle u_x u_y \rangle$ for supergranulation (Hanasoge et al., 2016, their figure 10) and larger-scale convection (Hathaway et al., 2013), respectively. For reference, the solar "torsional oscillation" has a typical amplitude of about ± 5 ms^{-1} (see, e.g., Lekshmi et al., 2018).

eigenfunctions of global-scale Rossby modes. Viscous critical layers form around latitudes where $c = U$. We find that only one symmetric mode, which we called the R mode, has an eigenvalue whose real part is close to that of the classical sectoral Rossby mode and whose imaginary part is close to the observed value when $Re \approx 300$. The real part of the vorticity eigenfunctions can be made to agree qualitatively with solar observations (unlike the imaginary part).

Treating this problem as a stability problem for a viscous Poiseuille flow in the β plane enabled us to connect our results to prior results in the fluids literature. For example, we used a well-established method to solve the Orr-Sommerfeld equation numerically, and we easily identified the known families of modes A, P, and S in the complex plane (eigenvalues and eigenfunctions). A new aspect of our work is that we identified the viscous R mode, which owes its existence to the β term in the equation. We find that the combination of the shear flow and the viscosity lead to chevron-shaped R-mode eigenfunctions, and thus to nonzero angular momentum transport by R modes. In our model, horizontal Reynolds stresses due to R modes lead to significant equatorial acceleration. Another original aspect of our work is that we studied the effect of the solar meridional flow on R modes. We found that the meridional flow affects the eigenfunctions to measurable levels. Reynolds stresses have significantly larger amplitudes when the meridional

flow is included, although the meridional flow plays a much smaller role than the differential rotation in shaping the eigenfunctions.

Sophisticated 3D models (but without background shear flow) also include Rossby waves as a possible mechanism to produce equatorial super-rotation in the atmospheres of planets (e.g., Liu & Schneider, 2011; Read & Lebonnois, 2018) and exoplanets (e.g., Showman & Polvani, 2011). Clearly, the present work will have to be extended to three dimensions (see, e.g., Watts et al., 2004, for the eigenvalues in the inviscid case) to account for the radial gradients of solar rotation measured by helioseismology. A better understanding of Rossby waves will also benefit from more realistic numerical experiments (see Bekki et al., 2019). Finally, we note that the model developed here can be used to estimate the temporal changes in the Rossby wave frequencies caused by the solar-cycle variations in the zonal flows (Goddard et al., 2020).

acknowledgements We thank Aaron Birch, Leonie Frantzen, Shravan Hanasoge (CSS), and Bastian Proxauf for useful discussions. Author contributions: L.G. proposed and designed research. L.G. and M.A. solved the inviscid problem analytically. D.F. solved the viscous problem numerically (code available at `https://edmond.mpdl.mpg.de/imeji/collection/50wepJqIODg7Jg13`). L.G. wrote the draft paper. All authors reviewed the final manuscript. Funding: L.G. acknowledges partial support from ERC Synergy Grant WHOLE SUN 810218 and NYUAD Institute Grant G1502. M.A. acknowledges funding from the Volkswagen Foundation and the Shota Rustaveli National Science Foundation of Georgia (SRNSFG grant N04/46). The computational resources were provided by the German Data Center for SDO through grant 50OL1701 from the German Aerospace Center (DLR).

3 Thesis discussion and conclusion

In recent years, Rossby waves attracted increased interest within the astrophysical research community. The growth of interest is related to the extensive data gathered by space missions, advances in data analysis techniques, and the development of new astrophysical areas such as asteroseismology. Following the observations of Rossby waves on the Sun (Löptien et al., 2018; Liang et al., 2019) and early-type stars (Van Reeth et al., 2016), there has been significant interest in developing tools to study the behavior of the waves inside stellar interiors. Theoretical study of r-modes requires consideration of certain approximations to solve the problem by analytical or numerical methods. Previous research mostly considered a slow rotation limit with corresponding expansion with a small parameter to get low-order Rossby wave solutions in spherical coordinates (Provost et al., 1981; Saio, 1982; Damiani et al., 2020)). Rossby waves were also studied for rapid rotation but only for high-order harmonics (Papaloizou & Pringle, 1978). On the other hand, it is important to consider a 3D problem for a star with any rotation rate and obtain a full spectrum of solutions. This thesis aimed to study the Rossby waves in three dimensions (horizontal + vertical) and to understand the potential impact of the waves on the dynamics of stellar interiors.

We initially incorporated latitudinal differential rotation and viscosity into the problem to investigate the dynamics of Rossby waves on a simple 2D β-plane (Gizon et al., 2020). The analysis provided a fundamental understanding of solar Rossby waves and enabled a comparison of theoretical results with observations obtained by Löptien et al. (2018). We first addressed the inviscid case, therefore eigenvalues were real and continuous, and velocity stream functions exhibited a singularity at the critical latitude. Upon introducing viscosity, the eigenvalues became complex and discrete. Our findings indicated that the real parts of the vorticity eigenfunctions could align well with observed modes, unlike the imaginary part, when $Re \approx 300$. The presence of viscosity and horizontal shear flow resulted in angular momentum transport toward the equator by Rossby waves. Additionally, the impact of meridional flow on the dynamics of Rossby waves has been explored. The impact was found to be significant but smaller compared to the influence of latitudinal differential rotation. This study provided valuable insights into the dynamics of Rossby waves in the presence of latitudinal differential rotation on a 2D plane.

In the following two papers (Albekioni et al., 2023a,b), we developed a three-

dimensional model considering vertical stratification of density and temperature. We used a traditional approximation of linear fluid equations in a rotating system and considered a rectangular frame. This method is widely used to study the equatorially trapped Rossby waves in Earth's atmosphere and oceans (Lindzen, 1967). The Cartesian coordinate system significantly simplifies the mathematics, while the dispersion relations of the waves are the same as those obtained in the spherical geometry (Matsuno, 1966; Zaqarashvili et al., 2021). To obtain the dispersion relations and vertical solutions of the waves, we employed the method of separation of variables, which allowed us to split the general equations in radial and horizontal parts connected by the separation constant h. From this stage, two different developments are possible. The first development considers solving the horizontal equations in corresponding boundary conditions and finding the separation constant, h. Then h can be used to solve the vertical equations and to obtain the vertical structure of the solutions. The solutions are usually called "forced oscillations" in the Earth context. Lee & Saio (1997) and Townsend (2003) used the spherical hydrodynamic equations in the traditional approximation to find the "forced oscillations" in stellar interiors. The second development considers solving the vertical equations in appropriate boundary conditions to find the separation constant, which then can be used to find the solutions of horizontal equations with corresponding dispersion relations. The solutions are called "free oscillations" in the Earth context. We used the second method and studied the free oscillations of Rossby waves in vertically stratified stellar interiors.

Vertical temperature gradient plays a significant role in shaping the stellar structure. Sub-adiabatic gradients usually lead to the radiative transfer of energy hence it yields the radiative envelope. While the super-adiabatic gradients lead to the convective envelope. We employed the linear vertical temperature gradient, which is a good approximation to show the general properties of Rossby waves in stratified fluids. The linear temperature gradient leads to the Bessel equation for the sub-adiabatic case (see Eq.35 in Paper I and Eq. 58 in Paper II) and to the modified Bessel equation for the super-adiabatic case. Then the solutions of vertical equations were obtained in terms of Bessel (modified Bessel functions) using appropriate boundary conditions at the stellar surface. We started to solve the first case of a sub-adiabatic temperature gradient, which corresponds to the radiative early-type stars with masses of $1.5 > m_{\odot}$. The next step obviously is to repeat the calculations for solar-type stars with a slightly super-adiabatic temperature gradient in the outer envelope. This will be done in the future as outlined below.

At the surface, we used a free boundary condition, which implies that the Lagrangian pressure vanishes at the surface. Note that the close boundary condition (i.e. when the vertical velocity vanishes at the surface) also gives the same solutions. both boundary conditions yield an infinite number of discrete values for the separation constant h, thereby leading to an infinite number of vertical modes. Each value of the separation constant, hence each vertical mode, corresponds to particular solutions of the horizontal equation with horizontal wavenumbers and frequencies governed by the dispersion equation. The horizontal solution must satisfy the polar boundary conditions i.e. should be bounded at poles. It is found that the horizontal solutions of Rossby waves are governed by the parabolic cylinder equation, therefore they exponentially decrease towards the poles i.e. they are trapped near the equator.

Paper I (Albekioni et al., 2023a) was focused on the first five vertical modes that satisfy both vertical and latitudinal boundary conditions. These modes demonstrate oscillatory behavior and penetrate to an approximate depth of 50 H_0, where H_0 is the surface scale height. This height is around 300 km in conditions of solar surface gravity and a surface temperature of about 10,000 K. The vertical wavelength of these modes is influenced by the vertical temperature gradient, represented as ϵ. In environments where ϵ is smaller, indicating the strongly sub-adiabatic environment, the wavelength is shorter, and the waves are predominantly concentrated near the surface. On the other hand, when the temperature gradient approaches the adiabatic limit ($\epsilon = 0.4$), the wavelength of the modes increases up to ten times. Through examining various values of the vertical temperature gradient and different vertical modes derived from both free and closed boundary conditions, we determined that the waves are typically confined within approximately 15 Mm of the surface area. The latitudinal solutions and dispersion relations of the problem significantly depend on the parameter $\varepsilon = 4\Omega^2 R^2/gh$, where Ω represents the rotation frequency of a star, R is the radius, and g is the surface gravitational acceleration.

As the massive stars located in the upper part of HRD are known to have faster rotation rates, we intended to study how different stellar rotation frequencies and vertical temperature gradients influence the horizontal and vertical structures of Rossby waves. Paper II (Albekioni et al., 2023b) deals with different sub-adiabatic temperature gradients from $\epsilon = 0.2$ to $\epsilon = 0.4$. This paper includes vertical structure plots and a detailed examination of latitudinal modes. It was found that faster rotation leads to more pronounced trapping of waves near the equator. For a rota-

tion rate of $\Omega = 5\Omega_\odot$, the waves are found to be confined within ± 30 degrees of latitude. The wave frequency also shows a significant dependence on the stellar rotation rate. This dependence is more noticeable at slower rotation rates but becomes less apparent with rapid rotations. Vertical modes are crucial for constructing period-spacing patterns, which are usually used to correlate the theory with observations. For instance, we plotted the period-spacing patterns for Rossby and inertia-gravity waves for $\epsilon = 0.39$. We calculated the first ten vertical modes for a stellar angular frequency of $\Omega = \Omega_\odot$.

As previously mentioned, the rate of the temperature gradient significantly influences the equivalent depth, h, which in turn defines the vertical structure and frequency of the modes. Therefore, systematic observations of wave frequency in stars can facilitate the estimation of internal stellar parameters. By determining the equivalent depth of a specific mode, one can approximately evaluate the vertical temperature gradient within the stellar interior. This approach may provide a useful tool in the field of stellar seismology.

Several key points remain to be addressed in the near future:

1) Our analysis concerned only early-type stars with outer radiative envelopes. It is relatively simple to repeat the whole analysis for solar-like stars with outer convective envelopes. The vertical structure of Rossby waves then will be changed from the ordinary Bessel functions to the modified Bessel functions, which will obviously modify the separation constant and hence the dispersion relation of the waves. It is of significant importance to compare the resulting vertical structure and dispersion relations with the dynamics of solar Rossby waves as obtained by Bekki et al. (2022).

2) Our 3D analysis used the simplest solid body rotation. On the other hand, the differential rotation significantly affects the dynamics of Rossby waves including the dispersion relations and stability (Zaqarashvili et al., 2010; Gizon et al., 2020, 2021). We plan to include the latitudinal differential rotation in the formalism and solve the resulting equations for radiative stars. Horizontal equations will probably remain similar to that of those studied by Gizon et al. (2020), therefore the analysis will result in the influence of latitudinal differential rotation on the spectrum of 3D Rossby waves. Then the systematic observations of the frequency of the waves in other stars may lead to the estimation of stellar differential rotation, which is a challenging task in nowadays astrophysics. The convective stars will probably give similar results as obtained by Gizon et al. (2021).

3) Our 3D analysis excluded the influence of magnetic fields. However, it was

shown that magnetic fields play a vital role in shaping the dynamics of Rossby waves (Zaqarashvili et al., 2007; Márquez-Artavia et al., 2017; Zaqarashvili, 2018; Dikpati et al., 2018, 2020). We plan to include the horizontal magnetic field in the calculations and study its influence on the dispersion relations and vertical strictures of the Rossby waves in the stellar interior. Then the combination of theoretical results and observations may provide a tool for the estimation of magnetic field strength in stellar interiors hence making a big step forward in asteroseismology.

4 Bibliography

References

Aerts, C. 2021, Reviews of Modern Physics, 93, 015001

Aerts, C., Christensen-Dalsgaard, J., & Kurtz, D. W. 2010, Asteroseismology

Albekioni, M., Zaqarashvili, T. V., & Kukhianidze, V. 2023a, , 671, A91

Albekioni, M., Zaqarashvili, T. V., Kukhianidze, V., Gurgenashvili, E., & Bourdin, P. 2023b, Astronomische Nachrichten, 344, e20230083

Balmforth, N. J. & Morrison, P. J. 1995, Annals of the New York Academy of Sciences, 773, 80

Beck, J. G. 2000, , 191, 47

Bekki, Y., Cameron, R., & Gizon, L. 2019, Poster at conference "Physics at the equator: from the lab to the stars", ENS Lyon, France, 16–18 October, https://equatorial-phys.sciencesconf.org/data/Bekki_poster.pdf

Bekki, Y., Cameron, R. H., & Gizon, L. 2022, , 666, A135

Bennett, J. R. & Young, J. A. 1971, Monthly Weather Review, 99, 202

Bonomo, A. S. & Lanza, A. F. 2012, , 547, A37

Brajša, R., Wöhl, H., Vršnak, B., et al. 2001, , 374, 309

Chelton, D. B. & Schlax, M. G. 1996, Science, 272, 234

Damiani, C., Cameron, R. H., Birch, A. C., & Gizon, L. 2020, , 637, A65

Dellar, P. J. 2011, Journal of Fluid Mechanics, 674, 174

Dikpati, M., Gilman, P. A., Chatterjee, S., McIntosh, S. W., & Zaqarashvili, T. V. 2020, , 896, 141

Dikpati, M., Gilman, P. A., Guerrero, G. A., et al. 2022, , 931, 117

Dikpati, M., McIntosh, S. W., Bothun, G., et al. 2018, , 853, 144

Drazin, P. & Howard, L. 1966, in (Elsevier), 1–89

Drazin, P. G., Beaumont, D. N., & Coaker, S. A. 1982, Journal of Fluid Mechanics, 124, 439

Drazin, P. G. & Reid, W. H. 2004, Hydrodynamic Stability

Driscoll, T. A., Hale, N., & Trefethen, L. N. 2014, Chebfun Guide (Oxford: Pafnuty Publications, https://www.chebfun.org/)

Duvall, Jr., T. L. & Gizon, L. 2000, , 192, 177

Eliasen, E. & Machenhauer, B. 1965, Tellus, 17, 220

Frederiksen, J. S. & Webster, P. J. 1988, Reviews of Geophysics, 26, 459

Gachechiladze, T., Zaqarashvili, T. V., Gurgenashvili, E., et al. 2019, , 874, 162

Geisler, J. E. & Dickinson, R. E. 1974, Journal of the Atmospheric Sciences, 31, 946

Gill, A. E. 1982, Atmosphere-Ocean Dynamics (New York: Academic Press)

Gilman, P. A., Dikpati, M., & Miesch, M. S. 2007, , 170, 203

Gilman, P. A. & Fox, P. A. 1997, , 484, 439

Gizon, L., Cameron, R. H., Bekki, Y., et al. 2021, , 652, L6

Gizon, L., Fournier, D., & Albekioni, M. 2020, , 642, A178

Goddard, C. R., Birch, A. C., Fournier, D., & Gizon, L. 2020, , 640, L10

Gurgenashvili, E., Zaqarashvili, T. V., Kukhianidze, V., et al. 2017, , 845, 137

Gurgenashvili, E., Zaqarashvili, T. V., Kukhianidze, V., et al. 2016, , 826, 55

Gurgenashvili, E., Zaqarashvili, T. V., Kukhianidze, V., et al. 2022, , 660, A33

Hadley, G. 1735, Philosophical Transactions of the Royal Society of London Series I, 39, 58

Hanasoge, S., Gizon, L., & Sreenivasan, K. R. 2016, Annual Review of Fluid Mechanics, 48, 191

Hanasoge, S. & Mandal, K. 2019, The Astrophysical Journal Letters, 871, L32

Hanson, C. S., Hanasoge, S., & Sreenivasan, K. R. 2022, Nature Astronomy, 6, 708

Hathaway, D. H., Upton, L., & Colegrove, O. 2013, Science, 342, 1217

Haurwitz, B. 1940, Transactions, American Geophysical Union, 21, 262

Haynes, P. H. 2003, in Encyclopedia of Atmospheric Sciences, ed. J. R. Holton, J. A. Pyle, & J. A. Curry (London: Elsevier)

Henneco, J., Van Reeth, T., Prat, V., et al. 2021, , 648, A97

Hill, K. L., Robinson, I. S., & Cipollini, P. 2000, , 105, 21927

Hirooka, T. & Hirota, I. 1989, Pure and Applied Geophysics, 130, 277

Horstmann, G. M., Mamatsashvili, G., Giesecke, A., Zaqarashvili, T. V., & Stefani, F. 2023, , 944, 48

Hough, S. S. 1897, Philosophical Transactions of the Royal Society of London Series A, 189, 201

Hough, S. S. 1898, Philosophical Transactions of the Royal Society of London Series A, 191, 139

Hovmöller, E. 1949, Tellus, 1, 62

Jeffery, C. S. 2020, , 496, 718

Keller, H. B. 1968, Numerical Methods for Two-point Boundary-value Problems (London: Blaisdell)

Kraft, R. P. 1967, , 150, 551

Krista, L. D. & Reinard, A. A. 2017, , 839, 50

Kuhn, J. R., Armstrong, J. D., Bush, R. I., & Scherrer, P. 2000, , 405, 544

Kuo, H.-L. 1949, Journal of the Atmospheric Sciences, 6, 105

Lanza, A. F., Gizon, L., Zaqarashvili, T. V., Liang, Z. C., & Rodenbeck, K. 2019, , 623, A50

Lanza, A. F., Pagano, I., Leto, G., et al. 2009, , 493, 193

Laplace, P. S. 1893, Oeuvres, 9, 71

Lee, U. & Saio, H. 1997, , 491, 839

Lekshmi, B., Nandy, D., & Antia, H. M. 2018, , 861, 121

Li, G., Van Reeth, T., Bedding, T. R., Murphy, S. J., & Antoci, V. 2019, , 487, 782

Liang, Z.-C., Gizon, L., Birch, A. C., & Duvall, T. L. 2019, , 626, A3

Lindzen, R. D. 1967, Monthly Weather Review, 95, 441

Lindzen, R. S., Straus, D. M., & Katz, B. 1984, Journal of the Atmospheric Sciences, 41, 1320

Liu, J. & Schneider, T. 2011, Journal of the Atmospheric Sciences, 68, 2742

Longuet-Higgins, M. S. 1965, Proceedings of the Royal Society of London Series A, 284, 40

Longuet-Higgins, M. S. 1968, Philosophical Transactions of the Royal Society of London Series A, 262, 511

Löptien, B., Gizon, L., Birch, A. C., et al. 2018, Nature Astronomy, 2, 568

Mack, L. M. 1976, Journal of Fluid Mechanics, 73, 497

Madden, R. A. 2007, Tellus Series A, 59, 571

Márquez-Artavia, X., Jones, C. A., & Tobias, S. M. 2017, Geophysical and Astrophysical Fluid Dynamics, 111, 282

Matsuno, T. 1966, Journal of the Meteorological Society of Japan, 44, 25

McIntosh, S. W., Cramer, W. J., Pichardo Marcano, M., & Leamon, R. J. 2017, Nature Astronomy, 1, 0086

Newton, H. W. & Nunn, M. L. 1951, , 111, 413

Orr, W. . 1907, Proc. R. Irish Acad., A27, 69

Orszag, S. A. 1971, Journal of Fluid Mechanics, 50, 689

Papaloizou, J. & Pringle, J. E. 1978, , 182, 423

Pedlosky, J. 1987, Geophysical Fluid Dynamics (New York: Springer)

Platzman, G. W. 1968, Quarterly Journal of the Royal Meteorological Society, 94, 225

Provost, J., Berthomieu, G., & Rocca, A. 1981, , 94, 126

Proxauf, B., Gizon, L., Löptien, B., et al. 2020, , 634, A44

RayleighLord Rayleigh. 1879, Proc. London Math. Soc., s1-11, 57

Read, P. L. & Lebonnois, S. 2018, Annual Review of Earth and Planetary Sciences, 46, 175

Ripa, P. 1997, Journal of Physical Oceanography, 27, 633

Rossby, C. G. 1939, Journal of Marine Research, 2, 38

Rüdiger, G. 1989, Differential Rotation and Stellar Convection (Berlin: Akademie-Verlag)

Saio, H. 1982, , 256, 717

Saio, H. & Kurtz, D. W. 2022, , 511, 560

Saio, H., Kurtz, D. W., Murphy, S. J., Antoci, V. L., & Lee, U. 2018, , 474, 2774

Salby, M. L. 1984, Reviews of Geophysics and Space Physics, 22, 209

Samadi-Ghadim, A., Lampens, P., Jassur, D. M., & Jofré, P. 2020, , 638, A57

Schensted, I. V. 1961, PhD thesis, The University of Michigan, Ann Arbor

Showman, A. P. & Polvani, L. M. 2011, , 738, 71

Simon, G. W. & Weiss, N. O. 1997, , 489, 960

Snodgrass, H. B. 1984, , 94, 13

Snodgrass, H. B. & Ulrich, R. K. 1990, , 351, 309

Sommerfeld, A. 1909, in Atti del IV Congresso Internazionale dei Matematici (Roma, 6–11 Apr 1908), 116–124

Stewartson, K. 1977, Geophysical and Astrophysical Fluid Dynamics, 9, 185

Suess, S. T. 1971, , 18, 172

Takata, M., Ouazzani, R. M., Saio, H., et al. 2020, , 644, A138

Taylor, G. I. 1936, Proceedings of the Royal Society of London Series A, 156, 307

Timothy, A. F., Krieger, A. S., & Vaiana, G. S. 1975, , 42, 135

Townsend, R. H. D. 2003, , 340, 1020

Vallis, G. K. 2006, Atmospheric and Oceanic Fluid Dynamics

Van Reeth, T., Mombarg, J. S. G., Mathis, S., et al. 2018, , 618, A24

Van Reeth, T., Tkachenko, A., & Aerts, C. 2016, , 593, A120

Watson, M. 1981, Geophysical and Astrophysical Fluid Dynamics, 16, 285

Watts, A. L., Andersson, N., & Williams, R. L. 2004, , 350, 927

Webster, P. J. 1973, Monthly Weather Review, 101, 58

Williams, P. E., Hathaway, D. H., & Cuntz, M. 2007, , 662, L135

Yanai, M. & Lu, M.-M. 1983, Journal of the Atmospheric Sciences, 40, 2785

Zaqarashvili, T. 2018, , 856, 32

Zaqarashvili, T. V., Albekioni, M., Ballester, J. L., et al. 2021, , 217, 15

Zaqarashvili, T. V., Carbonell, M., Oliver, R., & Ballester, J. L. 2010, , 709, 749

Zaqarashvili, T. V., Oliver, R., Ballester, J. L., & Shergelashvili, B. M. 2007, , 470, 815